Modeling of periodic non-smooth motion using the harmonic balance method

Amey N. Vasulkar

Technische Universiteit Delft

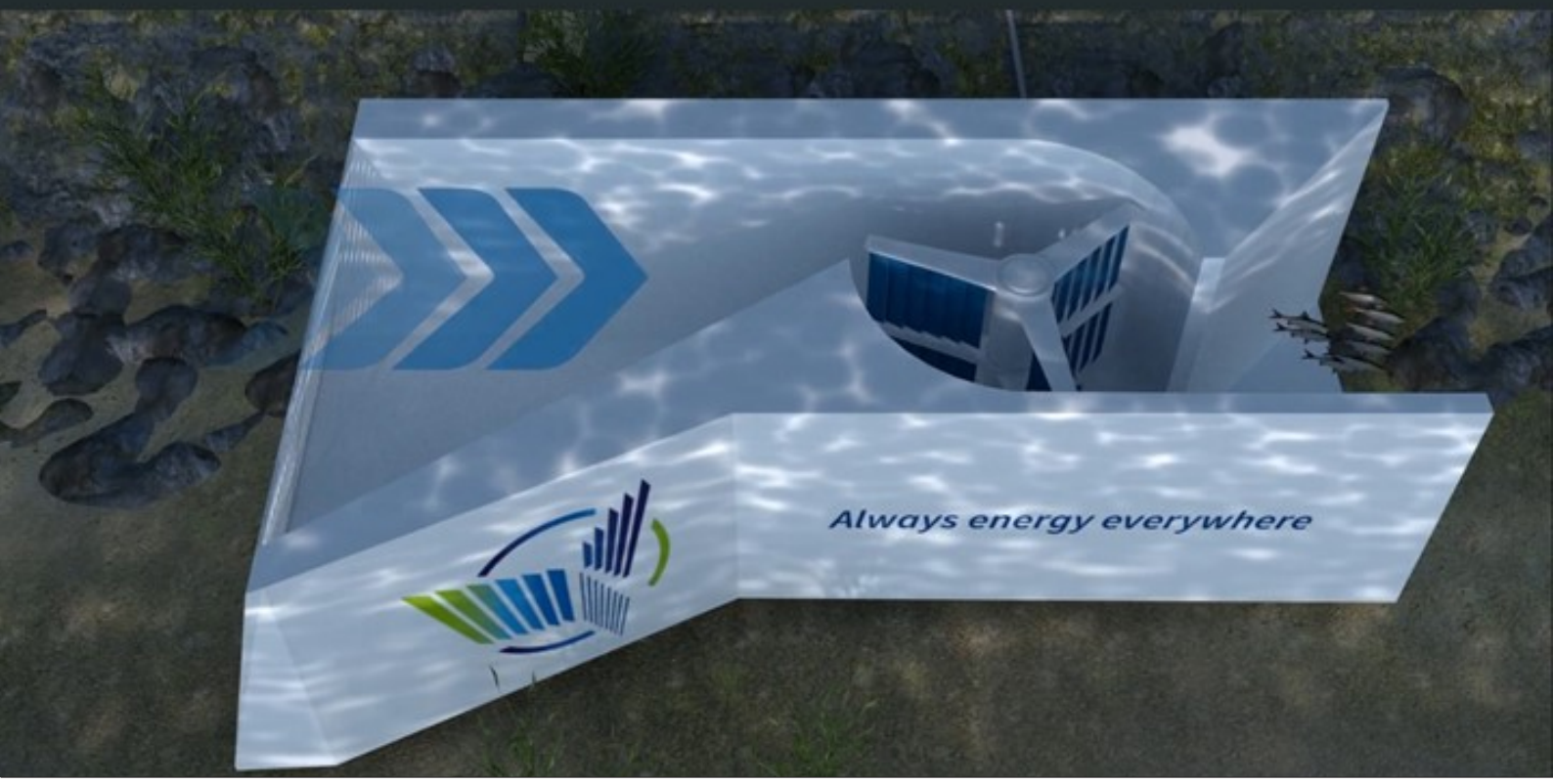

TU Delft Delft University of Technology

Challenge the future

MODELING OF PERIODIC NON-SMOOTH MOTION USING THE HARMONIC BALANCE METHOD

by

Amey N. Vasulkar

in partial fulfillment of the requirements for the degree of

Master of Science

in Applied Mathematics

at the Delft University of Technology,

to be defended publicly on Friday August 31, 2018 at 12:00 PM.

Supervisor:	Dr. ir. D. R. van der Heul	
Thesis committee:	Prof. dr. ir. C. Vuik,	TU Delft
	Prof. dr. ir. A. W. Heemink.	TU Delft

This thesis is confidential and cannot be made public until August 30, 2018.

TU Delft Delft University of Technology

ABSTRACT

The company Deepwater Energy BV, Netherlands developed a unique water turbine called as the Oryon Watermill (OWM). It was the aim of the company to obtain an efficient numerical model for the turbine. A numerical model, which serves as a good starting point, has already been developed by Maniyara [1]. This model suffered from certain limitations and to tackle these it was realized that a smaller and simpler problem needs to be solved. The current thesis deals with developing a numerical model for this smaller problem.

In this problem, an airfoil is hinged at its leading edge and rotating under the influence of a periodic water flow. Further, the rotation of the airfoil is restricted by a stopper. This restriction leads to a collision between the airfoil and the stopper due to which the motion of the airfoil is changed suddenly. This is a Fluid-Structure Interaction (FSI) problem.

To model the structural part i.e. the airfoil motion, a *non-smooth* dynamical analysis is needed. Then, the entire FSI problem is solved in a faster and efficient way using the harmonic balance method. For this purpose, the non-smooth dynamics of the airfoil have to be solved using the harmonic balance method. In the thesis, a novel approach is developed to solve the non-smooth dynamics problem using the harmonic balance method. Initially, this new approach is implemented and verified in MATLAB on a 1D level. Later, a *MATLAB-OpenFOAM coupled* solver is developed to compute the solution to the airfoil problem using this newly developed approach.

ACKNOWLEDGEMENTS

I would like to thank the Computer Simulations for Science and Engineering (COSSE) consortium, in particular, Dr. Michael Hanke, Dr. Reinhard Nabben, and Dr. Kees Vuik, for providing me with the opportunity of studying in such a unique programme through which I will be obtaining two master's degrees. A Master in Scientific Computing from TU Berlin and a Master in Applied Mathematics from TU Delft.

I feel a master's journey can be related to the process of computations. For a year and a half, a 'pre-processing' is done through the various courses you opt during your study. Then, the actual 'simulation' process is the time you write your thesis. And on the day of your defence, the 'simulations' are complete and you know the quality of your 'results'.

Nearly 10 months ago, I started the 'simulation' of my master's thesis project in the Numerical Analysis group at TU Delft. My supervisor for this project was Dr. Duncan van der Heul, whom I would like to extend my heartfelt gratitude for guiding me throughout the project. He has been my supervisor-cum-mentor and has directly or indirectly taught me a lot of things.

But this 'simulation' of my master's thesis is a very long one, and there have been a lot of 'acceleration techniques'. These have been in the form of my friends, family and thesis roommates. In particular, I would like to thank my friends, Sharayu, Giulia, Palash, Kartik, Sourabh, Komal, and Anudeep for helping me with editing and proofreading my thesis and being a constant source of motivation. A big shout-out to Jenny, Pascal, and Edoardo for being the best master's thesis roommates. We had fun and interesting conversations during lunch and coffee breaks.

A special mention of Mr. Yashasvi Giridhar who lent me his laptop for running simulations on Ubuntu platform. He is also my friend who has helped me a lot during this time.

But, above all, I would like to thank my parents and both my sisters for supporting me throughout this journey, both, emotionally and financially.

Amey N. Vasulkar
Delft, August 2018

Though the road's been rocky, it sure feels good to me
- Bob Marley

CONTENTS

1

THE ORYON WATERMILL-A BRIEF INTRODUCTION

The Oryon Water Mill (OWM) is an innovative water turbine developed by Deep Water Energy BV (DWE). In the view of optimizing the design and obtaining a better efficiency, numerical simulations are inevitable. So, the company plans on developing a reliable and efficient numerical model of the OWM. A numerical model, which serves as a good starting point, has already been developed by Maniyara [1]. This chapter gives a brief introduction to the OWM and its existing numerical model. The research questions come naturally in the process of understanding the limitations of the existing numerical model.

1.1. Oryon Water Mill

The OWM is a turbine which generates power from low-speed currents, typically, rivers, and open water channels with currents of $1-2\,m/s$. A few of the important characteristics of the turbine are:

- It has a modular build making it economically adaptable to local flow conditions.
- It has an ability to operate under low-pressure head conditions (rivers, etc.)
- It is eco-friendly as it operates at low speeds and has large clearances which do not adversely affect the morphology and wildlife (like fishes) of the local water body.
- It has an innovative design (described later) of the rotor arm which increases the torque and power delivered by the turbine.

1.1.1. Details of the construction of the OWM

The turbine primarily consists of a three-armed rotor with its axis mounted vertically and perpendicular to the flow. Each arm of the rotor has 4 equally sized movable flaps (referred to as *lamellas*). These lamellas are allowed to rotate with respect to the rotor arm. The angle of rotation of individual lamella depends on the stoppers effected in the design. This entire assembly is encased in a housing. The rotor shaft is connected to an electric generator. Figure 1.1 is an illustration of the OWM as given by DWE.

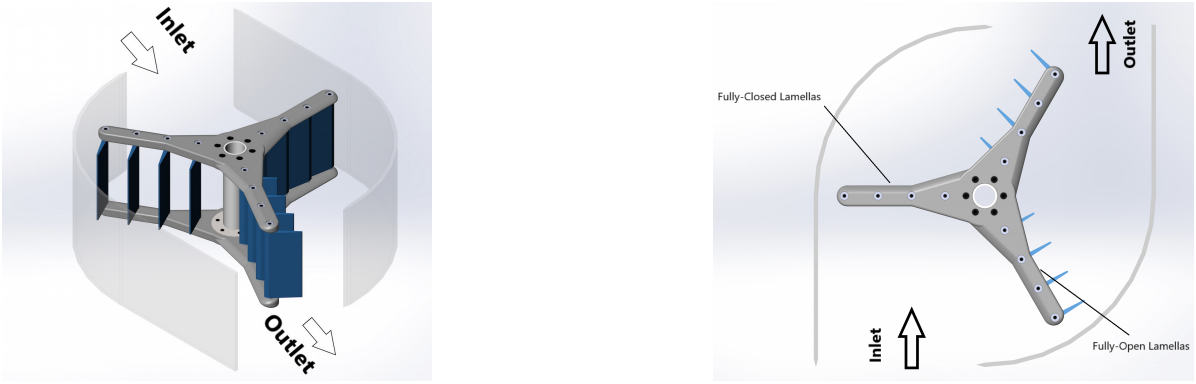

(a) Iso view (b) Top view

Figure 1.1: Figure (a) shows the isometric view of the OWM with inlet and outlet for water. Figure (b) shows the top view of the OWM with *lamellas* in fully-open and fully-closed positions.

1.1.2. Working of the OWM

The flowing water entering the turbine causes the rotor arms along with their lamellas to move. The independent motion of the lamellas with respect to the rotor is a result of the changing angle of attack of the water on the lamellas. Here, a convention for the lamellas is defined, which, from now on, will serve as a standard. The situation when the lamellas are aligned with the rotor arm (i.e. 0° angle) is referred to as-*fully-closed*, and when they are at the outermost position is referred to as-*fully-open*. Figure 1.1(b) illustrates these positions.

The turbine's working principle is of a three-armed *drag-based* rotor turbine. In a drag-based turbine, a drag force is exerted by the flowing water which propels the rotor arms. Likewise, the incoming water transfers momentum to the lamellas which in turn, based on their position with respect to the rotor, transfer momentum to the rotor arm and this results in the motion of the rotor arm. It is imperative to note that the direct transfer of momentum from water to the rotor arm is negligible and nearly all the momentum is transferred from the water to the rotor arms through the lamellas. The physics of momentum transfer can be explained in the following way.

The incoming water transfers momentum to the lamellas which are in the fully-open position. In this case, the angular momentum of the water closes the lamellas while the linear momentum is transferred from the lamellas to the rotor arm. Once lamellas are in the fully-closed position, (nearly) the entire momentum of the water is transferred to the rotor arm. As the rotor arm passes near the outlet, the moving water impinges at an angle such that it causes the lamellas to open again. In this case, too, only linear momentum is transferred while the angular momentum results in the movement of the lamellas with respect to the rotor arm. When the lamellas reach the fully open position, they align themselves with the flow. This means that the area of the rotor obstructing the upstream flow is minimized, effectively minimizing the drag in the recovery phase. Thus, the combined torque of all the lamellas and the power delivered by the water are increased. The rotor arm moves towards the inlet and the cycle continues. The design of the housing ensures that the upstream water impinges suitably on the lamellas and leaves at the right point. The housing and the lamella motion facilitates the existence of the wildlife in the water body.

Stoppers at fully-closed and fully-open positions

'Towing tank' experiments were conducted by MARIN on the OWM. The details of the experiment are described in the next section. From the experiments, videos were obtained which described the motion of the lamellas. It is clear from these videos that the lamella motion is restricted at the fully-closed position by a 'mechanical' stopper.

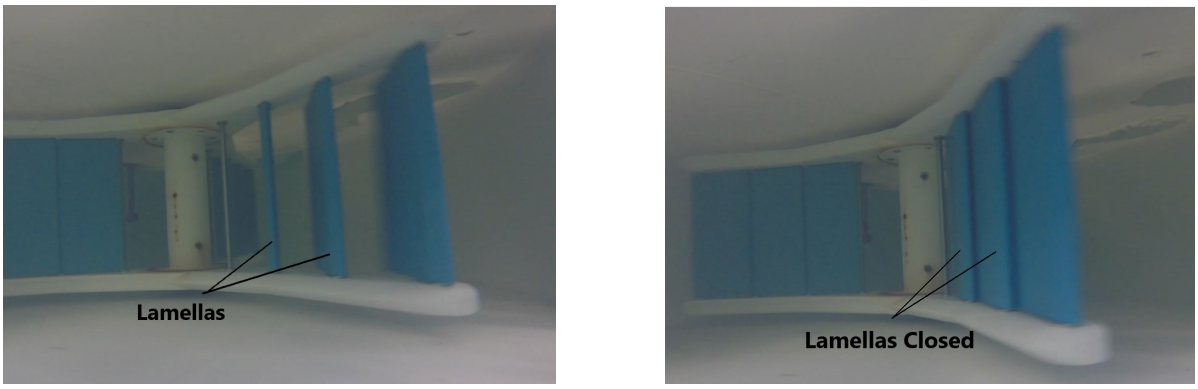

(a) Lamellas just before closing

(b) Fully-closed lamellas

Figure 1.2: Snapshots reproduced from the videos of the experimental tests performed on the OWM taken with a camera mounted near its inlet. Figures show the lamellas on a single rotor arm during the closing process.

Figure 1.2 illustrates the orientation of lamellas through the closing process. Here, one can verify that the lamella motion is restricted by collision with the neighboring lamella on the same rotor arm. This neighboring lamella acts as a 'mechanical' stopper. Similarly, the videos are observed to understand the stopper at the fully-open position.

Figure 1.3: Snapshots reproduced from the testing of the OWM depicting the lamellas at the fully-open condition aligned with the flow

For the fully-open position, the lamellas are aligned with the flow because of which there is no torque induced by the flow on the lamellas to cause the rotation of the lamellas. The lamellas are opened to the extent that they are aligned with the flow. Here, the stopper is not a mechanical one but a property of the flow. Figure 1.3 illustrates this operation. It should be noted here that the numerical model of the OWM should accurately model the behavior of the lamellas between and at the fully-open and fully-closed positions.

1.1.3. Experimentally obtained characteristics of OWM

For the OWM, like any other turbine, characteristic curves like the torque v/s the speed curve are essential for design optimization and performance analysis. To obtain these results, experimental tests were performed on the OWM by MARIN[1]. These tests are expensive and not the best option for design optimization in today's age of computing and so, a numerical model is preferred. Nonetheless, experimental results serve as a benchmark for the numerical results. Once the numerical results are in accordance with the experimental results, further efforts in design optimization of the OWM and testing of the various lamella designs and configurations can be done numerically as opposed to experimentally. This is cost-effective and faster.

In [1], the author has mentioned the experimental tests performed on the turbine which were used as a benchmark to evaluate his numerical model. The tests were conducted in a controlled laboratory environment in the 'Shallow Water Basin' (Binnenvaart) of MARIN. The test setup consisted of a six-component measurement frame with an attached mounting frame for an electric generator and an attached drive shaft. The shaft of the OWM contains a torque sensor which measures forces in the x, y and z directions, with the positive direction of turbine rotation defined as clockwise when viewed along the shaft from above the water surface. Additionally, the setup included flow meters installed at several locations at the inlet and outlet of the turbine housing. This setup was then mounted under the towing carriage of the 'shallow water basin' facility. The model tests were conducted for several variants of the turbine housing and for a number of different towing speeds. The above description of the model setup is reproduced from [1].

The following is a review of the variant, among the five variants tested by MARIN, with the highest evaluated power generation co-efficient (described later) at a single selected towing velocity of 2.5m/s (requested by DWE). This variant which is referred to as *Type IIA* consists of only the curved housing segments and is illustrated schematically in figure 1.4.

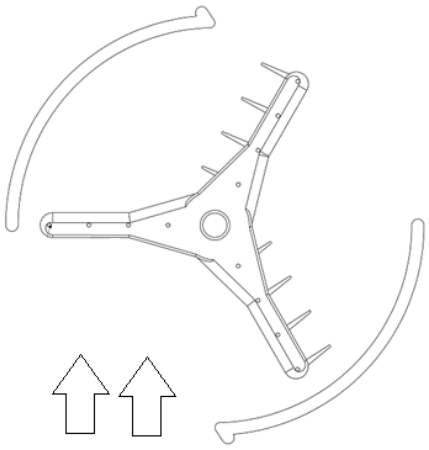

Figure 1.4: Schematic representation of the OWM (*Type IIA*). The arrows indicate the inlet for water

[1] Maritime Research Institute in Netherlands

Nomenclature of the turbine characteristics

The amount of power, P, generated by a turbine is given by:

$$P = 2\pi QN,$$

where Q is the net torque generated by the turbine and N is the frequency of rotations in Hertz (Hz). Furthermore, the available power in unrestricted water (no obstructions in the flow of water) based on the total kinetic energy of the incoming water in the rotor is defined by:

$$P_{available} := \frac{1}{2}\rho A v^3,$$

where ρ is the density of water, A is the projected area perpendicular to the inlet and v is the velocity of incoming water.

This leads to the definition of power coefficient in unrestricted water as:

$$C_p := \frac{P}{P_{available}} = \frac{2\pi QN}{\frac{1}{2}\rho A v^3}.$$

The Tip Speed Ratio (TSR) is the ratio of the tangential velocity of the tip of the rotor arm and the velocity of the incoming water. Its mathematical representation is:

$$TSR := \frac{v_{tip}}{v} = \frac{2\pi RN}{v},$$

where v_{tip} is the velocity of the rotor tip and R is the radius of the turbine.

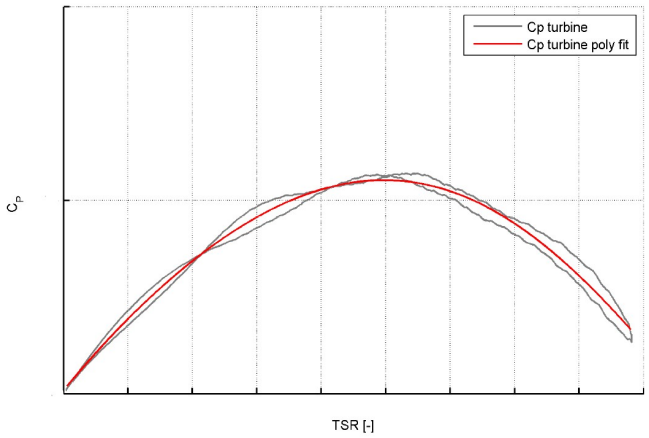

Figure 1.5: Experimental test results:C_p v/s TSR-at 2.5m/s for the OWM Type IIa

The performance characteristic curve of the OWM is the C_p v/s TSR plot. Figure 1.5 shows three curves depicting the C_p v/s TSR relation obtained from the experimental tests performed by MARIN. One of the grey colored curves is obtained by increasing the TSR from 0 to around 0.9 and plotting the corresponding C_p value, while the other is obtained by decreasing the TSR from maximum to 0. The red curve is then obtained by fitting an appropriate polynomial of degree 4. This curve has a maximum as seen from figure 1.5. Hence, it can be inferred that there is an optimum TSR and thus, a turbine operating speed for which the power generated from the turbine is maximum. An increase of the TSR beyond this optimum reduces the power obtained from the turbine.

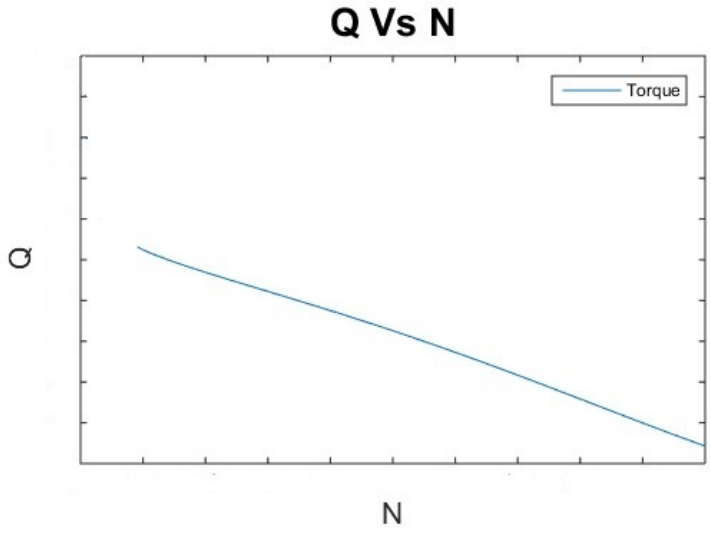

Figure 1.6: Experimental test results:Q v/s N- at 2.5m/s for OWM IIa

The performance can also be expressed with the Q v/s N curve. This curve is derived from the previous plot and is an alternative way to visualize the same results. Observation of figure 1.6 shows that the frequency versus torque relation is linear. The torque reduces as the frequency increases. Extrapolating the curve beyond N = 1, it is seen that the torque produced becomes negative, implying that the turbine will consume instead of produce power. The section of the curve between 0 to 0.1 is omitted because the Q v/s N curve becomes non-linear as $N \rightarrow 0$ with $Q \rightarrow \infty$. This is not true in reality and Q is finite. This discrepancy can be attributed to the fact that the experiment is started with the turbine being stationary when the water impinges on the rotor arm. Thus, implying that at $C_p = 0$ the TSR = 0. But the curve fitting polynomial in figure 1.5 doesn't pass through the point (0,0) which leads to the non-linear behavior of the derived Q v/s N curve. Hence the rotational speeds are restricted to less than 1 and greater than 0.1.

1.2. The baseline 2D model of the OWM developed by Maniyara

In this section, the previous work done on the numerical modeling of the OWM is discussed briefly. The numerical model of the OWM developed by Maniyara will be referred to as the *baseline 2D model*. The baseline model is 2D as the problems faced in the 2D case will also appear in 3D, so correctly modeling a 2D case is the first step towards modeling in 3D. Also, the 2D model already incorporates most of the essential parts of the 3D model and has lesser complexity. It must be clear by now that modeling of the lamellas will be the most crucial task as they are the link for momentum transfer to the rotor arm. OpenFOAM® is used as a solver for the baseline 2D numerical model. The results produced by the baseline 2D are discussed in the following sub-section.

1.2.1. Results and Discussion

It is understood that the baseline 2D model produces results that significantly differ from the experimental results.

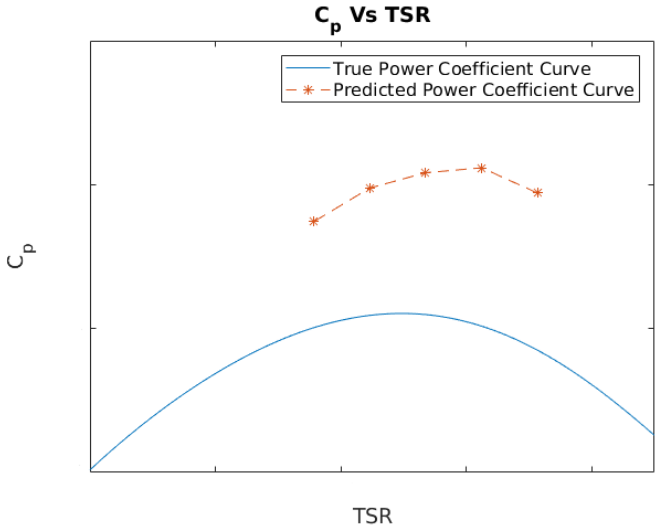

Figure 1.7: The C_p v/s TSR curve observed experimentally (blue) and predicted numerically (red dotted).

Figure 1.7 shows the comparison of C_p v/s TSR curve between the numerical and experimental results. This clearly illustrates that the model has some deficiencies. The conclusions and recommendations in [1] need to be carefully studied to make the model more accurate.

The C_p v/s TSR comparison has shown over-prediction in torque. The author attributes this to the gap between the turbine and the casing in the axial direction that only exists in 3D, which cannot be accounted for in the 2D model. Also, the shift in the optimal turbine performance is accredited to the difference in the velocities used to calculate the TSR in the experiments and the numerical results. In the experiments, the average inlet velocity is considered while in the numerical results the velocity just in front of the rotor is considered. It should be noted that the incorrect modeling of the motion of the lamellas will also affect the turbine torque calculation.

1.2.2. Limitations of the baseline 2D model

As noted in the previous section, the results from the baseline 2D model are not accurate, nonetheless, they serve as a good starting point towards a better numerical model. To develop a better model, the limitations in the baseline 2D model are studied and noted as follows:

- A laminar flow model is used, as it is cited in [1] that the Reynolds number of the flow is well below the turbulent regime. But the lamellas move very fast when they are closing or opening. The motion is recorded in the videos of the experiments. This fast motion of lamellas will lead to separation of the fluid near thir surface. Thus, a low-Reynolds Turbulence model would be more appropriate as it will model the separation in the turbine dynamics more precisely.
- The developed solver for the model is currently serial. The fact that it is serial means the computation time is determined by the speed of the single core. Also, parallelization of the solver is essential if the model is to be extended to 3D.

- There are sudden spikes in the torque versus time signal over a single period.

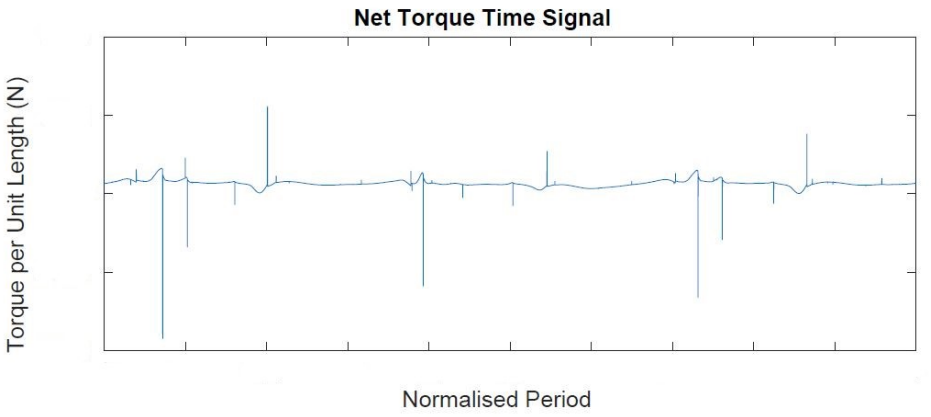

Figure 1.8: Torque time signal curve showing the unphysical spikes in the torque calculated using the numerical solution from the baseline 2D model.

Figure 1.8 depicts the torque calculated using the numerical solution from the baseline 2D model over a single period of operation. The sudden spikes in the signal are presumed to be numerical artifacts as such high torque spikes are not physical. The spikes are actually because of pressure corrections to reestablish the continuity of the flow after the (sudden) movement of the lamella. This implies that the coupling between the fluid flow and the lamella dynamics should be enforced more correctly.

- The baseline 2D model solved the problem as an IVP (initial value problem). The periodic solution is then the limit solution of the transient problem. The erratic motion of the lamellas leads to a slower convergence to this periodic solution. The model was simulated for 10 periods of rotation to achieve sufficient periodicity. This increases the computation time significantly with no gain in terms of output. A faster method to obtain only the periodic solution can be incorporated.

- The lamellas, in each period of the rotor rotation, should have the same angular position i.e. the lamellas should open and close at the same time instant. This defines the *lamella periodicity*. The lamella dynamics predicted from the baseline numerical model show a lack of periodicity. Figure 1.9 clearly illustrates that the respective lamellas of each arm show a small shift in their periodicity curves. A clear lack of overlap in their period of operation versus the angle of operation curve is visible. This discrepancy is a result of the fact that the motion of the lamellas is not modelled in a physically correct way. In the baseline 2D model, it is assumed that at the instant when the lamella collides with the stopper, all the momentum of the lamella is lost i.e. a perfectly inelastic collision. This approximation is leads to an erratic motion of the lamellas.

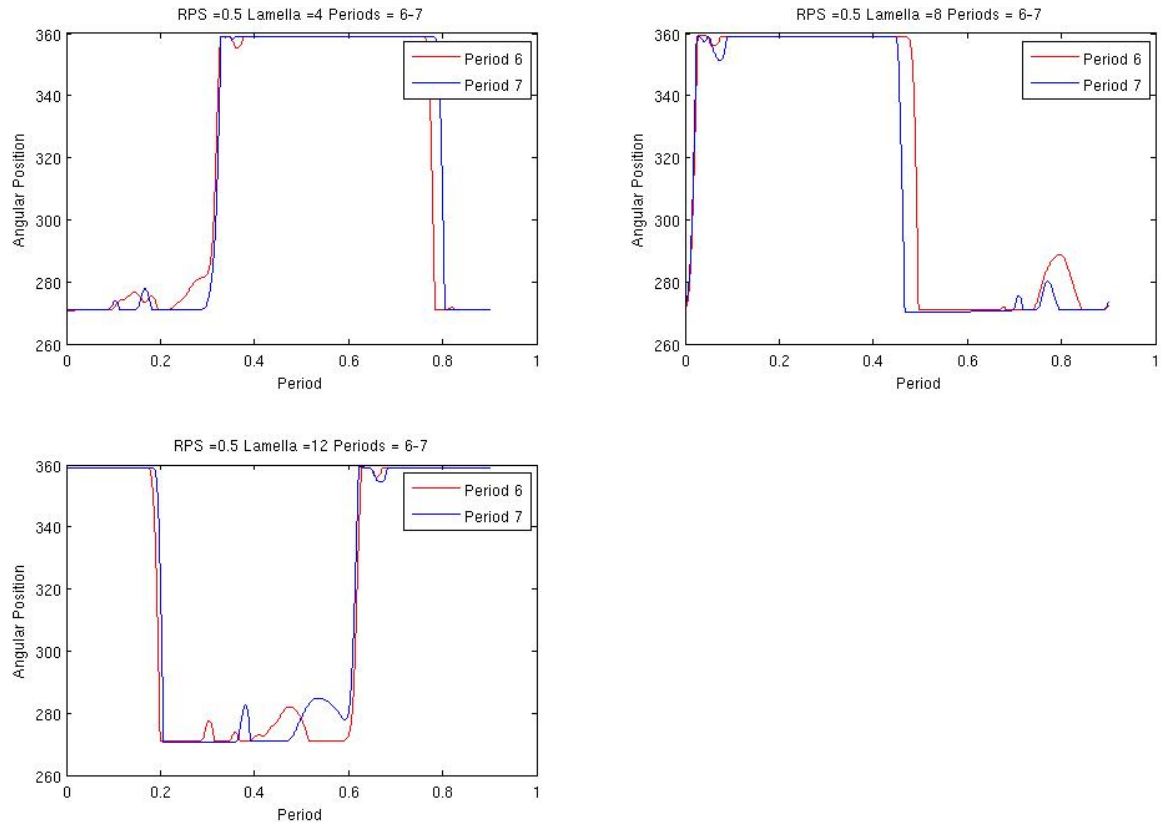

Figure 1.9: Depicts lamella periodicity for three lamellas located at the same position on respective rotor arms for two periods. Lamellas 4, 8, 12 are shown in periods 6 and 7. The figure is reproduced from [1]

1.3. Research Questions

Studying the baseline 2D model and its limitations, it is realized that correctly modeling the motion of the lamellas and the coupling between the fluid and structure part are two important aspects that need to be addressed to improve the accuracy. The research questions for this project follow from these limitations. These research questions are:

- What is the correct way to model the motion of a lamella considering its collision with the stopper? The collision with the mechanical stopper makes the lamella motion *non-smooth* which hints at focusing on non-smooth dynamics of bodies. This naturally leads to questions about how to numerically solve for this non-smooth motion?
- Is there any efficient and faster method to obtain the limit, periodic, solution of the motion of the lamellas? If yes, how to couple this method with the numerical solution procedure for the *non-smooth* motion of the lamella?
- How should the coupling between the fluid and structure models be improved to eliminate the non-physical pressure fluctuations and obtain a better solution for the coupled Fluid-Structure Interaction (FSI) problem of the motion of lamellas?

In this project, the modeling of the full OWM will *not* be considered. Instead, the project focuses on the development of a model of the motion of a single lamella under periodic flow whose positions are limited by stoppers. The model for this simpler problem will serve as first step towards modeling the full OWM. In the process of the development of this simpler model the above research questions are addressed. The lamella has a cross-section of a symmetric airfoil and hence, the problem to be tackled in this project is:

Numerical modeling of the non-smooth motion of a symmetric airfoil under periodic fluid flow using the harmonic balance method

The fluid flow is assumed to be laminar with small angles of attack ($\pm 10°$) which are varied periodically. Following the development of the numerical model, a MATLAB®-OpenFOAM® coupled solver is developed which solves for this model.

1.4. Schematic of the model problems

In this thesis, there a lot of model problems that are solved to verify certain numerical procedures and developed solvers. In this section, there are two schematics which show the type of model problems and their hierarchy. Figure 1.10 shows the hierarchy of the model problems, while figure 1.11 shows the model problems under each category.

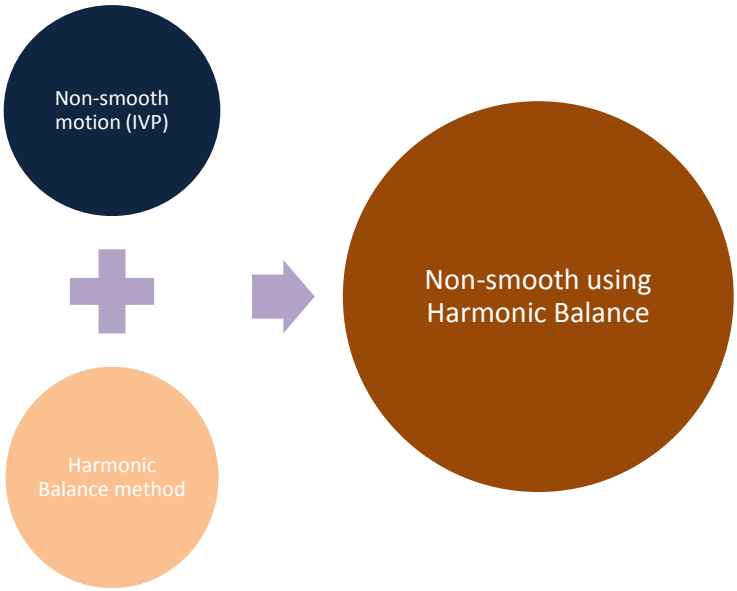

Figure 1.10: Schematic showing three categories under which the model problems lie.

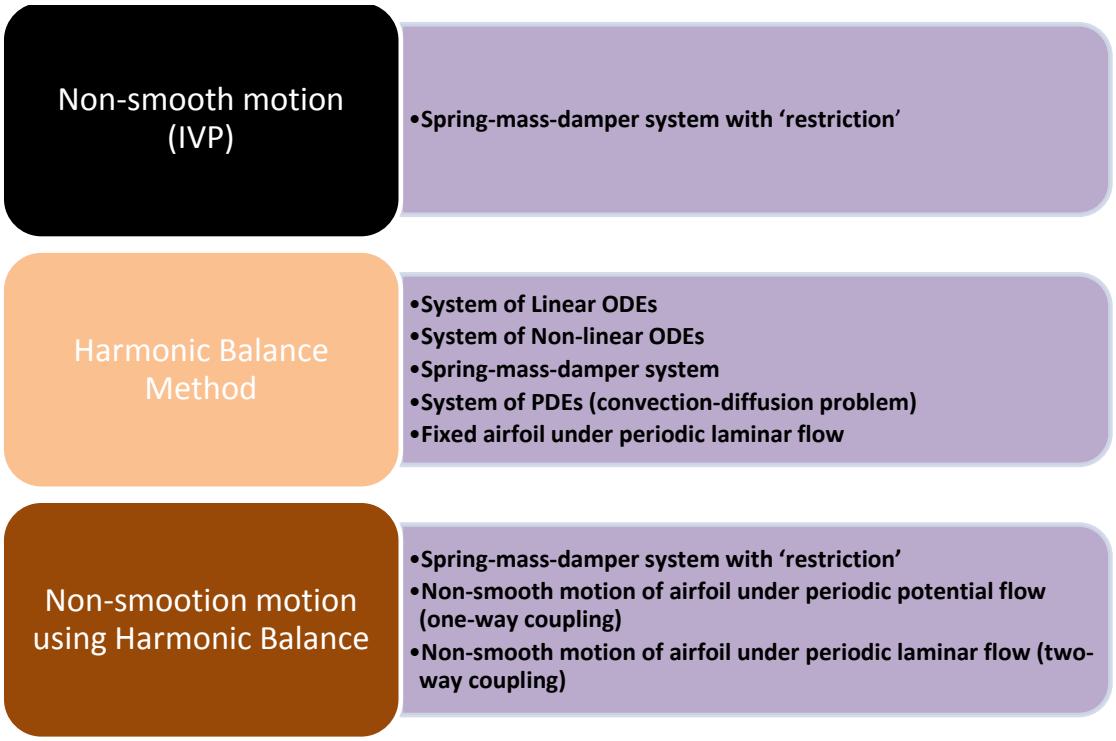

Figure 1.11: Schematic showing the problems under each category.

2

NON-SMOOTH DYNAMICS OF RIGID BODIES

In the previous chapter, it was show how the motion of the lamellas is restricted by a 'mechanical' stopper at the fully-closed position. There is a collision of the lamella with the stopper at the fully-closed position which hints that the modeling of the lamella dynamics requires understanding of the collision dynamics. The lamellas are considered as rigid bodies as there is no deformation in the shape of the lamellas during the operation of the turbine. Thus, the collision dynamics of rigid bodies is studied in order to develop a model for the motion of a single lamella/airfoil.

2.1. Rigid body equations of motion

This section introduces the dynamics of rigid bodies which is described by their equation of motion. The equation of motion provides the relation between the forces acting on the body and its resulting acceleration. In classical mechanics, Newton's Laws of Motion (mostly, Second Law) describes the behavior of the physical system. Newtonian mechanics can be a possible option to develop the equation of motion, but Lagrangian mechanics is preferred when there are constraints to the motion of the body. The reason being that the constraints can be made implicit in the Lagrangian formulation as opposed to the Newtonian formulation, where the constraints are explicit. The solution procedures for complying with explicit constraints are, generally, more complicated than for implicit constraints. The rigid body equations of motion developed using the Lagrangian mechanics are presented here.

At time t, $\mathbf{x}(t)$ is a vector defining the position coordinates of the Center of Gravity (COG) of the rigid body and $\mathbf{v}(t)(=\dot{\mathbf{x}}(t))$ is the vector defining the velocity of the COG of the rigid body. The *Lagrangian function* (L) is defined as the excess of kinetic energy over the potential energy. This Lagrangian function is the most fundamental quantity in the mathematical analysis of mechanical problems.

The Lagrangian function is given by:

$$\begin{aligned} L(\mathbf{x},\mathbf{v},t) &= T - U - \lambda(\phi), \\ T &= \frac{1}{2}\mathbf{v}^T \boldsymbol{M}\mathbf{v}, \end{aligned} \tag{2.1}$$

where T is the kinetic energy of the system, $\boldsymbol{M}$ is a symmetric positive definite mass matrix, λ is called the Lagrangian multiplier, ϕ denotes the algebraic constraints in the system, and U is the potential energy associated with the system. The mass matrix will be constant throughout the problems considered in this project as only the motion of single airfoil is analyzed.

The Euler-Lagrange equation of motion for a rigid body is given by:

$$\frac{\mathrm{d}}{\mathrm{dt}}\left(\frac{\partial \mathrm{L}}{\partial \mathbf{v}}\right)-\frac{\partial \mathrm{L}}{\partial \mathbf{x}}=0. \tag{2.2}$$

It should be noted that the Euler-Lagrange equations of motion when evaluated, essentially leads to Newton's Second Law. The formulation can be represented in the form of-*Force=Mass* × *Acceleration*. To illustrate the application of this equation, a simple example without an algebraic constraint is discussed.

Consider a rigid ball in the x−y plane. It is dropped from a height Y to the ground. The equations of motion of the ball until it hits the ground which is located at y = 0 are developed here.

The position coordinate vector of the ball at time 't' is $\mathbf{x}(\mathrm{t}) = (\mathrm{x}(\mathrm{t}), \mathrm{y}(\mathrm{t}))$.
The Lagrangian function (L) is given by:

$$\mathrm{L}(\mathbf{x}, \mathbf{v}, \mathrm{t}) = \frac{1}{2}\mathbf{v}^{\mathrm{T}}\boldsymbol{M}\mathbf{v} - \mathbf{g}^{\mathrm{T}}\boldsymbol{M}\mathbf{x},$$

where $\mathbf{g}$ is the gravitational acceleration in the y– direction. Note that the ball has no constraints to its motion so there is no term with a Lagrangian multiplier (λ). Applying the Euler-Lagrange equation of motion (2.2):

$$\begin{aligned} \mathrm{m}_1\ddot{\mathrm{x}}(\mathrm{t}) &= 0, \\ \mathrm{m}_2\ddot{\mathrm{y}}(\mathrm{t}) + \mathrm{m}_2|\mathbf{g}| &= 0, \\ \mathrm{m}_1 &= (\boldsymbol{M})_{1,1}, \\ \mathrm{m}_2 &= (\boldsymbol{M})_{2,2}, \end{aligned} \tag{2.3}$$

where $\ddot{\mathrm{x}}(\mathrm{t})$ and $\ddot{\mathrm{y}}(\mathrm{t})$ are the accelerations in x and y directions respectively.

The above system of equations clearly describes the motion of the ball before it hits the ground. It can be seen that the equations are in accordance with Newton's Second Law. During impact (collision), the above equation of motion will have constraints associated with it. The next section deals with these constraints.

2.2. Smooth/Non-Smooth dynamics in rigid body motion

In rigid body dynamics, it is generally assumed that the position and velocity are smooth functions of time when the bodies involved do not touch each other. This is referred to as *smooth dynamics*.

When the rigid bodies in the system are interacting (i.e. colliding or sliding), there are discontinuities in velocity at the time of collision or sliding. In literature [2] [3], this is referred to as *non-smooth dynamics*. A classic example of this phenomenon is a rigid ball hitting the ground. Just before hitting the ground, the ball has a pre-impact velocity which changes instantaneously on hitting the ground. This creates a discontinuity in the velocity function of the ball.

The field of non-smooth dynamics is vast and to not deviate from the main aim of modeling the motion of airfoil, only a few relevant aspects of this field are presented. The lamellas collide with the stopper which is similar to a ball bouncing on the ground. Hence, studying the dynamics of the motion of the ball or any other similar physical phenomena can aid in applying a similar analysis to the case of airfoil motion. As mentioned in [2], the ball bouncing dynamics is a case of *unilateral contacts*. Furthermore, it is assumed that the contact between the lamella and its corresponding 'mechanical' stopper is frictionless on the grounds of reasoning that the presence of water will make the contact frictionless.

The phenomenon of collision/impact can be modeled by impact laws. Two important types of such laws, as given in [4], are: *Newton's kinematic impact law* and *Poisson's impact law*. Poisson's impact law is more useful for collisions involving deformation of the bodies (flexible bodies)[4]. In this case, the bodies are considered rigid and thus, Newton's kinematic impact law is chosen. Newton's kinematic impact law for rigid bodies is given by:

$$\mathbf{v_{rel}}^{-} = \epsilon \mathbf{v_{rel}}^{+},$$

where $\mathbf{v_{rel}}^{-}$ is the relative velocity before impact, $\mathbf{v_{rel}}^{+}$ is the relative velocity after impact and ϵ is the coefficient of restitution between the impacting bodies. Thus, the equations of motion along with the analysis of impacts will give the exact description of the motion of the lamellas.

2.2.1. Equations for non-smooth motion

Having understood the non-smoothness of the motion of rigid bodies, this section initially introduces the generalized equation of non-smooth rigid body system and later, its form in the case of unilateral contacts, as given in [4], is presented.

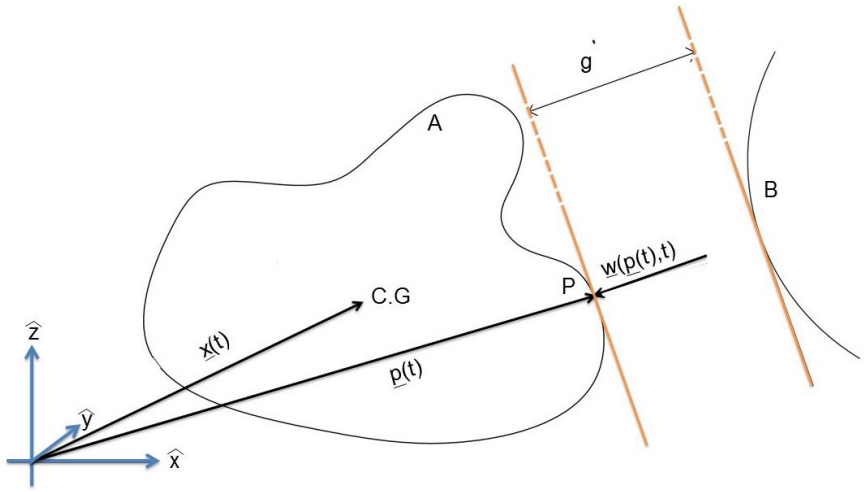

Figure 2.1: Schematic showing a collision between two rigid bodies A & B and the nomenclature used in the generalized rigid body equation of motion (2.4)

Figure 2.1 shows two bodies A and B colliding at point P. The formulation of the generalized equations of motion for such a system of rigid bodies is:

$$\boldsymbol{M}\mathbf{a_p}(t) = \mathbf{h}(\mathbf{p}(t), \mathbf{v_p}, t) - \mathbf{w}(\mathbf{p}(t), t)\Lambda = 0, \tag{2.4}$$

where $\mathbf{p}(t)$ and $\mathbf{v_p}$ are the position vector and velocity vector associated with the point of contact P, $\mathbf{a_p}(t)$ is the acceleration vector associated with point P, $\boldsymbol{M}$ is a symmetric positive definite mass matrix, $\mathbf{h}$ is the vector accounting for external forces, (Coriolis forces, centrifugal forces, etc.,) and $\mathbf{w}$ accounts for the generalized force direction of the contact force whose magnitude is given by Λ. $\mathbf{w}$ is essentially a unit vector. Equation (2.4) is also referred to as the *projected Newton-Euler equation*. The next concern is to determine $\mathbf{w}\Lambda$, for which the unilateral contact constraints need to be understood.

Unilateral contact constraints

The value of the gap function ($g(\mathbf{p},t)$) of the contact points determines the nature of interaction between the two bodies. The corelation between the value of the gap function and nature of interaction is defined as:

- $g > 0 \rightarrow$ the bodies are separated.
- $g = 0 \rightarrow$ the bodies are in contact.
- $g < 0 \rightarrow$ the bodies are penetrating.

Thus, the *unilateral constraint equation* between two colliding/impacting bodies is $g \geq 0$. It is important to note that the equation (2.4) along with the constraint equation form a system of Differential Algebraic Equations (*DAE*). Further, $\gamma(=\dot{g})$ defined as the normal relative velocity of the point of contact of one body with respect to the other, is given by $\gamma = \mathbf{w}^T\mathbf{v_p}$ [4].

As per [4], on integrating the equation (2.4) over singleton (t_o) the following impact equation is obtained:

$$\begin{aligned} \boldsymbol{M}(\mathbf{v}^+ - \mathbf{v}^-) &= \mathbf{w}\Lambda, \\ \gamma^{\pm} &= \mathbf{w}^T\mathbf{v}^{\pm}. \end{aligned} \tag{2.5}$$

where the + and – signs indicate velocities after and before the impact. Next important step is to determine Λ. For this, the Newton's impact law comes into picture.
Applying the law for two model conditions, $g = 0$ and $g > 0$:

$$\begin{aligned} g > 0: &\quad \boldsymbol{M}(\mathbf{v}^+ - \mathbf{v}^-) = 0, \\ g = 0: &\quad \boldsymbol{M}(\mathbf{v}^+ - \mathbf{v}^-) = \mathbf{w}\Lambda; \qquad \gamma^{\pm} = \mathbf{w}^T\mathbf{v}^{\pm}; \\ &\quad \gamma^+ + \epsilon\gamma^- \geq 0; \quad \Lambda \geq 0; \quad (\gamma^+ + \epsilon\gamma^-)\Lambda = 0, \end{aligned} \tag{2.6}$$

where again ϵ is the coefficient of restitution between the impacting bodies.

The first line of (2.6) is same as (2.5). The second line represents the set of all the complementarity conditions as referred in [4][2]. The impulsive force, if there is any, should be compressive, $\Lambda \geq 0$. This is clear from the physics of the motion. In the case of non-vanishing impulse ($\Lambda > 0$) apply the Newton's impact law as usual, i.e. $\gamma^+ = -\epsilon\gamma^-$, which is expressed in the third condition. Suppose now that, for any reason the contact does not participate in the impact, i.e. that the value of the impulsive force is zero, although the contact is closed. (Note: This happens for multi-contact situations). In such a situation, the post-impact relative velocities are allowed to be higher than prescribed by Newton's impact law, in the case of non-vanishing impulse, $\gamma^+ \geq -\epsilon\gamma^-$. Tnis is in order to express that the contact is superfluous and could be removed without changing the contact-impact process.

Equation (2.6) is developed for a general rigid body system. The second line of (2.6) is referred to as a *Linear Complementarity Problem*. The numerical approach to solve equation (2.6) is discussed in the next section

2.3. Numerical solution procedure for non-smooth motion

After studying the mathematical formulation of the motion of the lamella/airfoil the next question that arises is *how to solve this problem numerically* In literature, there are many approaches provided to solve (2.6), but not all the approaches are discussed here in order to avoid diverging from the main topic. Given that the approach should be straightforward to implement within OpenFOAM without much modification and that it should be able to model partially inelastic contacts, the event-driven approach is selected in this project[2]. The equation (2.6) and the governing equations of the motion of lamella/airfoil are second order ODEs and hence, ODE integrators will be an essential tool in this approach.

2.3.1. The event-driven approach

In the event-driven approach, one must separate the non-smooth motion into piecewise smooth parts and *switching points* (points of discontinuity). These smooth parts and switching points are referred to as 'states' or 'events' (σ). So, the approach specifies to evaluate the smooth and non-smooth parts separately. This means to integrate the ODE till the point of collision in the usual smooth way using an appropriate time integration method (an ODE integrator). At the switching points or discontinuities as referred before, solve the impact problem as referred in section 2.2.1 and determine the new underlying ODE. Note that, it is important to determine the post-impact velocities which will serve as the initial conditions for future ODE integration into the smooth part after the discontinuity. Figure 2.2 shows the flow chart for the event-driven approach.

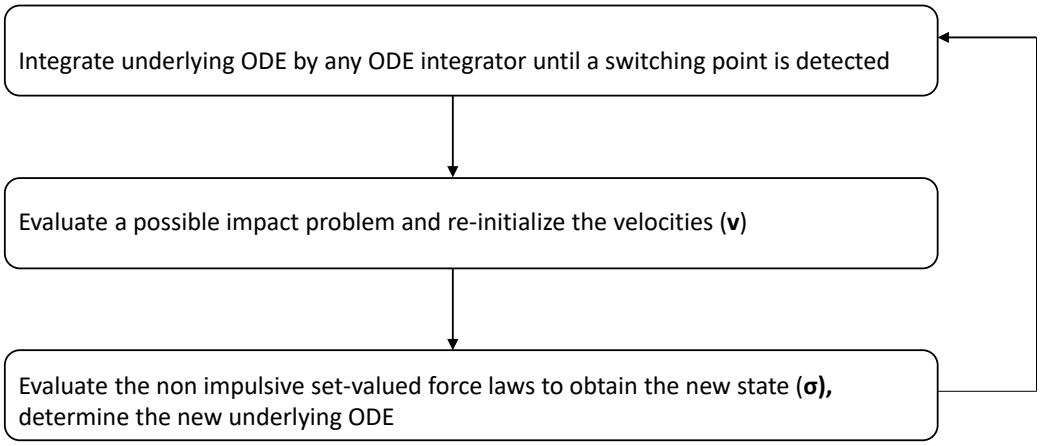

Figure 2.2: Flowchart of the event-driven approach

The event-driven approach solves the model equation in an initial value problem (IVP) formulation. The equation of motion of lamella/airfoil is an ODE but with some *constraints* because of the stoppers. These constraints add extra contact forces and constraint equations to the ODE which make it difficult to solve. The constraints are referred to, in literature, as *Nonpenetration Constraints*[3]. For such contact constraints, there are two types of contact: colliding contact and resting contact.

Colliding contact is used when the two bodies are colliding with each other and have a discontinuity in velocity after the collision (i.e. instantaneous change in velocity). The bodies separate after collision.

Resting contact is used when the two bodies after the collision are resting on each other i.e. they have (nearly) zero relative velocity with respect to each other.

Colliding Contact

In the case of colliding contact, the integration of the equation is continued until the time when the collision occurs (t_c). At this instant, the integration is stopped and the changes in the pre-collision velocities of the bodies are computed. It requires the application of Newton's impact law. This will help compute the velocities post the collision which will be used to continue the integration. Thus, the problem of impact discussed in section 2.2.1 is solved. But there are a few concerns like how to compute the time of the collision, the changes in velocity and the contact forces that prevent the inter-penetration of the two bodies.

The foremost thing is computing the time of collision (t_c). Consider the position of the body at different time steps through the integration of the ODE. Call these time steps $t_n; 1 \leq n \leq N$.

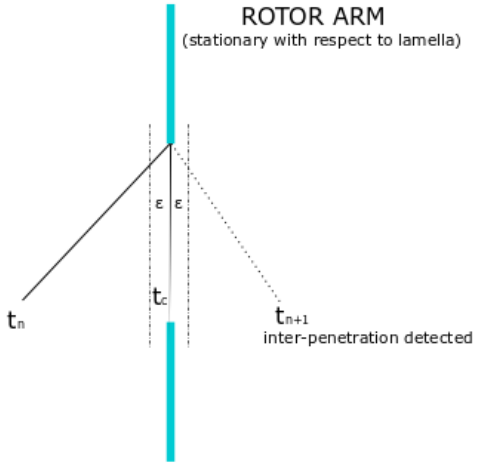

Figure 2.3: The position of the lamella is shown at different instants of time. The solid line shows position at t_n and dotted line shows position at t_{n+1}. ϵ represents the numerical tolerance up to which the bisection algorithm computes the time of collision t_c.

Consider that t_c lies between t_n and t_{n+1} as shown in the figure 2.3. Then, use a numerical root finding algorithm to determine t_c. The method is as follows:

- As t_c lies between t_n and t_{n+1}, it means that an inter-penetration is detected at time instant t_{n+1}. In this case, simply determine when the lamella has crossed the rotor arm as the inter-penetration condition.
- Inform the ODE solver to restart at time t_n and proceed with time step $\frac{\Delta t}{2}$. Note that, Δt is the time step between two instants. In this case, $\Delta t = t_{n+1} - t_n$.
- If no collision (or inter-penetration) is encountered that means, t_c lies between $t_n + \frac{\Delta t}{2}$ and t_{n+1}. And then, restart the ODE solver with the starting point as $t_n + \frac{\Delta t}{2}$ and time step $\frac{\Delta t}{4}$. Otherwise, t_c is less than $t_n + \frac{\Delta t}{2}$ and try to simulate from t_n to $t_n + \frac{\Delta t}{4}$.
- Repeating the above step, the collision time is computed with some suitable numerical tolerance ϵ.

With the time of impact (collision) computed, the next step is to determine the velocities post the collision and the contact forces. Before going into the details of this step, a small detour is taken to clarify a few concepts which will help to determine whether the contact between two bodies is colliding, resting or if there is no contact at all.

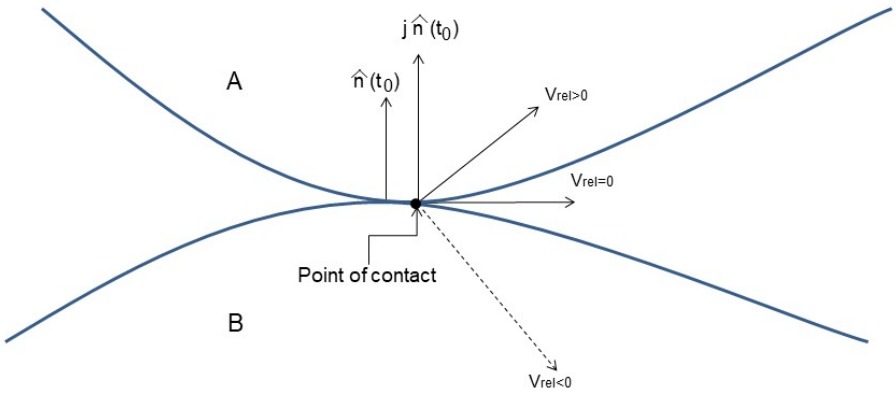

Figure 2.4: Depiction of the nomenclature used in describing the contacts between two bodies A and B.

Figure 2.4 shows two bodies (A and B) with different individual velocities at time instant (t_o). The vector ($\hat{\mathbf{n}}(t_o)$) is a unit normal vector acting from body B towards body A. Reference this as the positive direction. It is defined that $\mathbf{v_{rel}}$ is the relative velocity of body A with respect to body B at t_o. Then γ, as defined earlier in section 2.2.1, will now be equal to $\mathbf{v_{rel}}^T\hat{\mathbf{n}}$. The value of this γ determines the type of contact.

- $\gamma > 0$ (pointing outwards (towards A)) → The bodies are not contacting after t_o.
- $\gamma < 0$ (pointing inwards (towards B)) → The bodies are in colliding contact after t_o.
- $\gamma = 0$ → The bodies are in resting contact after t_o.

The vector $j\hat{\mathbf{n}}$ represents the impulse required to avoid the penetration of the bodies whose magnitude is j and direction given by the unit normal vector. If the bodies are in colliding contact it is necessary to compute the relative velocity post impact and the contact force responsible for the instantaneous change in the relative velocity. For computing the relative velocity post impact, Newton's impact law is applied. The equation states:

$$\gamma^+ = -\epsilon\gamma^-,$$

where γ^- is the relative velocity before impact and γ^+ is the relative velocity post impact. ϵ is the coefficient of restitution as before.

Next, it is necessary to determine the contact force. When two bodies collide there is an instantaneous change in the velocity. According to Newton's laws, this change is caused by an impulse. This impulse has to be determined so that the integration of the ODE can be continued after the collision instant with new initial velocities and external force conditions. Calculating the impulse involves a lengthy derivation which can be referred in [3].

In the case of the motion of the lamellas, the stoppers are stationary in a frame of reference fixed to the rotor. Applying the condition when one of the interacting bodies is fixed, the formulation for the impulse magnitude j as given in [3] is:

$$j = -M_a(1+\epsilon)\gamma^-,$$

where M_a is the mass of the body A.

To conclude this section, it is now known how to estimate the time of collision, calculate the changes in relative velocity and determine the underlying contact forces in the case of colliding contact. The next sub-section will deal with resting contact.

Resting Contact

It is clear that resting contact occurs when the relative velocities between the impacting bodies are zero. In numerical modeling, achieving this 'zero' is an ideal case and hence, it is approximated by considering that the relative velocity is within a certain numerical tolerance (e.g. $|\gamma| \leq \epsilon_r$). In the case of the motion of the lamella, this will occur when all the lamella oscillations are damped out and the lamella is stationary with respect to the rotor arm in the fully-closed position.

The resting contact problem for lamellas is very simple as it is a case of pure rotation with a single contact. Using the physical understanding of the lamella problem, the contact force during resting contact for the lamella is equal to the external force from water on the lamella. This provides the contact force during the resting contact situation. Note that, the contact force goes to zero as soon as the force from water changes direction (to open the lamella).

To sum it up, the lamella dynamics are evaluated using an event-driven approach where the collision between the lamella and the mechanical stopper is evaluated using colliding or resting contact based on the criteria discussed before. Thus, a clear numerical approach is developed to correctly evaluate the motion of the lamella/airfoil.

2.4. Governing equation of the motion of the lamella/airfoil

The collision dynamics to model the non-smooth motion of a single lamella/airfoil is described completely. It is now possible to describe the governing equation of *the non-smooth motion of an airfoil under periodic fluid flow*. This problem, as mentioned in chapter 1, is also the main problem addressed in this thesis.

As the motion of the airfoil is due to the fluid forces, the problem is a coupled Fluid-Structure-Interaction problem. The equations governing the fluid motion in FSI problems are still the Navier-Stokes equations. And for the structural part, (lamella) the equation is dependent on the motion of the lamella. Knowing that the lamella rotates with the hinge point at its leading edge, the equation of motion of the lamella is given by:

$$I\ddot{\theta}(t) = T_f + T_{ns}, \tag{2.7}$$

where $\theta(t)$ is the angle made by the lamella with the reference axis, I is the mass moment of inertia of the lamella/airfoil about its leading edge, T_f is the external torque on the lamella exerted by the flowing water, T_{ns} is the external torque because of the non-smooth contact force. The value of T_{ns} is determined by solving the linear complementarity problem (2.6) using the numerical approach discussed in section 2.3. The equation (2.7) is similar to the Newton-Euler equation (2.4). Note that T_f is the torque obtained from the force which is calculated by the integration of the pressure and viscous stresses on the airfoil.

The equation (2.7) will not be solved directly in this chapter. Initially, the non-smooth solution procedure described previously (2.3) is implemented for some model problem. The motion of the lamella is similar to many physical phenomena like a ball bouncing off the ground, a pendulum colliding with a wall, a spring-mass-damper with external excitation. But the spring-mass-damper system is considered here because it is known that the external fluid torque can be decomposed into three components-torque due to a stiffness force, torque due to a damping force, and the torque due to a force which is the remainder after subtracting the stiffness and damping components from the total fluid force. Hence, it is chosen as a model problem to implement the *non-smooth IVP solver* based on the numerical approach discussed in section 2.3. This is the reason why in the flow chart of chapter 1 the spring-mass-damper problem is given as one of the model problems.

2.5. Non-smooth dynamics for the spring-mass-damper problem

As discussed in the previous section, a spring-mass-damper problem is chosen to verify the non-smooth IVP solver. But there are certain restrictions on the parameters and the nature of the spring-mass-damper problem for it to correspond to the lamella/airfoil problem. For instance, the external excitation of the spring-mass-damper should be periodic. This is because of the fact that the lamella motion achieves periodicity after a large number of rotor rotations when all the transients have died out and a steady state is achieved. Hence, the solution of the spring-mass-damper should also have a periodic steady state solution which is achieved only when the external excitation is periodic. The model problem of a spring-mass-damper with periodic external excitation is described without considering any non-smooth forces.

2.5.1. Spring-mass-damper system with periodic external excitation

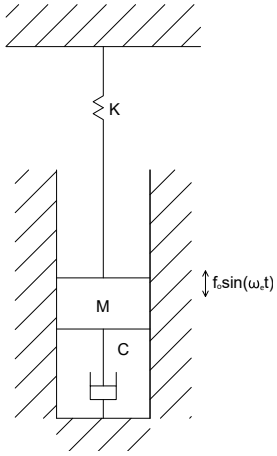

Figure 2.5: Schematic of a spring-mass-damper system which has periodic external excitation given by $f_0\sin(\omega_e t)$. The mass is denoted by M while the spring stiffness and damping constants by K and C respectively.

The following description is adapted from [5]. The governing equation of motion of the spring-mass-damper system as shown in figure 2.5 is:

$$m\ddot{y} + c\dot{y} + ky = f_0\sin(\omega_e t), \tag{2.8}$$

where m is the mass of the body under consideration, c is the viscous damping constant, k is the spring stiffness constant, f_0 is the magnitude of the external excitation (in this case force) and ω_e is the excitation frequency. The above equation can also be written as:

$$\ddot{y} + 2\zeta\omega_n\dot{y} + \omega_n^2 y = f_0\sin(\omega_e t), \tag{2.9}$$

where $\omega_n \left(= \sqrt{\frac{k}{m}}\right)$ is called the *natural frequency* and $\zeta \left(= \frac{c}{2m\omega_n}\right)$ is called *proportional damping* or *damping ratio*.

The value of ζ determines the type of system.

- $\zeta > 1 \rightarrow$ over-damped.
- $\zeta < 1 \rightarrow$ under-damped.
- $\zeta = 1 \rightarrow$ critically damped.

Another term is ω_d, called as the damped natural frequency and is given by $\omega_n\sqrt{1-\zeta^2}$. The exact solution of equation (2.8) is composed of two parts: the homogeneous (unsteady) and the particular (steady state) solution. The form of the solution in the case of under-damped system is given by:

$$y(t) = e^{-\zeta\omega_n t}(\tilde{C}\sin(\omega_d t + \phi)) + (A\cos(\omega_e t) + B\sin(\omega_e t)), \tag{2.10}$$

where the first part (exponential) of the solution is referred to as the homogeneous solution while the second part is the particular solution. Note that only under-damped system is considered here, but one can also use critically, or over-damped systems, in that case, the homogeneous solution will change. In this project, the steady state solutions are of importance, and hence, the homogeneous solutions can be of any form as long as they decay over a period of time. The type of external excitation determines the nature of the steady state solution. As the excitation is periodic, the steady state solution is also periodic, which is clear from the solution (2.10). The description of the spring-mass-damper system with periodic external excitation is complete. The next important aspect is devising a problem with some model parameters such that the system is under-damped and obtaining a solution for it.

Solutions with appropriate model parameters.

In this section, an exact solution to the equation (2.8) is computed using some initial conditions. This solution is compared to the one obtained from a standard IVP solver of MATLAB®, viz. ODE45. The model parameters are assumed to be:

$$m = 1; \quad k = 4; \quad c = 3; \quad f_0 = 5; \quad \omega_e = 4.$$

The value of $\zeta = 0.75$, which is less than 1 and hence, these model parameters satisfy the condition discussed previously. The equation (2.8) with above model parameters is given by:

$$\ddot{y} + 3\dot{y} + 4y = 5\sin(4t), \tag{2.11}$$

with initial conditions,

$$y(0) = -\frac{\pi}{3}; \quad \dot{y}(0) = 0. \tag{2.12}$$

The exact solution of (2.11) with initial conditions (2.12) is given by:

$$y(t) = e^{-\frac{3}{2}t}\left(\frac{-5}{9\omega_d}\sin(\omega_d t) + \left(-\frac{\pi}{3} + \frac{5}{24}\right)\cos(\omega_d t)\right) - \frac{5}{24}(\sin(4t) + \cos(4t)) \tag{2.13}$$

where $\omega_d = \sqrt{7}/2$. The first part of the above solution is the transient part while the second is the steady state part.

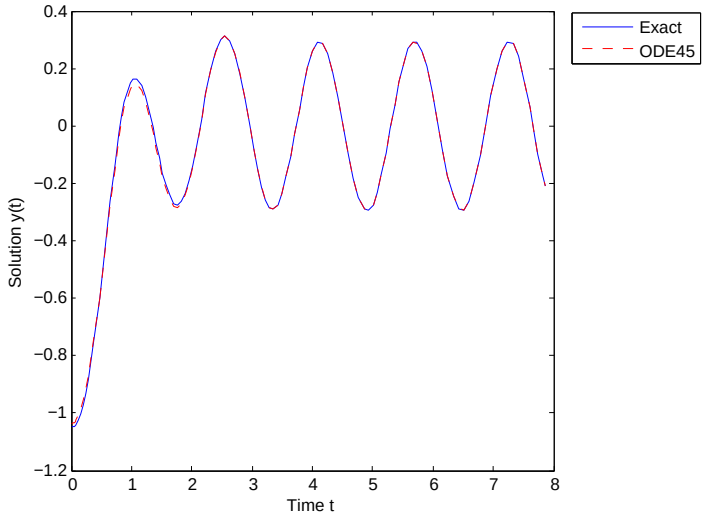

Figure 2.6: Solutions of the spring-mass-damper problem with periodic external excitation having model parameters m = 1; k = 4; c = 3; f_0 = 5; ω_e = 4 and initial conditions defined by (2.12). The numerical solution is obtained using the standard ODE45 solver of MATLAB® and compared to the exact solution (2.13) for time period $[0, 2.5\pi]$

From figure 2.6 it is clear that the solution from the IVP solver of MATLAB® (in this case ODE45) and the analytically computed solution are in agreement. It is also worthwhile to see when the transients die out and the solution reaches a steady state. For the above problem it can be determined analytically from the exact solution. But, in the case of *non-smooth* solutions, the exact solution is not known. Hence, it is important to have a numerical way of obtaining this point.

To determine this point, when the transients have died out, a standard is defined using the time period (T_{ss}) of the steady state solution. The aim is to determine after how many periods of (T_{ss}) do the initial transients die out and the steady state solution is reached. The idea is given below:

1. Compute the time period of the steady state solution. This is determined using the frequency of external excitation in the system and is given by $T_{ss} = \frac{2\pi}{\omega_e}$.
2. Divide the solution over the total time period $[0, T]$ into equal parts of size T_{ss}. Let $M = \lfloor \frac{T}{T_{ss}} \rfloor$ then T_i is the i^{th} element of the time period $[0, T]$ where $1 \leq i \leq M-1$.
3. Calculate error as the difference between the solution at two consecutive time periods. Mathematically written as:
$$err_i = ||\mathbf{Y_{i+1}} - \mathbf{Y_i}||_2, \qquad 1 \leq i \leq M-1, \tag{2.14}$$
where $\mathbf{Y_i}$ is a vector whose elements are values of the solution y(t) for the period T_i.
4. The first value of i for which $err_i = 10^{-10}$ gives the required number of periods of T_{ss} after which the steady state solution is reached.

For the solution shown in figure 2.10, it is seen that $T_{ss} = \frac{\pi}{2}$ and it requires 3 of these T_{ss} periods to obtain a steady state solution. Hence, a steady state solution is obtained after $t = 3\pi/2$. The model problem defined by (2.11) will be used for all the further analysis of the spring-mass-damper system. The next section deals with a non-smooth version of the same problem.

2.5.2. Restricted spring-mass-damper system with periodic external excitation

To formulate a non-smooth problem in the case of spring-mass-damper system consider that the motion of the mass is restricted at y = 0 by a 'restriction' as shown in figure 2.7.

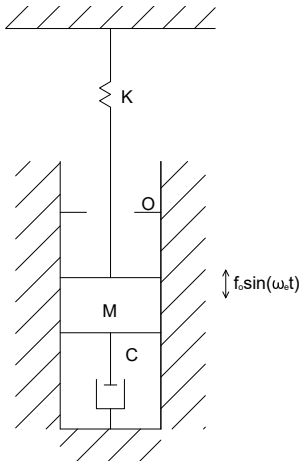

Figure 2.7: Schematic of a spring mass damper system with harmonic external excitation in which the mass is restricted to y = 0 position

The 'restriction' at y = 0 acts similar to the mechanical stopper from the lamella motion. As the mass strikes this 'restriction' there is an impact and the velocity of the mass changes suddenly. This leads to a discontinuity in the velocity curve of the mass, and hence, the problem falls under the realm of non-smooth dynamics. As there is an impact, one needs to apply unilateral constraints through a non-smooth contact force. The mathematical formulation for this spring-mass-damper problem with 'restriction' is given by:

$$m\ddot{y} + c\dot{y} + ky = f_0 \sin(\omega_e t) - \lambda(t), \tag{2.15}$$

where $\lambda(t)$ is the contact or collision force with positive in upwards direction. It was discussed in section 2.3 that this problem can be solved using the event-driven approach involving the concepts of colliding and resting contact. A *non-smooth IVP solver* is developed using this approach and implemented for the model problem (2.11) with 'restriction' at y = 0 and initial conditions $y(0) = 0; \quad \dot{y}(0) = -\frac{\pi}{3}$. The following is a detailed description of the non-smooth IVP solver:

1. Divide the total time period ($[0, T]$) into N small steps given by $t_i; (0 \leq i \leq N)$. For each time step compute the solution to the spring-mass-damper problem without the 'restriction' (2.8) with using the ODE45 solver. Note that the starting initial conditions should be such that the mass in figure 2.7 is below the 'restriction'.

2. Compare the computed solution at each step with the maximum value y can attain, given by y_{max}. This value is determined by the position of the 'restriction' (in this case $y_{max} = 0$). Stop the computation of the solution at the first instant when the mass crosses the 'restriction' limit (i.e. $y(t_m) \geq y_{max}$).

3. Apply interpolation or bisection algorithm between instants t_{m-1} and t_m to compute the time instant t_c, up to a certain tolerance (ϵ_r), when the mass collides with the 'restriction' i.e. $y(t_c) = y_{max} \pm \epsilon_r$.

4. At t_c, compute the velocity of the mass $\dot{y}(t)$ which is also the relative velocity of the mass with respect to the 'restriction' as the 'restriction' is fixed in space. Depending on the value of the velocity determine the type of contact and treat accordingly.

- **Colliding Contact**
  When the relative velocity $(\dot{y}(t)) \geq \epsilon_r$, it is a case of colliding contact. For the colliding contact, the 'restriction' applies an impulse to the mass which reverses the velocity of the mass. This impulse is given by: $J = -m(1+\epsilon)\dot{y}(t_c)$. The impulsive force is mathematically represented as $F_J = J\delta(t)$ where $\delta(t)$ is the Dirac function. From physics it is well known that the impulse leads to a sudden change in velocity of the mass and hence, instead of applying an impulsive force one can also change the velocity of the mass at t_c from $\dot{y}(t_c)$ to $\dot{y}_{new}(= -\epsilon\dot{y}(t_c))$, where ϵ is the coefficient of restitution between the impacting bodies. Thus, with the new initial conditions of $[y_{max}, \dot{y}_{new}]$ start computing the solution for $t_i; (m \leq i \leq N)$.

- **Resting Contact**
  When the relative velocity $(-\epsilon_r \leq \dot{y}(t_c) \leq \epsilon_r)$, then it is a case of resting contact. In this case, the mass is assumed to be resting on the 'restriction'. This implies that the contact force $\lambda(t)$ is equal and opposite to the external excitation of the spring-mass-damper system. And the contact force becomes zero as soon as the external excitation becomes negative, implying that the mass is starting to travel downwards. The mathematical representation is:

$$\lambda(t) = \begin{cases} -f_0 \sin(\omega_e t), & \text{if } (f_0 \sin(\omega_e t) \geq 0) \\ 0. & \text{otherwise} \end{cases}$$

5. Continue steps 2,3,4 until the N^{th} time step.

Depending on the total time T one can obtain a solution where the transient (or homogeneous) part of the solution eventually dies to leave behind only the steady state solution.

It is imperative to verify the implementation of this non-smooth IVP solver. For this verification, a non-smooth exact solution is computed for the problem (2.15). To compute the non-smooth exact solution, the exact solution for the smooth problem ((2.10)) is used along with the previously discussed event-driven approach. This leads to the development of an exact solution which is referred to as the *pseudo-exact solution*. This pseudo-exact solution will be used to compare the solution from the non-smooth IVP solver.

2.5.3. Pseudo-exact solution for the non-smooth spring-mass-damper problem

The exact solution of the spring-mass-damper problem without 'restriction' is given by (2.10). The solution can also be written as:

$$y(t) = e^{-\zeta\omega_n t}(\tilde{A}\sin(\omega_d t) + \tilde{B}\cos(\omega_d t)) + (A\cos(\omega_e t) + B\sin(\omega_e t)). \tag{2.16}$$

The coefficients $\tilde{A}$ andd $\tilde{B}$ are determined from the initial conditions for the problem while the coefficients A and B are determined from the inhomogeneous part. A pseudo-exact solution using the event-driven approach is calculated in the following manner:

1. The time $[0, T]$ is divided into N equal steps. With the given initial conditions compute the solution given by (2.16) for each of the time steps.
2. Stop the computation at the first instant the solution crosses the limit y_{max}. Referring to this instant as t_m, apply the bisection or interpolation algorithm to compute the instant t_c, where the solution $y(t_c) = y_{max} \pm \epsilon_r$.
3. From the exact solution, the derivative can be computed and hence the velocity is known. The velocity is used to determine the type of contact.

- **Colliding Contact**
  In colliding contact, calculate a new exact solution using a new set of initial conditions and the same expression (2.16). These initial conditions are a result of the impulse at the collision instant t_c. The initial conditions are given by $[y_{max}, -\epsilon\dot{y}(t_c)]$. Compute the solution for the time instants starting from t_c then t_m and further.

- **Resting Contact**
  For the resting contact case, when the contact force balances the external excitation, the equation (2.15) reduces to a homogeneous equation and the solution of which is only given by the exponential part of (2.16). The initial condition $[y_{max}, 0]$ will help determine the exact solution. This will lead to a new exact solution from t_c and further time steps. Remember, one needs to check at every instant if $f_0 \sin(\omega_e t_i); \quad i \geq m$ is greater than zero. If it is less than zero, then the contact force vanishes and have the steady state component along with a different unsteady component.

4. Go back to step 2 and proceed till the last step N.

Using the above procedure one can compute a pseudo-exact solution. As the point of impact is determined numerically this solution is referred to as the pseudo-exact solution. Nonetheless, the solution can be used as a best possible benchmark to compare the solution obtained from the non-smooth IVP solver.

2.5.4. Verification of the non-smooth IVP solver

Consider the same model parameters as (2.11) with initial conditions $y(0) = 0$ and $\dot{y}(0) = -\frac{\pi}{3}$. The motion of the mass is restricted at $y_{max} = 0$. The nonsmooth solution to this problem is obtained using the IVP solver and compared to the pseudo-exact solution.

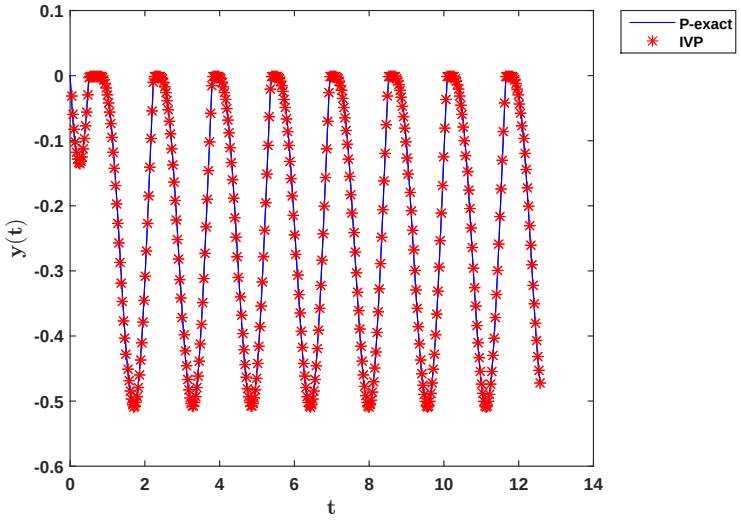

Figure 2.8: Non-smooth solution using the non-smooth IVP solver and pseudo-exact solution. The time period $[0, 4\pi]$ is divided into N = 2000 steps. The tolerance $\epsilon_r = 10^{-4}$.

Figure 2.8 shows that the solution obtained from the non-smooth IVP solver is in agreement with the pseudo-exact solution. Hence, the implementation of non-smooth IVP solver is verified.

Another aspect that can be studied is, after how many time periods of the steady state solution do the transients die. Using the same process as discussed in the previous section and computing the error using (2.14) it can be seen that for $T_{ss} = \frac{\pi}{2}$ the initial transients die after 3 time periods. The velocity curves are also plotted and can be visualized for confirming the implementation of the IVP solver.

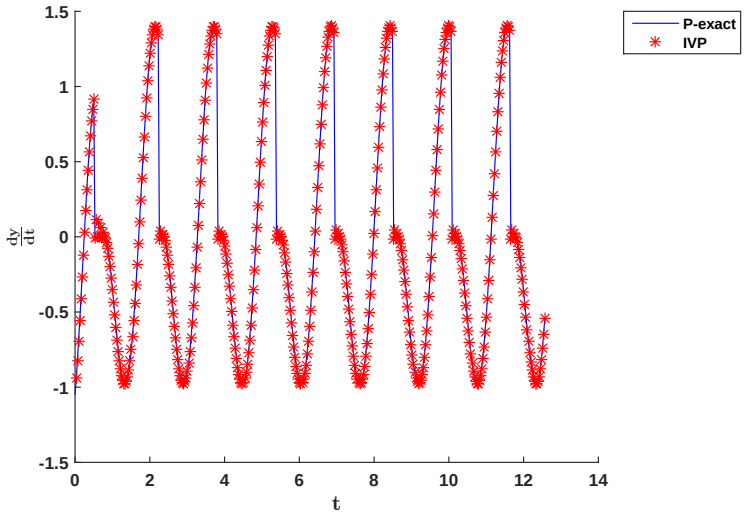

Figure 2.9: Non-smooth solution for the velocity ($\dot{y}(t)$) using the non-smooth IVP solver and the pseudo-exact solution. The time period $[0, 4\pi]$ is divided into N = 2000 steps. The tolerance $\epsilon_r = 10^4$.

Figure 2.9 shows that the respective solutions are in agreement. Also, a sharp discontinuity in velocity can be observed which is attributed to the fact that there is a sudden change in the velocity of the mass when it collides with the 'restriction'. It can be observed from figures 2.6 and 2.8 that the steady state solutions have different lower limits. The smooth solution has a lower limit of around -0.25 i.e. the mass travels up to that position. While the non-smooth solution has a lower limit of around -0.5. Thus, due to the collision with the 'restriction', the steady state solution is changed.

2.6. Conclusion

In this chapter, the governing equation of the non-smooth motion of the lamella/airfoil along with a numerical solution procedure for the non-smooth part, of this governing equation, is presented. A *non-smooth IVP solver* is developed using the standard ODE45 solver of MATLAB® to implement the numerical solution. The solver is described in detail for a model problem of the spring-mass-damper system with external periodic excitation. In this model problem, there is a 'restriction' to the motion of the mass, similar to the 'mechanical' stopper of the lamella, making the spring-mass-damper system to become non-smooth. The implementation of the solver is verified using a *pseudo-exact solution* developed for the non-smooth spring-mass-damper system. In this pseudo-exact solution, only the point of impact is determined numerically while the rest of the solution is determined analytically. Thus, the first research question of the project about modeling the non-smooth motion of the lamella/airfoil was addressed in this chapter.

3

HARMONIC BALANCE METHOD FOR SMOOTH PERIODIC SOLUTIONS

In this chapter the focus is on an efficient and faster method to obtain solutions for periodic fluid flows. Periodic fluid flows mostly occur in turbomachinery and rotary machines, and CFD analysis of such turbomachines has been done for decades. This prompts to investigate the type of method that should be used in these applications to obtain a steady state periodic flow solution. A thorough literature study was performed on the possible methods to obtain steady state periodic flow solutions. On the grounds of easy implementation in OpenFOAM® and efficient simulations, it was decided to use the harmonic balance method for the current application of flow around a lamella/airfoil. The harmonic balance method is presented in detail in the following section.

3.1. The harmonic balance method

The harmonic balance method has been used in the analysis of non-linear circuits for decades[6]. Its application to problems in fluid dynamics was first proposed by Hall, et al., [7] in 2001. This harmonic balance method was initially developed for modeling unsteady non-linear periodic flows in turbomachinery applications and airfoil pitching, but has now found many other applications. The main requirement for this method is the periodic nature of the flow. The fluid flow in the case of the motion of the lamella is governed by the Navier-Stokes equations. The Navier-Stokes equations when semi-discretized on a spatial grid provide a system of ODEs for the momentum equation. In the case of the continuity equation, the semi-discretization on a spatial grid provides only a set of algebraic equations. In the harmonic balance method, the system of ODEs obtained for the momentum equation are of importance and are represented as:

$$\rho \frac{d\mathbf{U}}{dt} + \hat{\mathbf{R}}(\mathbf{U}) = 0, \tag{3.1}$$

where $\hat{\mathbf{R}}(\mathbf{U})$ contains the semi-discretized forms of the convection, diffusion, and pressure gradient terms. More details on the Navier-Stokes will be given in chapter 5. In the current context, only the system of ODEs given by (3.1) is discussed. The basic concept of this method is to modify the time derivative term in equation (3.1) to a source term and thus, form a set of steady state equations. Then, the harmonic balance method solves a set of coupled steady state equations, where the temporal term is modeled as an additional source term and the periodicity is externally enforced. This is an advantage of the method as it is not required to simulate for many periods until periodicity

is achieved, like in the case when an initial boundary value problem formulation is used. The next section gives the derivation of the harmonic balance method.

3.1.1. Derivation of the harmonic balance method for a non-linear ODE

The expression (3.1) is, in fact, a non-linear system of ODEs. So, in this section a general non-linear ODE is used for the derivation of the harmonic balance implementation. Consider a general non-linear ODE having periodic steady state solutions:

$$\frac{du}{dt} + R(u) = 0, \tag{3.2}$$

where R(u(t)) is the non-linear function of u(t). As the solutions are periodic in nature, they are represented in Fourier series. This is one of the main aspects of the harmonic balance method. The description of the method given here is adapted from [8]. From the equation (3.2), the scalars u and R are represented as a truncated Fourier series in time.

Fourier series expansion of u(t) with n harmonics is given by:

$$u(t) = \sum_{j=0}^{n} \mathcal{U}_j e^{ij\omega t}, \tag{3.3}$$

and the expansion for R(t) reads:

$$R(t) = \sum_{j=0}^{n} \mathcal{R}_j e^{ij\omega t}, \tag{3.4}$$

where $\mathcal{U}_j$ and $\mathcal{R}_j$ are the Fourier coefficients given by:

$$\begin{array}{rcll} \mathcal{U}_j & = & u_{s_j} - iu_{c_j}; & j > 0; \\ \mathcal{U}_0 & = & u_0; & j = 0; \end{array} \tag{3.5}$$

$$\begin{array}{rcll} \mathcal{R}_j & = & R_{s_j} - iR_{c_j}; & j > 0; \\ \mathcal{R}_0 & = & R_0; & j = 0. \end{array} \tag{3.6}$$

Inserting equations (3.3) and (3.4) in equation (3.2):

$$\omega \sum_{j=0}^{n} ij\mathcal{U}_j e^{ij\omega t} + \sum_{j=0}^{n} \mathcal{R}_j e^{ij\omega t} = 0.$$

The above equation can be expanded using (3.5) and (3.6) in terms of the sine and cosine terms. The respective sine and cosine terms, when equated to zero, give the following set of equations:

$$\text{n equations for sine} \begin{cases} -1\omega u_{c_1} + R_{s_1} = 0; \\ -2\omega u_{c_2} + R_{s_2} = 0; \\ \vdots \\ -n\omega u_{c_n} + R_{s_n} = 0; \end{cases} \tag{3.7}$$

$$\text{center-} \quad R_0 = 0 \tag{3.8}$$

$$\text{n equations for cosine} \begin{cases} 1\omega u_{s_1} + R_{c_1} = 0; \\ 2\omega u_{s_2} + R_{c_2} = 0; \\ \vdots \\ n\omega u_{s_n} + R_{c_n} = 0; \end{cases} \tag{3.9}$$

A Fourier series expansion up to n harmonics involves 2n+1 terms and so, the above set of equations should also be 2n + 1. These equations can be represented in a matrix form as:

$$\omega \boldsymbol{A}\mathbf{u} + \mathbf{R} = 0, \tag{3.10}$$

where the matrices have the following form:

$$\boldsymbol{A} = \begin{bmatrix} & & & & 0 & -1 & 0 & \dots & 0 \\ & & & & 0 & \ddots & -2 & \ddots & \vdots \\ & & 0 & & \vdots & & \ddots & \ddots & 0 \\ & & & & \vdots & & & 0 & n \\ 0 & 0 & \dots & 0 & 0 & 0 & \dots & 0 & 0 \\ 1 & \ddots & & & \vdots & & & & \\ 0 & 2 & \ddots & & \vdots & & & & \\ \vdots & \ddots & \ddots & 0 & 0 & & 0 & & \\ 0 & \dots & 0 & n & 0 & & & & \end{bmatrix}; \quad \mathbf{u} = \begin{bmatrix} u_{s_1} \\ u_{s_2} \\ \vdots \\ u_{s_n} \\ u_0 \\ u_{c_1} \\ u_{c_2} \\ \vdots \\ u_{c_n} \end{bmatrix}; \quad \mathbf{R} = \begin{bmatrix} R_{s_1} \\ R_{s_2} \\ \vdots \\ R_{s_n} \\ R_0 \\ R_{c_1} \\ R_{c_2} \\ \vdots \\ R_{c_n} \end{bmatrix}. \tag{3.11}$$

Equation (3.10) gives a set of 2n + 1 equations which requires to store 2n + 1 Fourier coefficients for each flow variable (**u** and **R**). The variables have been transformed to a frequency domain. This was the proposition in the harmonic balance approach by Hall et. al [7]. Gopinath et. al [9] went further to have the variables in time domain.

Gopinath et. al, propose to reconstruct the Fourier coefficients of **u** and **R** from knowledge of the temporal behavior of u(t) and R(t) at 2n + 1 equally spaced points over one temporal period. Let $\hat{\mathbf{u}}$(t) and $\hat{\mathbf{R}}$(t) be the values at the 2n+1 points over the temporal period. A discrete Fourier transform operator (***E***) is required to connect these time domain and frequency domain vectors. The dimensions of this operator are: (2n + 1) × (2n + 1). The transformation is given by:

$$\mathbf{u} = \boldsymbol{E}\hat{\mathbf{u}}(\mathrm{t}),$$

where the operator ***E*** is:

$$\boldsymbol{E} = \frac{2}{2n+1} \begin{bmatrix} \sin(\omega t_1) & \sin(\omega t_2) & \sin(\omega t_3) & \dots & \sin(\omega t_{2n+1}) \\ \sin(2\omega t_1) & \sin(2\omega t_2) & \sin(2\omega t_3) & \dots & \sin(2\omega t_{2n+1}) \\ \vdots & \vdots & \vdots & & \vdots \\ \sin(n\omega t_1) & \sin(n\omega t_2) & \sin(n\omega t_3) & \dots & \sin(n\omega t_{2n+1}) \\ \frac{1}{2} & \frac{1}{2} & \frac{1}{2} & \dots & \frac{1}{2} \\ \cos(\omega t_1) & \cos(\omega t_2) & \cos(\omega t_3) & \dots & \cos(\omega t_{2n+1}) \\ \cos(2\omega t_1) & \cos(2\omega t_2) & \cos(2\omega t_3) & \dots & \cos(2\omega t_{2n+1}) \\ \vdots & \vdots & \vdots & & \vdots \\ \cos(n\omega t_1) & \cos(n\omega t_2) & \cos(n\omega t_3) & \dots & \cos(n\omega t_{2n+1}) \end{bmatrix}. \tag{3.12}$$

The matrix ***E*** is a discrete Fourier transform operator, thus, its inverse will be the inverse discrete Fourier transform operator. The inverse operator is given by:

$$\boldsymbol{E}^{-1} = \begin{bmatrix} \sin(\omega t_1) & \dots & \sin(n\omega t_1) & 1 & \cos(\omega t_1) & \dots & \cos(n\omega t_1) \\ \sin(\omega t_2) & \dots & \sin(n\omega t_2) & 1 & \cos(\omega t_2) & \dots & \cos(n\omega t_2) \\ \sin(\omega t_3) & \dots & \sin(n\omega t_3) & 1 & \cos(\omega t_3) & \dots & \cos(n\omega t_3) \\ \vdots & & \vdots & \vdots & \vdots & & \vdots \\ \vdots & & \vdots & \vdots & \vdots & & \vdots \\ \sin(\omega t_{2n+1}) & \dots & \sin(n\omega t_{2n+1}) & 1 & \cos(\omega t_{2n+1}) & \dots & \cos(n\omega t_{2n+1}) \end{bmatrix}. \tag{3.13}$$

This allows the representation of the equation (3.10) as:

$$\omega \boldsymbol{AE}\hat{\mathbf{u}}(\mathrm{t}) + \boldsymbol{E}\hat{\mathbf{R}}(\mathrm{t}) = 0.$$

Multiplying from left with the inverse transform operator ($\boldsymbol{E}^{-1}$):

$$\omega(\boldsymbol{E}^{-1}\boldsymbol{AE})\hat{\mathbf{u}} + \hat{\mathbf{R}} = 0. \tag{3.14}$$

Using the trigonometric sum identity ($\sin(\mathrm{A}+\mathrm{B}) = \sin(\mathrm{A})\cos(\mathrm{B}) + \cos(\mathrm{A})\sin(\mathrm{B})$), the expressions in operator ($\boldsymbol{E}^{-1}\boldsymbol{AE}$) are simplified. Ultimately, the operator has the following form:

$$\boldsymbol{E}^{-1}\boldsymbol{AE} = \frac{2}{2\mathrm{n}+1}\begin{bmatrix} 0 & \mathrm{B}_1 & \mathrm{B}_2 & \mathrm{B}_3 & \dots & \dots & \mathrm{B}_{2\mathrm{n}} \\ -\mathrm{B}_1 & 0 & \mathrm{B}_1 & \mathrm{B}_2 & \mathrm{B}_3 & & \mathrm{B}_{2\mathrm{n}-1} \\ -\mathrm{B}_2 & -\mathrm{B}_1 & 0 & \mathrm{B}_1 & \mathrm{B}_2 & & \vdots \\ -\mathrm{B}_3 & -\mathrm{B}_2 & -\mathrm{B}_1 & 0 & \mathrm{B}_1 & & \vdots \\ \vdots & & & & \ddots & & \mathrm{B}_2 \\ \vdots & & & & & \ddots & \mathrm{B}_1 \\ -\mathrm{B}_{2\mathrm{n}} & \dots & \dots & -\mathrm{B}_3 & -\mathrm{B}_2 & \mathrm{B}_1 & 0 \end{bmatrix}, \tag{3.15}$$

where $\mathrm{B}_\mathrm{j} = \sum_{\mathrm{k}=1}^{\mathrm{n}} \mathrm{k}\sin(\mathrm{k}\omega\mathrm{j}\mathrm{t}_1); \quad \mathrm{j} = \{1, \dots, 2\mathrm{n}\}$.

This completes the derivation of the harmonic balance method where the time derivative term in equation (3.2) has been transformed to look as a source term and a set of $2\mathrm{n}+1$ coupled steady state equations are required to be solved. The extra source term in (3.14) obtained from the time derivative term will be referred to as *temporal source term*. As R(t) is a function of u(t), the equation (3.14) is essentially of the form f(x(t)) = 0. And such an equation can be solved mathematically in many different ways depending on the nature of the terms in the equation.

Now, the second research question of this project is revisited. It requires developing an efficient approach for solving a coupled FSI problem. In this case, not only the fluid part but also structural part has periodicity which means the harmonic balance method should be applied to the governing equation of the motion of the lamella/airfoil (2.7) too. In the next section, the approaches to solve (3.14) are discussed.

3.2. Approaches to solve equation resulting from HB transformation

Consider a system of ODEs of the same form as equation (3.2):

$$\dot{\mathbf{y}} + \mathbf{R}(\mathbf{y}) = 0, \tag{3.16}$$

where R is any general non-linear function. The solution of this system of ODEs is assumed to be periodic. In the harmonic balance method, the temporal term is converted to a source term by using a Fourier series expansion of the solution up to n harmonics.

$$\dot{\mathbf{y}} + \mathbf{R}(\mathbf{y}) = 0 \quad \xRightarrow[\text{Transformation}]{\text{Harmonic Balance}} \quad \omega \boldsymbol{B}\hat{\mathbf{y}} + \hat{\mathbf{R}}(\hat{\mathbf{y}}) = 0, \tag{3.17}$$

where $\boldsymbol{B}$ is a simplified representation of the operator $\boldsymbol{E}^{-1}\boldsymbol{AE}$. It is a block matrix of size $(2\mathrm{n}+1) \times (2\mathrm{n}+1)$ with each block being a diagonal matrix of size determined by the length of the vector $\dot{\mathbf{y}}$. The

vectors $\hat{\mathbf{y}}$ and $\hat{\mathbf{R}}(\hat{\mathbf{y}})$ are composed of $2n+1$ sub-vectors whose length is determined by the number of elements in $\dot{\mathbf{y}}$. The form of vectors in the equation (3.17) is given by:

$$\hat{\mathbf{y}} = \begin{bmatrix} (\mathbf{y})^1 \\ (\mathbf{y})^2 \\ \vdots \\ (\mathbf{y})^{2n} \\ (\mathbf{y})^{2n+1} \end{bmatrix}; \quad \hat{\mathbf{R}}(\hat{\mathbf{y}}) = \begin{bmatrix} (\mathbf{R}(\mathbf{y}))^1 \\ (\mathbf{R}(\mathbf{y}))^2 \\ \vdots \\ (\mathbf{R}(\mathbf{y}))^{2n} \\ (\mathbf{R}(\mathbf{y}))^{2n+1} \end{bmatrix}. \tag{3.18}$$

The superscript indices on the elements of the vectors $\hat{\mathbf{y}}$ and $\hat{\mathbf{R}}$ represent the $2n+1$ time instants obtained from n harmonics. There are different approaches to solve equation (3.17), but the following approaches are considered here for their ease of application to existing solvers and possibility of coupling with fluid equations.

- **Sylvester's equation approach**

  This approach can be only used when R(y) is a linear function in y.

- **Pseudo-time stepping approach**

  This approach can be used when R(y) is non-linear function in y. It is also a preferred approach in this project, as it can be easily implemented in the OpenFOAM framework.

3.2.1. Sylvester's equation approach

In ODEs, when R(y) is a linear function of y the Sylvester's equation approach can be used. For example, consider a linear system of ODEs comprised of two ODEs. Then, $\mathbf{R(y)}$ can be written as $\boldsymbol{C}\mathbf{y}+\mathbf{f}(t)$, where $\mathbf{y}$ is a vector of length 2. The equation (3.17) for such an ODE is written as:

$$\omega \boldsymbol{B}\hat{\mathbf{y}} + \boldsymbol{C_I}\hat{\mathbf{y}} = -\hat{\mathbf{f}}(t), \tag{3.19}$$

where $\boldsymbol{C_I} = (\boldsymbol{I} \otimes \boldsymbol{C})$ and $\boldsymbol{I}$ is 2×2 identity matrix. As $\boldsymbol{C}$ is a constant matrix (R is linear), the above is a linear algebraic equation. One can also represent this as a Sylvester's equation in the following way:

$$\omega \boldsymbol{BY} + \boldsymbol{YC}^{\mathrm{T}} = -\boldsymbol{F} \tag{3.20}$$

where $\boldsymbol{B} \in \mathbb{R}^{2n+1 \times 2n+1}$, $\boldsymbol{Y} \in \mathbb{R}^{2n+1 \times 2}$ and $\boldsymbol{F} \in \mathbb{R}^{2n+1 \times 2}$. The matrix $\boldsymbol{B}$ has the size of individual blocks as 1×1. The other two matrices have the following form:

$$\boldsymbol{Y} = \begin{bmatrix} (y_1)^1 & (y_2)^1 \\ (y_1)^2 & (y_2)^2 \\ \vdots & \vdots \\ (y_1)^{2n} & (y_2)^{2n} \\ (y_1)^{2n+1} & (y_2)^{2n+1} \end{bmatrix}; \quad \boldsymbol{F} = \begin{bmatrix} (f_1)^1 & (f_2)^1 \\ (f_1)^2 & (f_2)^2 \\ \vdots & \vdots \\ (f_1)^{2n} & (f_2)^{2n} \\ (f_1)^{2n+1} & (f_2)^{2n+1} \end{bmatrix}. \tag{3.21}$$

It is clear that the approach can be implemented easily, when R is a linear function in y. For a non-linear R, the pseudo-time stepping approach is preferred as has been cited in [9][10]. This approach is discussed in the next sub-section.

3.2.2. Pseudo-time stepping approach

The equation (3.17) for pseudo-time stepping approach is written as:

$$\frac{\mathrm{d}\hat{\mathbf{y}}}{\mathrm{d}\tau} + \omega \boldsymbol{B}\hat{\mathbf{y}} + \hat{\mathbf{R}}(\hat{\mathbf{y}}) = 0, \tag{3.22}$$

where τ represents pseudo-time. Approaching a steady state in pseudo-time, it is known that $\frac{\mathrm{d}\hat{\mathbf{y}}}{\mathrm{d}\tau} = 0$. Thus, the steady state solution of equation (3.22) will provide the solution to equation (3.17). The form of the operators in the above equation suggests that the equations are coupled. And hence, the harmonic balance approach reduces to solving coupled steady state problems with the pseudo-time stepping approach.

The equation (3.22) can be solved using an implicit method for which one step is written as:

$$\frac{\hat{\mathbf{y}}^{k+1} - \hat{\mathbf{y}}^{k}}{\Delta\tau} = -[\omega \boldsymbol{B}\hat{\mathbf{y}} + \hat{\mathbf{R}}(\hat{\mathbf{y}}^{k+1})]. \tag{3.23}$$

Note that the time level for the source term $\omega \boldsymbol{B}\hat{\mathbf{y}}$ is not yet defined as it can be explicit or implicit[10]. As $\hat{\mathbf{R}}(\hat{\mathbf{y}}^{k+1})$ is unknown, it is linearized using a Taylor Series expansion. The linearization is given by:

$$\hat{\mathbf{R}}(\hat{\mathbf{y}}^{k+1}) = \hat{\mathbf{R}}(\hat{\mathbf{y}}^{k}) + \boldsymbol{J_R}\Delta\hat{\mathbf{y}} + \mathcal{O}(\Delta\hat{\mathbf{y}}^2), \tag{3.24}$$

where $\boldsymbol{J_R}$ is the Jacobian matrix of the residual vector. The block diagonal form of the Jacobian matrix is given by:

$$\boldsymbol{J_R} = \begin{bmatrix} \left.\frac{\partial \mathbf{R}}{\partial \mathbf{y}}\right|_{t_1} & 0 & \dots & 0 \\ 0 & \left.\frac{\partial \mathbf{R}}{\partial \mathbf{y}}\right|_{t_2} & \ddots & \vdots \\ \vdots & & \ddots & 0 \\ 0 & \dots & 0 & \left.\frac{\partial \mathbf{R}}{\partial \mathbf{y}}\right|_{t_{2n+1}} \end{bmatrix}. \tag{3.25}$$

Further, based on the time level of the temporal source term, the pseudo-time stepping approach can be further divided in to two sub-approaches:

- Explicit treatment of temporal source term
  - Fully uncoupled approach
  - Partially uncoupled approach
- Implicit treatment of temporal source term
  - Fully coupled approach

The above sub-approaches are now discussed in detail.

Explicit treatment of the temporal source term

If the temporal source term is treated explicitly the equation (3.23) using the linearization (3.24) and explicit source term can be written as:

$$\left[\frac{\boldsymbol{I}}{\Delta\tau}+\boldsymbol{J_R}\right]\Delta\hat{\mathbf{y}}=-\hat{\mathbf{R}}^{\mathrm{k}}-\omega\boldsymbol{B}\hat{\mathbf{y}}^{\mathrm{k}}. \tag{3.26}$$

The left-hand side operator is an augmented matrix composed of the Jacobian at the k^{th} snapshot and an identity matrix divided by the pseudo-time step size. The form of the operator is also block diagonal like the Jacobian operator. The block diagonal nature of the matrix makes it possible to solve independently for each of the $2\mathrm{n}+1$ time instants. These will be referred to as $2\mathrm{n}+1$ *sub-problems* where the coupling exists through the explicit temporal source term operator. Thus, the sub-problem for each level can be written as:

$$\left[\frac{\boldsymbol{I}}{\Delta\tau}+\boldsymbol{J_R}\right]_{\mathrm{i}}\Delta[\hat{\mathbf{y}}]_{\mathrm{i}}=-\left[\hat{\mathbf{R}}^{\mathrm{k}}\right]_{\mathrm{i}}-\left[\omega\boldsymbol{B}\hat{\mathbf{y}}^{\mathrm{k}}\right]_{\mathrm{i}}, \tag{3.27}$$

where the subscript index i denotes the i^{th} sub-problem of the $2\mathrm{n}+1$ sub-problems. As the sub-problems need to be solved, existing options like the SIMPLE algorithms or steady state ODE solvers can be easily implemented. Hence, for non-linear problems the pseudo-time stepping approach is preferred. There are two possible ways to solve (3.26) to convergence which further lead to two more sub-approaches.

Fully uncoupled approach

In this approach, for each global iteration step k, all the $2\mathrm{n}+1$ sub-problems are solved to convergence individually in pseudo-time keeping the temporal source term constant. Then, for the next global iteration step $\mathrm{k}+1$ the temporal source term and the $\hat{\mathbf{R}}$ term are updated and again all the individual sub-problems are solved to convergence in pseudo-time. In such a manner, the solution converges when the global error of $\hat{\mathbf{y}}$ between two iteration steps is within a certain specified limit. The name *fully uncoupled* comes from the fact that for each sub-problem the temporal source term is constant in one global iteration implying that the sub-problems are independent of each other for that global iteration step.

Partially uncoupled approach

In this approach, for each global iteration step k, each sub-problem is solved to convergence in a sequential way. The solution of each sub-problem is used to update the temporal source term for the next sub-problem. This continues for all the $2\mathrm{n}+1$ sub-problems and then, the solution is updated for the next global iteration step $\mathrm{k}+1$. In this approach too, the solution converges when the global error between successive iteration steps is within a certain limit. The name *partially uncoupled* is given because for each sub-problem the temporal source term changes in one global iteration step. Thus, the solution for one sub-problem is coupled with the solution for other sub-problem in the same iteration step.

To elucidate further, one can relate to the difference between block Gauss-Jacobi and block Gauss-Seidel iterative methods. The fully-uncoupled approach can be thought of as Gauss-Jacobi while the partially-uncoupled approach relates to Gauss-Seidel.

Implicit treatment of the temporal source term

The next option is to treat the temporal source term $\omega \boldsymbol{B}\hat{\mathbf{y}}$ implicitly. This would require linearization of the source term. As the operator $\boldsymbol{B}$ is linear, the source term linearization is the following:

$$\boldsymbol{B}\hat{\mathbf{y}}^{k+1} = \boldsymbol{B}\hat{\mathbf{y}}^{k} + \boldsymbol{B}\Delta\hat{\mathbf{y}}. \tag{3.28}$$

Substituting equations (3.24) and (3.28) in (3.23):

$$\left[\frac{\boldsymbol{I}}{\Delta\tau} + \boldsymbol{J_R}\right]\Delta\hat{\mathbf{y}} + \omega\boldsymbol{B}\Delta\hat{\mathbf{y}} = -\hat{\mathbf{R}}^{k} - \omega\boldsymbol{B}\hat{\mathbf{y}}^{k}; \tag{3.29}$$

In this case the operator, on the left hand side is not block diagonal but instead it is a full matrix of the form:

$$\boldsymbol{B_{imp}} = \left[\frac{\boldsymbol{I}}{\Delta\tau} + \boldsymbol{J_R} + \boldsymbol{B}\right] = \begin{bmatrix} \mathrm{E}_1 & \mathrm{H}_{1,2} & \mathrm{H}_{1,3} & \dots & \mathrm{H}_{1,2n+1} \\ \mathrm{H}_{2,1} & \mathrm{E}_2 & & \dots & \vdots \\ \vdots & & \ddots & & \vdots \\ & & & \mathrm{E}_{2n} & \mathrm{H}_{2n,2n+1} \\ \mathrm{H}_{2n+1,1} & \dots & \dots & & \mathrm{E}_{2n+1} \end{bmatrix}; \tag{3.30}$$

where $\mathrm{E_i} = \frac{\boldsymbol{I}}{\Delta\tau_\mathrm{i}} + \boldsymbol{J_{R_{i,i}}}$ and $\mathrm{H_{i,j}} = \omega\boldsymbol{B}_\mathrm{i,j}$. The full matrix implies that the solutions for all the sub-problems are coupled. This approach is, thus, referred to as a *fully coupled approach*. The description of the harmonic balance method is complete.

Comparison to select the appropriate approach

As the Navier-Stokes equations are non-linear, Sylvester's equation approach is not suitable for this project. Now it remains to see which of the pseudo-time stepping approaches are suitable.

It can be seen from the form of the matrices (3.30) and (3.25) that, the approach with an implicit treatment of the source term has higher memory storage requirements and is more complex to solve than the explicit one. In the explicit approach, the operator being block diagonal, individual *sub-problems* can be solved. But, the implicit approach will provide faster global convergence than the explicit. Hence, a tradeoff between faster convergence, complexity and memory requirements is necessary to select the best method.

But another prime requirement of this project is the ease of implementation of the method in the existing framework of OpenFOAM. As individual sub-problems are solved to steady state in the explicit approach, and OpenFOAM already having steady state Navier-Stokes equation solvers (SIMPLE) the *explicit treatment of source term* approach is selected in this project. But, it still remains to see whether it should be fully uncoupled or partially uncoupled approach out of the two explicit approaches. This will be clear in the next section when the spring-mass-damper problem is solved.

3.3. Application of the HB method to model problems

The harmonic balance method was implemented using the various approaches discussed in the previous section. The implementations are verified against the available exact solutions. This section presents all the model problems which were solved with the harmonic balance method.

3.3.1. System of Linear ODEs

A linear system of ODEs was developed whose exact solution is periodic and can be easily calculated analytically. Such a system of ODEs is:

$$\dot{\mathbf{x}}(t) = \boldsymbol{Q}\mathbf{x} + \mathbf{f}(t); \quad \mathbf{x}(0) = \mathbf{x}(T); \quad \mathbf{x} = [0 \quad 1]^T; \tag{3.31}$$

where $\boldsymbol{Q} = \begin{bmatrix} 0 & -\omega \\ \omega & 0 \end{bmatrix}$ and $\mathbf{f}(t) = \begin{bmatrix} \sin(\omega t) \\ \cos(\omega t) \end{bmatrix}$. As the matrix $\boldsymbol{Q}$ has purely imaginary eigen values, the system is known to have a periodic solution. The exact solution of the above system is computed to be:

$$\begin{bmatrix} x_1(t) \\ x_2(t) \end{bmatrix} = \begin{bmatrix} -\sin(\omega t) \\ \cos(\omega t) + \frac{1}{\omega}(\sin(\omega t)) \end{bmatrix} \tag{3.32}$$

Applying harmonic balance method to equation (3.31), gives:

$$\omega(\boldsymbol{E}^{-1}\boldsymbol{A}\boldsymbol{E})\hat{\boldsymbol{X}} + \hat{\boldsymbol{R}} = 0.$$

where, for n harmonics:

$$\boldsymbol{E}^{-1}\boldsymbol{A}\boldsymbol{E} \in \mathbb{R}^{2n+1\times 2n+1}; \quad \hat{\boldsymbol{X}} \in \mathbb{R}^{2n+1\times 2}; \quad \hat{\boldsymbol{R}}^{2n+1\times 2},$$

with

$$\hat{\boldsymbol{R}} = -\hat{\boldsymbol{X}}\boldsymbol{Q}^T - \boldsymbol{F}.$$

The final system is:

$$\omega(\boldsymbol{E}^{-1}\boldsymbol{A}\boldsymbol{E})\hat{\boldsymbol{X}} - \hat{\boldsymbol{X}}\boldsymbol{Q}^T = \boldsymbol{F}.$$

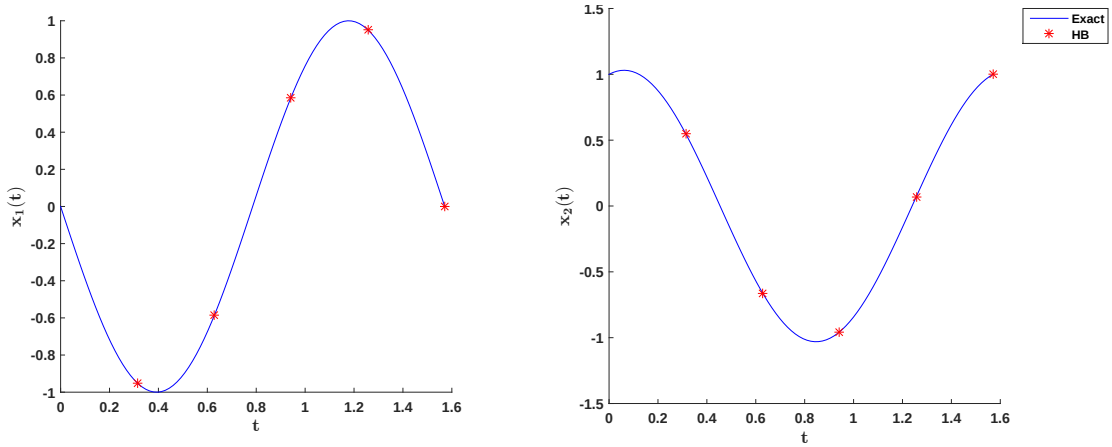

(a) Solution for x_1

(b) Solution for x_2

Figure 3.1: Solution for (3.31) obtained using the Sylvester's approach of the harmonic balance method for n = 2 harmonics and $\omega = 4$. The exact solution is represented in blue and given by the expression (3.32)

Figure 3.1 shows the solution obtained for the equation (3.31) using Sylvester's equation approach of the harmonic balance method. As n = 2 harmonics were used for the computation, the solution is obtained for 2n + 1 = 5 time instants. It is seen that the solution time instants lie on the curve of the exact solution. This is because R(y) is linear and the harmonic balance method is expected to provide the exact coefficients of the Fourier modes for such equations. The accuracy of the above solution is determined by the solver used for Sylvester's equation. For the current implementation, the standard Sylvester equation solver[11] available in MATLAB® was used.

3.3.2. System of non-linear ODEs

The harmonic balance method is also capable of solving a system of non-linear ODEs which have a periodic solution. To implement the method, a van der Pol's equation was used. The van der Pol's equation is given by:

$$\ddot{y} - \mu(1-y^2)\dot{y} + y = 0. \tag{3.33}$$

This equation appears in the study of circuits containing vacuum tubes. The equation is a second order non-linear ODE. As the harmonic balance method is applied to a system of first order ODEs, the equation (3.33) is reduced to a system of first order non-linear ODEs using order reduction.

Such a system of first order ODEs for the van der Pol's equation is:

$$\begin{bmatrix} \dot{y}_1(t) \\ \dot{y}_2(t) \end{bmatrix} = \begin{bmatrix} y_2 \\ (1-y_1^2)y_2 - y_1 \end{bmatrix}, \tag{3.34}$$

where μ is considered to be 1. The $\mathbf{R}(\mathbf{y})$ term in this equation is $\begin{bmatrix} y_2 \\ (1-y_1^2)y_2 - y_1 \end{bmatrix}$. This term is non-linear and hence, the Jacobian ($\boldsymbol{J_R}$), needed for iterations in pseudo time is not constant. To elucidate further, consider the harmonic balance formulation with an explicit version of the temporal source term for equation (3.34).

$$\left[\frac{\boldsymbol{I}}{\Delta\tau} + \boldsymbol{J_R}\right]\Delta\hat{\mathbf{y}} = \begin{bmatrix} y_2 \\ (1-y_1^2)y_2 - y_1 \end{bmatrix}^k - \omega \boldsymbol{B}\hat{\mathbf{y}}^k, \tag{3.35}$$

where $\boldsymbol{J_R} = \begin{bmatrix} 0 & -1 \\ 1-2y_1y_2 & y_1^2-1 \end{bmatrix}^k$. Note that the Jacobian is at k^{th} iteration level. A MATLAB solver was developed to implement this and provide a steady state solution.

It is known that this equation has no exact or analytical solution and can only be solved numerically. The MATLAB® ODE45 solver provides a numerical solution for this equation which is used, here, as a benchmark.

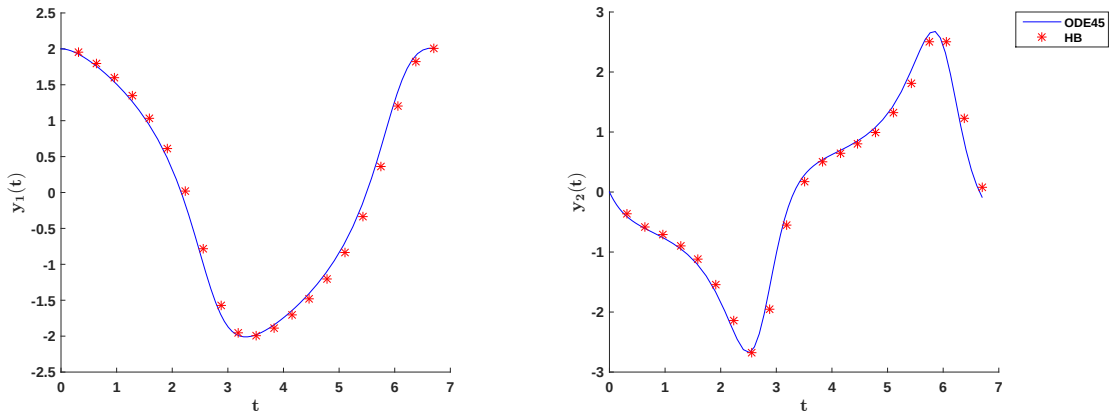

(a) Solution for y_1

(b) Solution for y_2

Figure 3.2: Solution for (3.34) obtained using the fully coupled approach of the harmonic balance method. n = 10 harmonics were used for computing the solution. The convergence criteria for the global iterations was set to 10^{-5}. In blue, the solution computed from the ODE45 solver of MATLAB® is plotted.

Figure 3.2 shows the steady state solution for the van der Pol's equation (3.34) obtained using the fully coupled implementation from the pseudo-time stepping approach of the harmonic balance method on MATLAB®. This solution is compared to the ODE45 solution. Note that the ODE45 provides both the transient and steady state solution, in the above figure 3.2 the transient part is truncated and only the steady state part is shown for one single period. It is seen that the harmonic balance solution, obtained for $2n+1 = 21$ time instants, doesn't lie exactly on the curve as observed previously with the linear ODE system. This is because the global iterations have been set a convergence limit of 10^{-5} in a L^2 norm which reduces the accuracy of the computed solution. Also, there are numerical errors in the approximation of the Jacobian for R as it is a non-linear function. Additionally, the solution being highly non-linear it might require more harmonics for the harmonic balance approach for providing the exact solution (in this case ODE45 solution).

3.3.3. Spring-mass-damper

It is necessary to implement this method for the motion of the lamella/airfoil, but as previously discussed the spring-mass-damper system has a similar model equation as the governing equation of the motion of the lamella/airfoil. So, in this section, the spring-mass-damper system is solved with the harmonic balance method. Here, the harmonic balance method is only implemented for the smooth problem i.e. the spring-mass-damper system without any restriction. The analysis for the non-smooth problem will be dealt with in the next chapter.

The same model problem defined by equation (2.11) is treated here. This equation is a linear second order ODE which is reduced to a system of first order ODEs using order reduction. The form of this system of first order ODEs is:

$$\begin{bmatrix} \dot{y} \\ \ddot{y} \end{bmatrix} = \begin{bmatrix} 0 & 1 \\ -\frac{k}{m} & -\frac{c}{m} \end{bmatrix} \begin{bmatrix} y \\ \dot{y}. \end{bmatrix} + \begin{bmatrix} 0 \\ f_0 \sin(\omega_e t) \end{bmatrix}, \tag{3.36}$$

where $m = 1$, $k = 4$, $c = 3$, $f_0 = 5$ and $\omega_e = 4$. For ease of representation the above equation is written as:

$$\dot{\mathbf{y}} = \boldsymbol{A}\mathbf{y} + \mathbf{f}(t). \tag{3.37}$$

The harmonic balance transformation on the above equation gives:

$$\dot{\mathbf{y}} - \boldsymbol{A}\mathbf{y} - \mathbf{f}(t) = 0 \quad \xrightarrow[\text{Transformation}]{\text{Harmonic Balance}} \quad \omega \boldsymbol{B}\hat{\mathbf{y}} - \boldsymbol{A_I}\hat{\mathbf{y}} - \hat{\mathbf{f}}(t) = 0. \tag{3.38}$$

where B is the same operator as (3.15), $\boldsymbol{A_I} = (\boldsymbol{I} \otimes \boldsymbol{A})$. The equation (3.36) has R(t) as a linear function, hence, Sylvester's approach can be applied to the equation. The steady state solution to (3.36) is obtained using all the approaches discussed for the harmonic balance method.

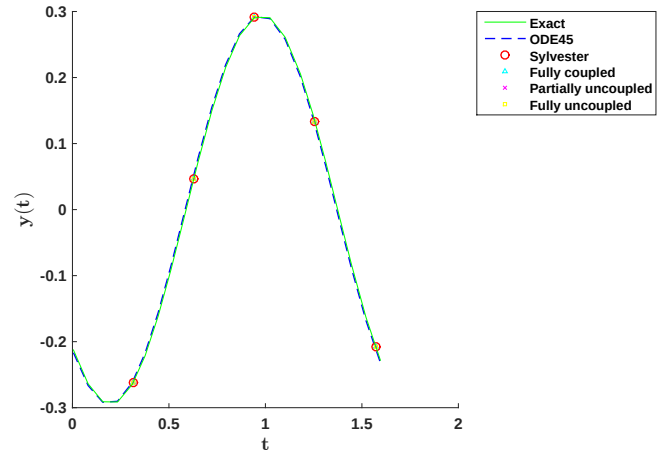

(a) Solution for y(t)

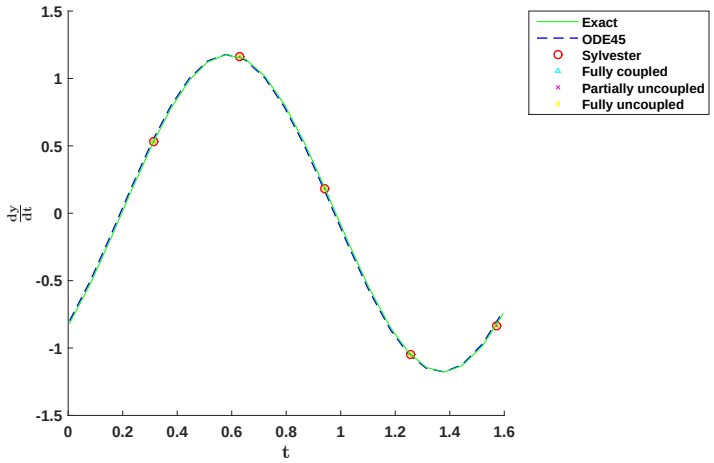

(b) Solution for $\frac{dy}{dt}$

Figure 3.3: Steady state solutions of the spring-mass-damper problem (2.11) computed using the various harmonic balance approaches for n = 2 harmonics. The time period is $\frac{\pi}{2}$. All the sub-problems in the fully uncoupled and partially uncoupled approaches are run to an accuracy of 10^{-8}. The global iterations in all the three pseudo-time approaches are set a convergence limit of 10^{-6}.

Figure 3.3 shows the steady state solutions for the equation (3.36) using the harmonic balance method for its various solution approaches. The exact and ODE45 solutions are also shown. The exact solution, in this case, is the particular solution from (2.13), while for the ODE45 solution, the steady state part is obtained by truncating the transient solution and only considering the steady state component for a single period. Note that, as expected all the approaches indeed give the same harmonic balance solution. This completes the verification of the implementation of the various harmonic balance approaches.

Problems with fully uncoupled approach

It was seen that increasing the number of harmonics to 4 or more, the fully uncoupled approach did not converge in its global iterations. This creates a limit to the applicability of that approach to various problems and hence, will not be considered. Thus, the *partially uncoupled* approach will be used further, in this project.

The exact reason for the fully uncoupled approach to not converge for higher harmonics is not completely understood, but it is thought that the convergence issues in this approach can be linked to the issues with block Gauss-Jacobi. Nonetheless, it requires more research on that front and is not the focus of this project.

Another aspect that is analyzed here, is the number of global iterations that are required to obtain a converged solution.

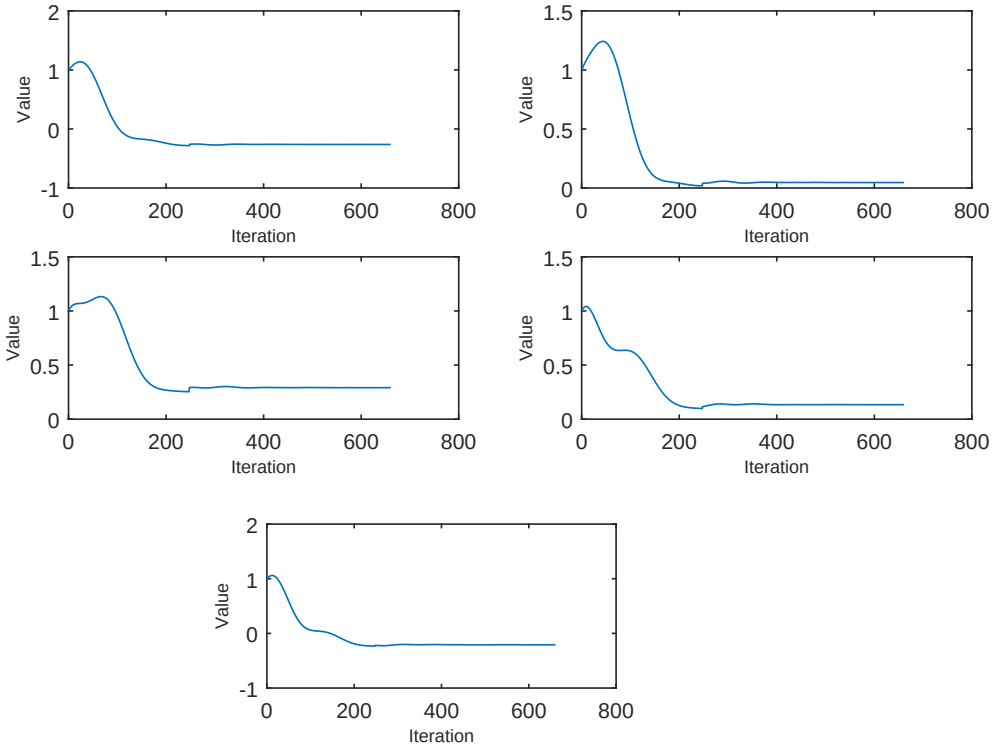

Figure 3.4: Global convergence results for the $2n+1 (=5)$ sub-problems in the case of the partially uncoupled approach

Figure 3.4, on the right, shows the number of iterations required to obtain global convergence in the case of the partially uncoupled approach. It is seen that as much as 659 iterations are required for convergence. But it can be concluded from the results that one can obtain a solution of lower accuracy by running around 250 iterations. Hence, the speed can be increased further by lowering the convergence limit of the global iterations. Only partially uncoupled approach is treated here, because this approach is the one that will be used to solve the problem of airfoil motion.

3.3.4. Partial Differential Equation

In all the previous problems the model equations were ODEs. In this project, the harmonic balance method is also applied to the Navier-Stokes equations which are, in fact, partial differential equations. In this section, as a more representative problem to the Navier-Stokes equations, the harmonic balance method is implemented for the convection-diffusion equation.

Consider an unsteady convection-diffusion equation for temperature (T) in 1D bar:

$$\frac{\partial T}{\partial t} + u\frac{\partial T}{\partial x} - \epsilon\frac{\partial^2 T}{\partial x^2} = q, \quad 0 \le x \le 1, \quad 0 \le t \le 1, \tag{3.39}$$

where u is the (prescribed) velocity and ϵ is the diffusion coefficient.

The method of manufactured solutions is used to verify the implementation of the harmonic balance method for such a convection diffusion equation. Assume a periodic solution of the equation (3.39) as:

$$\mathrm{T}(\mathrm{t},\mathrm{x}) = \cos(\beta(\mathrm{x}-\mathrm{ut})), \tag{3.40}$$

where β is any constant. With the knowledge of the exact solution, the scalar source term q is determined from the equation (3.39). The value of the source term is:

$$\mathrm{q}(\mathrm{t},\mathrm{x}) = \beta^2\epsilon\cos(\beta(\mathrm{x}-\mathrm{ut})).$$

The boundary conditions are determined as:

$$\begin{aligned}\mathrm{T}(\mathrm{t},0) &= \cos(\beta\mathrm{ut}),\\ \mathrm{T}(\mathrm{t},1) &= \cos(\beta(1-\mathrm{ut})).\end{aligned}$$

And the initial condition is $\mathrm{T}(0,\mathrm{x}) = \cos(\beta\mathrm{x})$. The complete boundary value problem with initial condition for a 1D bar having a periodic solution is now given by:

$$\begin{aligned}\frac{\partial \mathrm{T}}{\partial \mathrm{t}} + \mathrm{u}\frac{\partial \mathrm{T}}{\partial \mathrm{x}} - \epsilon\frac{\partial^2 \mathrm{T}}{\partial \mathrm{x}^2} &= \beta^2\epsilon\cos(\beta(\mathrm{x}-\mathrm{ut})), \quad 0 \le \mathrm{x} \le 1, \quad 0 \le \mathrm{t} \le 1,\\ \mathrm{T}(\mathrm{t},0) &= \cos(\beta\mathrm{ut}),\\ \mathrm{T}(\mathrm{t},1) &= \cos(\beta(1-\mathrm{ut})),\\ \mathrm{T}(0,\mathrm{x}) &= \cos(\beta\mathrm{x}).\end{aligned} \tag{3.41}$$

The problem (3.41) is initially solved using the harmonic balance approach implemented in MATLAB. The first step is a spatial discretization using finite volume techniques. A central difference approximation on a cell centered grid for the problem (3.41) gives an ODE of the form:

$$\frac{\mathrm{d}\tilde{\mathbf{T}}}{\mathrm{dt}} + \boldsymbol{L_h}\tilde{\mathbf{T}} = \tilde{\mathbf{q}} \tag{3.42}$$

where

$$\boldsymbol{L_h} = \begin{bmatrix} (\frac{\mathrm{u}}{2\mathrm{h}}+\frac{3\epsilon}{\mathrm{h}^2}) & (\frac{\mathrm{u}}{2\mathrm{h}}-\frac{\epsilon}{\mathrm{h}^2}) & 0 & \dots & 0\\ -(\frac{\mathrm{u}}{2\mathrm{h}}+\frac{\epsilon}{\mathrm{h}^2}) & (\frac{2\epsilon}{\mathrm{h}^2}) & (\frac{\mathrm{u}}{2\mathrm{h}}-\frac{\epsilon}{\mathrm{h}^2}) & & \vdots\\ 0 & \ddots & \ddots & \ddots & 0\\ \vdots & & -(\frac{\mathrm{u}}{2\mathrm{h}}+\frac{\epsilon}{\mathrm{h}^2}) & (\frac{2\epsilon}{\mathrm{h}}) & (\frac{\mathrm{u}}{2\mathrm{h}}-\frac{\epsilon}{\mathrm{h}^2})\\ 0 & \dots & 0 & -(\frac{\mathrm{u}}{2\mathrm{h}}+\frac{\epsilon}{\mathrm{h}^2}) & (\frac{3\epsilon}{\mathrm{h}^2}-\frac{\mathrm{u}}{2\mathrm{h}}) \end{bmatrix}, \quad \tilde{\mathbf{T}} = \begin{bmatrix} \mathrm{T}_1\\ \mathrm{T}_2\\ \vdots\\ \vdots\\ \mathrm{T}_{\mathrm{J}-1}\\ \mathrm{T}_{\mathrm{J}} \end{bmatrix},$$

$$\tilde{\mathbf{q}} = \begin{bmatrix} \mathrm{q}_1 + (\frac{\mathrm{u}}{\mathrm{h}}+\frac{2\epsilon}{\mathrm{h}^2})\cos(\beta\mathrm{ut})\\ \mathrm{q}_2\\ \vdots\\ \vdots\\ \mathrm{q}_{\mathrm{J}-1}\\ \mathrm{q}_{\mathrm{J}} + (\frac{2\epsilon}{\mathrm{h}^2}-\frac{\mathrm{u}}{\mathrm{h}})\cos(\beta(1-\mathrm{ut})) \end{bmatrix}.$$

The equation (3.42) due to constant coefficients of $\boldsymbol{L_h}$ is also a system of linear ODEs. It can be solved using the same implementation as done previously for (3.31).

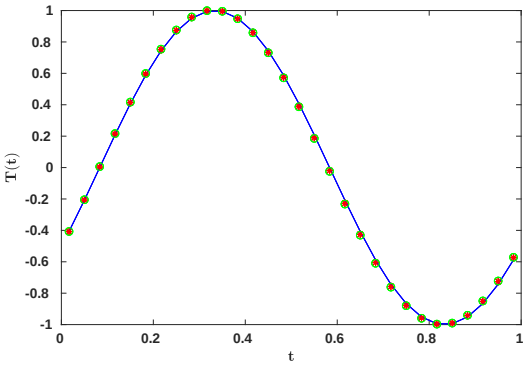

(a) Solution T(t) for t = $\frac{1}{3}$

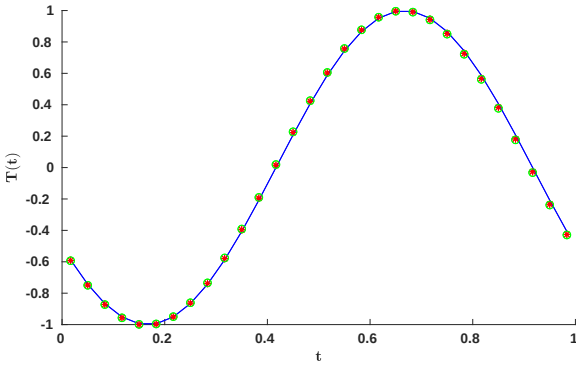

(b) Solution T(t) for t = $\frac{2}{3}$

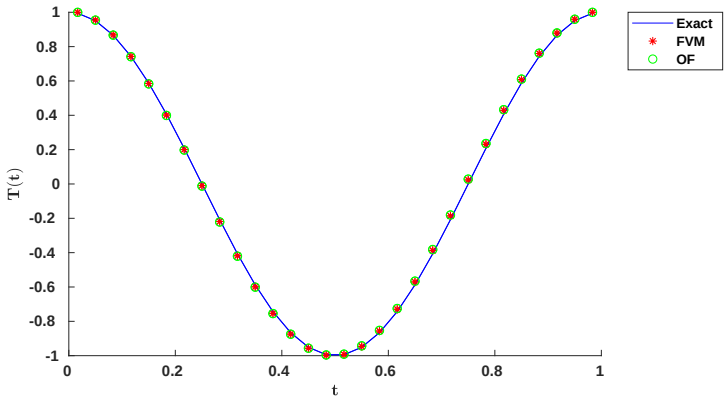

(c) Solution T(t) for t = 1

Figure 3.5: Solutions for the convection diffusion problem (3.41) obtained using the finite volume implementation (3.42) (red asterisks) and the OpenFOAM solver (green circles). The solutions are compared to the exact solution (3.40). The model parameters are u = 1, ϵ = 0.0025.

Figure 3.5 shows the solution for the convection diffusion problem (3.41) with u = 1 and ϵ = 0.0025 obtained using a finite volume implementation given by (3.42) applied to a harmonic balance implementation for a system of linear ODEs given in section 3.3.1. Note that the solution is in agreement with the exact solution (3.40). This verifies the implementation of the harmonic balance method for a partial differential equation.

It is imperative to solve using OpenFOAM as this will be a first step towards solving the Navier-Stokes equations using OpenFOAM. Hence, at this point, a solver has been developed in OpenFOAM to obtain a steady state solution to the equation (3.41). Figure 3.5 depicts the solution obtained using the *scalarTransportFoam* solver of OpenFoam. Thus, it can be said that the OpenFOAM based solver for the convection-diffusion equation using the harmonic balance method provides the correct solution.

For the harmonic balance implementation, the scalarTransportFoam solver was modified by removing the time derivative term and adding a source term. As expected the finite volume method base solution is in agreement with the OpenFOAM based solution as OpenFOAM solvers also incorporate the same finite volume schemes. Also, the framework of OpenFOAM is such that it treats the problem as a 3D one, so the 1D problem above is no simplification in terms of OpenFOAM implementation.

3.4. Conclusion

In this chapter, a harmonic balance method to solve for steady state solutions of flow and structural problems having periodic solutions was discussed. This is a faster and efficient method to obtain a steady state solutions of such problems as has been noted in [7][9]. The method is implemented for a variety of model problems as given in schematic 1.11. Thus, a part of the second research question was addressed here but there is still the problem of: How to solve the non-smooth problem using the harmonic balance method? The next chapter presents approaches for obtaining non-smooth solutions using the harmonic balance method.

4

HARMONIC BALANCE METHOD FOR *non-smooth* PERIODIC SOLUTION

In chapter 2, the numerical solution procedure to solve for the motion of the lamella was presented. A non-smooth IVP solver was developed and tested for a model problem of a spring-mass-damper system with 'restriction'. While in chapter 3, a harmonic balance method was introduced to obtain faster and efficient solutions to problems with smooth periodic solutions. It now remains to see how to solve for the motion of the lamella/airfoil, which is a non-smooth periodic motion, using the harmonic balance method. The problem of solving the equations of non-smooth dynamics which have periodic solutions with the harmonic balance method is very nascent and not much research has been done on this front. The chapter discusses three approaches to solve this problem, out of which, two are newly developed as a part of this thesis research. The third approach is from the solution methods used in the of analysis of vibro-impact-oscillators.

The real lamella/airfoil problem is not solved here. Instead the model problem of spring-mass-damper with a 'restriction' is solved as the solution for this problem is already known (2.5.3).

4.1. Model problem of spring-mass-damper with 'restriction'

As discussed in chapter 2, the spring-mass-damper system with a 'restriction' is modeled by equations which have the same form as the governing equation of the motion of the lamella (2.7).

Figure 4.1 shows the same spring-mass-damper system presented in chapter 2. Again, the mathematical formulation of this spring-mass-damper problem with 'restriction' is given by:

$$m\ddot{y} + c\dot{y} + ky = f_0 \sin(\omega_e t) - \lambda(t), \tag{4.1}$$

where $\lambda(t)$ is the contact or collision force with positive in the upwards direction. The pseudo-exact and non-smooth IVP solver solutions are already available for this problem with model parameters as given in (2.11).

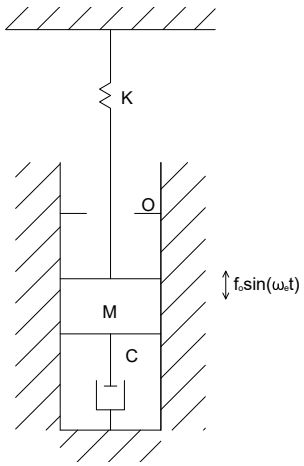

Figure 4.1: Schematic of a spring mass damper system with harmonic external excitation in which the mass is restricted to y = 0 position

4.2. Approaches to solve non-smooth motion using HB method

In solving the non-smooth problem using the harmonic balance method it is clear that one needs to obtain the contact force. This contact force is modeled as a differential inclusion problem whose solution is obtained by a numerical solution procedure as described in chapter 2. It is not possible to apply that procedure directly to the harmonic balance method as the procedure requires an IVP solver. However, the harmonic balance method is not a time integration method. In fact, it directly provides the steady state solution. Nonetheless, it is necessary to obtain this contact force, and the approaches discussed in this section give different ways of obtaining this force directly or indirectly.

4.2.1. Using a non-smooth dynamical force

It is clear that one needs to obtain the contact force and then the harmonic balance implementation is quite straightforward. As it is a single contact problem, the contact force is formulated in such a way that it takes care of the entire non-smooth solution procedure discussed previously. This force is referred to as *non-smooth dynamical force*.

Mathematical modeling of the non-smooth dynamical force

Colliding contact can be modeled by using an impulsive force. The general formulation of an impulsive force is given by:

$$\int_{0^-}^{0^+} F^I(t)dt = J, \tag{4.2}$$

where J is the impulse which acts at t = 0[12]. The force F^I is a distribution of the form of a Dirac function. Thus, the value of F^I is zero everywhere except at t = 0, where (in some heuristic sense) its value is infinity. The integral of F^I over the real line is finite and equal to the impulse J. Knowing that the Dirac function ($\delta(t)$) has the following property[12][13]:

$$\int_{0^-}^{0^+} \delta(t)dt = 1,$$

Setting $F^I(t) = J\delta(t)$ satisfies equation (4.2)[12]. Now the colliding contact force at the instant of collision t_c can be written as:

$$F_{col}(t-t_c) = J\delta(t-t_c), \tag{4.3}$$

where $J = -m(1+\epsilon)\dot{y}(t)$.

The resting contact can be modeled as:

$$F_{res} = H(f_0 \sin(\omega_e t))(-f_0 \sin(\omega_e t)),$$

where $H(f_0 \sin(\omega_e t))$ is the *Heaviside function* which assumes a value of one when $f_0 \sin(\omega_e t) > 0$. The total external force function that gives the contact force $\lambda(t)$ in (4.1) is given by:

$$\begin{aligned} & \Lambda_{hb}(y,\dot{y},t) = H(y-y_{max})\left(H(\dot{y}-\epsilon_r)F_{col} + (1-H(\dot{y}-\epsilon_r))F_{res}\right), \\ \text{where} \quad & F_{col} = -m(1+\epsilon)\dot{y}(t)\delta\left((y-y_{max})\frac{1}{\dot{y}_{ref}}\right), \\ & F_{res} = H(f_0 \sin(\omega_e t))(-f_0 \sin(\omega_e t)). \end{aligned} \tag{4.4}$$

Note that the argument of the force from the colliding contact (4.3) is scaled on the reasoning that at $y = y_{max}$, $t = t_c$. Thus, circumventing the determination of time of collision t_c.

The force function $\lambda_{hb}(y,\dot{y},t)$ completely defines the non-smooth dynamics in action for the case of spring-mass-damper problem with 'restriction' at y_{max}. The Heaviside function $H(y-y_{max})$ necessitates the application of this force at the instant when the mass crosses the 'restriction', this also implies that the time of collision t_c is known implicitly. The second Heaviside function $H(\dot{y}-\epsilon_r)$ makes it possible to switch between the colliding and resting contact forces. The modified form of equation (4.1) is given by:

$$m\ddot{y} + c\dot{y} + ky = f_0 \sin(\omega_e t) + \Lambda_{hb}(y,\dot{y},t). \tag{4.5}$$

But in the current form, this cannot be used to obtain a solution using the harmonic balance method as the Heaviside function is highly non-linear, and the Dirac function is actually a distribution. One can regularize the Heaviside and Dirac functions and use these to formulate an approximation for $\Lambda_{hb}(y,\dot{y},t)$. This approximated force can then be used in the harmonic balance method. Note that the regularisation of the Dirac function changes the force from colliding contact to a function (from a distribution), and hence, it can be incorporated in the harmonic balance formulation.

Heaviside Function

The Heaviside function is given by:

$$H(x-\alpha) = \begin{cases} 1, & x \geq \alpha \\ 0. & x < \alpha \end{cases} \tag{4.6}$$

The Heaviside function is also called as a step function. This function can be approximated using many possible standard functions, one such approximation is the *logistic function* which will be used in this context as it is a continuous function whose derivative can be computed easily. The reason to compute the derivative will be clear in the later part of this section. Thus, the Heaviside function approximation using the logistic function is given by:

$$H(x-\alpha) \approx \frac{1}{2} + \frac{1}{2}\tanh(\kappa(x-\alpha)) = \frac{1}{1+e^{-2\kappa(x-\alpha)}}. \tag{4.7}$$

The values of κ decide the quality of approximation. It is known that $\kappa \geq 25$ can be considered the best possible approximation[13]. Another important aspect of Heaviside function is that it is dimensionless.

Dirac function

The Dirac function (also known as Delta function) can also be approximated in many possible ways. The choice of approximation is again based on the fact that the first derivative exists and can be easily computed.

The regularized form of the Dirac function that will be used here is given by:

$$\delta(x-\alpha) \approx \begin{cases} \frac{1}{2\eta}\left(1+\cos\left(\frac{\pi(x-\alpha)}{\eta}\right)\right), & \text{if } (\alpha-\eta) < x < (\alpha+\eta), \\ 0 & \text{otherwise,} \end{cases} \tag{4.8}$$

where η is the parameter that determines the size of the width of the smearing[13]. Note that the function value of the peak at $x = \alpha$ will be $1/\eta$. The form of the above approximation indicates that outside the range of η around $x = \alpha$ the Dirac function value is zero. The Dirac function always has an inverse dimension of its argument.

Using the regularized forms (4.7) and (4.8) of the Heaviside and Dirac functions respectively, the approximation of the non-smooth dynamical force of (4.4) is obtained. The equation (4.5) is now given by:

$$m\ddot{y} + c\dot{y} + ky = f_0 \sin(\omega_e t) + \Lambda_{ns}(y, \dot{y}, t). \tag{4.9}$$

where $\Lambda_{ns}(y, \dot{y}, t)$ is the approximation of $\Lambda_{hb}(y, \dot{y}, t)$ given in (4.4). This approximation of the non-smooth force is highly non-linear. One can use a similar approach discussed previously for the van der Pol's equation to solve the equation (4.9). The resulting steady state solution is expected to be an approximation of the pseudo-exact solution. It remains to be seen why are the derivatives of the Heaviside and Dirac functions so important. For this purpose, (3.26) applied to (4.9) is studied.

$$\left[\frac{\boldsymbol{I}}{\Delta\tau} + \boldsymbol{J_R}\right] \Delta\hat{\mathbf{y}} = \boldsymbol{A_I}\hat{\mathbf{y}}^k + \hat{\mathbf{f}}(t) + \left(\hat{\boldsymbol{\Lambda}}_{ns}(y, \dot{y}, t)\right)^k - \omega \boldsymbol{B}\hat{\mathbf{y}}^k, \tag{4.10}$$

The Jacobian $\boldsymbol{J_R}$ is obtained from the derivative of the $\hat{\mathbf{R}}(y, \dot{y}, t)$ term. In this case,

$$\hat{\mathbf{R}}(y, \dot{y}, t) = \boldsymbol{A_I}\hat{\mathbf{y}}^k + \hat{\mathbf{f}}(t) + \hat{\boldsymbol{\Lambda}}_{ns}(y, \dot{y}, t).$$

Hence one has to also differentiate the non-linear non-smooth force $\Lambda_{ns}(y, \dot{y}, t)$ to obtain the Jacobian. This explains the need to differentiate the regularized form of Heaviside and Dirac functions. Refer appendix A for details of the approximate non-smooth force ($\hat{\Lambda}_{ns}(y, \dot{y}, t)$) and its Jacobian.

Another important aspect is that the Dirac function in the force from the colliding contact is in terms of y_{max}. This force when approximated using the regularization (4.8) is given by:

$$F_{col} = -m(1+\epsilon)\dot{y}(t)\frac{1}{2\eta}\left(1+\cos\left(\frac{\pi(y-y_{max})}{\eta\dot{y}_{ref}}\right)\right). \tag{4.11}$$

Now, it is clear from the use of the Heaviside function $H(y-y_{max})$ that the above force is acting only when $y = y_{max}$. Thus, when $y = y_{max}$ the approximation (4.11) hints that cosine assumes a value of 1, and the Dirac function value is $\frac{1}{\eta}$. Although, this is an approximation because the Heaviside function is regularised and hence, y is not equal to y_{max} but lies in close tolerance to y_{max}. This close tolerance can mean that cosine ≈ 1. Such an approximation of the Dirac function is used in the current implementation. However, one can also continue using (4.11) with some appropriate $\dot{y}_{ref}$ but in that case, the derivative of the cosine function should be used in the Jacobian in (4.10). An appropriate value of $\dot{y}_{ref}$ can be obtained from the smooth analytical solution.

Simulations are performed to compare the solutions obtained using this method. The model equation for computing the solution using this method is:

$$\ddot{y} + 3\dot{y} + 4y = 5\sin(4t) + \Lambda_{ns}(y, \dot{y}, t). \tag{4.12}$$

This model equation is similar to the one considered for the solution in figure 2.8.

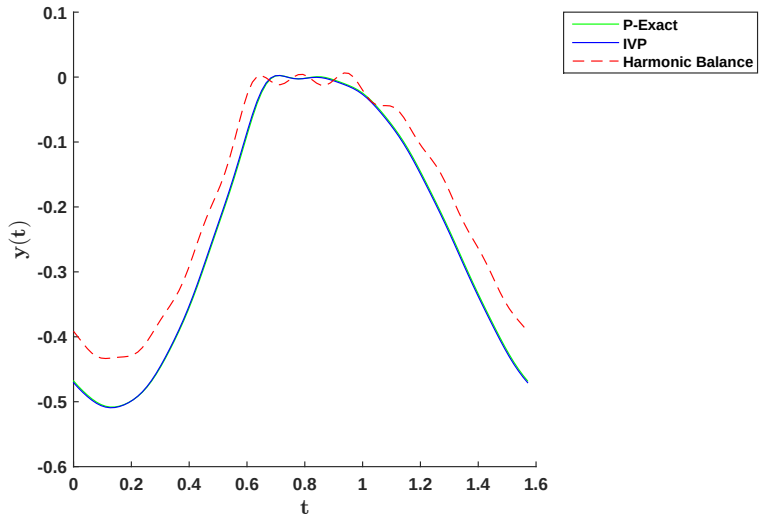

(a) Solution y(t)

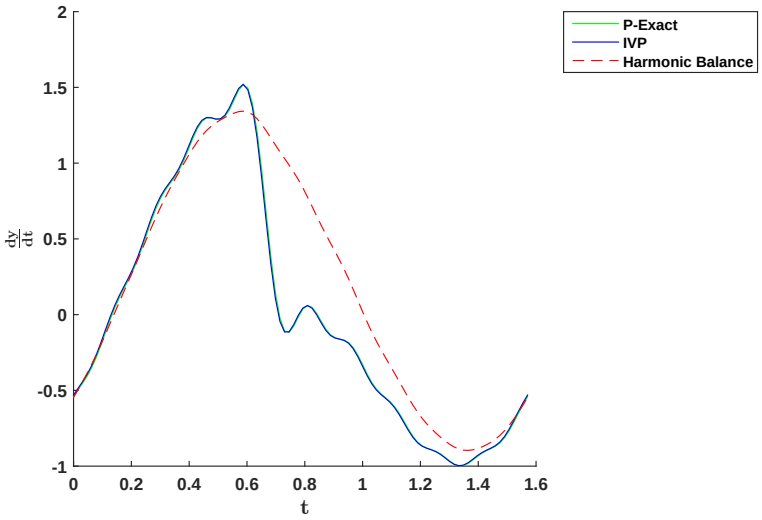

(b) Solution $\frac{dy}{dt}$

Figure 4.2: The signal constructed from the harmonic balance solution to (4.12) using n = 10 harmonics with the non-smooth dynamical force approach. The green and blue curves are the projection of the pseudo-exact and non-smooth IVP solver solutions on the n = 10 harmonic space. The parameters used are: $\epsilon = 0.1$, $\epsilon_r = 10^{-3}$, $\kappa = 500$, $\eta = 0.025$. The convergence limit for global iterations was set to 10^{-9}.

Figure 4.2 depicts the solution to the non-smooth problem of the spring-mass-damper system with 'restriction' using the approach of non-smooth dynamical force up to a convergence accuracy of 10^{-9} for the global iterations. As expected this solution is an approximation of the exact solution because of the approximations involved in the Heaviside and Dirac functions. Also, the harmonic balance method uses a Fourier series approximation of the non-smooth force. This leads to a further approximation in the solution. The percentage error of the above computed solution is 10%. One should note that the error varies on changing the parameters in the approximations of Heaviside and Dirac functions, viz-a-viz κ and η. Hence, another drawback of this approach is that one needs to know the optimum values of κ and η to obtain a good solution. Nonetheless, this method provides a faster but less accurate solution to the non-smooth problem and hence, can used where solutions of lower accuracy are acceptable.

4.2.2. *Modified non-smooth solver* in pseudo-time

In this method, the partially-uncoupled approach is used wherein each sub-problem is converged in pseudo-time with the contact force obtained using a modified version of the non-smooth IVP solver. The equation (3.26) is modified by adding an extra force which is motivated from the non-smooth dynamical force discussed in the previous section. The modified equation is given by:

$$\left[\frac{\boldsymbol{I}}{\Delta\tau}+\boldsymbol{J_R}\right]\Delta\hat{\mathbf{y}}=\boldsymbol{A_I}\hat{\mathbf{y}}^{k}+\hat{\mathbf{f}}(t)-\omega\boldsymbol{B}\hat{\mathbf{y}}^{k}+\hat{\mathbf{F}}_{\mathbf{ns}}, \tag{4.13}$$

where $\hat{\mathbf{F}}_{\mathbf{ns}}$ is the contact force. The superscript index k denotes the global iteration number. The value of this force will depend on the type of contact (colliding/resting/no contact). The above equation is obtained when one reduces the spring-mass-damper equation to first order and performs a harmonic balance transformation as seen in (3.36). The equation which is transformed to obtain (4.13) is the following:

$$m\ddot{y}+c\dot{y}+ky=f_0\sin(\omega_e t)+F_{ns}. \tag{4.14}$$

The equation (4.13) comprises of individual sub-problems which will be solved in pseudo-time. To elucidate further, one such sub-problem for a global iteration (k) has the following form:

$$\left[\frac{\boldsymbol{I}}{\Delta\tau}+\boldsymbol{J}\right](\Delta\mathbf{y})_i=\boldsymbol{A}(\mathbf{y})_i+\mathbf{f}(t_i)-(\omega\boldsymbol{B}\hat{\mathbf{y}})_i+(\mathbf{F_{ns}})_i. \tag{4.15}$$

where J is the Jacobian whose value is $-\boldsymbol{A}$. The non-smooth force $(\mathbf{F_{ns}})_i$ is a vector of the form $[0 \quad (F_{ns})_i]^T$. Similarly, $\mathbf{f}(t_i) = [0 \quad f_0\sin(\omega_e t_i)]^T$. The vector $(\mathbf{y})_i$ has two components-position and velocity. The subscript i denotes the i^{th} sub-problem of the total $2n+1$ sub-problems. For each sub-problem, the force $(F_{ns})_i$ is computed for every iteration in pseudo-time using a modified version of the non-smooth IVP solver referred to as *modified non-smooth solver*. Let s denotes the iteration number in pseudo-time. The solver description is as given below.

Modified non-smooth solver for computing $(F_{ns})_i$

This solver is motivated from the original non-smooth solver. The detailed steps are as follows:

1. Check if the position component from the previous iteration (s) is greater than the limit. Mathematically given as: $(y_1^s)_i \geq y_{max}$, where $(y_1^s)_i$ is the position component of $(\mathbf{y}^s)_i$. Similarly, $(y_2^s)_i$ is the velocity component. If the value is indeed greater, there is a collision (in pseudo-time) and proceed to step (2). Else, $(F_{ns})_i = 0$ and exit the modified non-smooth solver.

2. If $(y_2^{k+1})_i > \epsilon_r$, there is a colliding contact. In this case,

$$(F_{ns})_i = J\delta\left((y-y_{max})\frac{1}{\dot{y}_{ref}}\right),$$

   where J is the impulse given by $-m(1+\epsilon)(y_2^s)_i$ and $\delta\left((y-y_{max})\frac{1}{\dot{y}_{ref}}\right)$ is the Dirac function.

3. If $|(y_2^{k+1})_i| < \epsilon_r$, it is a resting contact. This case is same as the original non-smooth solver. Hence,

$$(F_{ns})_i = \begin{cases} -f_0\sin(\omega_e t_i), & \text{if } (f_0\sin(\omega_e t_i) \geq 0) \\ 0. & \text{otherwise} \end{cases}$$

The modified non-smooth solver provides with $(F_{ns})_i$ which is used to compute $(\mathbf{y}^{s+1})_i$ using equation (4.15). In such a manner, each sub-problem is converged for global iteration k. This process is further continued similar to a partially uncoupled approach until convergence.

The difference between the original non-smooth IVP solver and the modified non-smooth solver is the modeling of the colliding contact case. In the original non-smooth IVP solver, instead of an external impulse, the velocity is changed using Newton's impact law for a colliding case. This is because, in a single contact case, the change in velocity is equivalent to an impulsive force. In the original solver, as it incorporates an IVP solver the change in velocity was easily done by changing the initial conditions, but in the harmonic balance method, there is no such possibility. The harmonic balance method depends solely on the form of the equation. Thus, the modified non-smooth solver models the colliding case as an impulsive force as opposed to the change in velocity in the original solver.

It remains to see how to compute the impulsive force from the colliding contact. For this purpose, the Dirac function is regularized as done in the previous section and further approximation as noted in (4.11) is used. Hence, $\delta\left((y-y_{max})\frac{1}{\dot{y}_{ref}}\right) \approx \frac{1}{\eta}$ is used. The final formulation of impulsive force is:

$$(F_{ns})_i = -m(1+\epsilon)(y_2^s)_i\left(\frac{1}{\eta}\right). \tag{4.16}$$

Using (4.16) and the procedure described before, a harmonic balance solver is developed and the solution is compared to the solution obtained from the non-smooth IVP solver and pseudo-exact solution. Note that, the non-smooth force, in this approach, is calculated in pseudo-time.

It should be understood that the harmonic balance approach will not provide an exact solution to the non-smooth problem as it is a highly non-linear problem and a large number of harmonics will be needed to visualize the exact solution. But, increasing the number of harmonics will significantly increase the computation time. Hence, a tradeoff between the accuracy and the computation time is necessary to obtain a good approximation solution to the non-smooth motion using harmonic balance method. The harmonic balance solution is now computed with using a solver which incorporates the method described above.

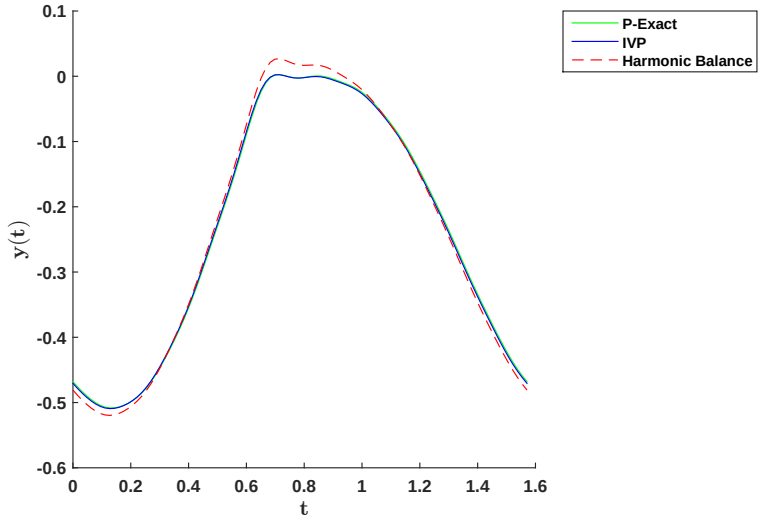

(a) Solution y(t)

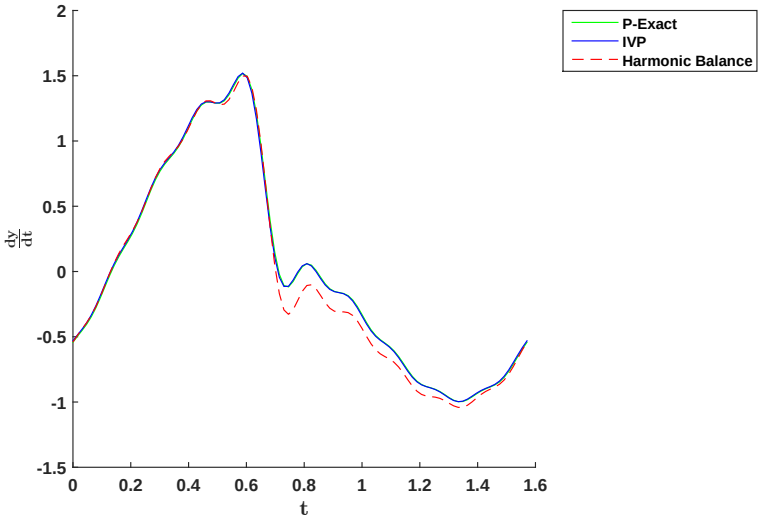

(b) Solution $\frac{dy}{dt}$

Figure 4.3: The signal constructed from the harmonic balance solution to (4.12) using n = 10 harmonics with a *modified non-smooth solver* in pseudo-time approach. The green and blue curves are the projection of the pseudo-exact and non-smooth IVP solver solutions on the n = 10 harmonic space. The parameters used are: $\epsilon = 0.1$, $\epsilon_r = 10^{-3}$, $\eta = 0.025$. The convergence limit for global iterations was set to 10^{-9}.

Figure 4.3 shows the solution for the non-smooth problem computed using this new approach. The percentage error of this solution compared to the pseudo-exact solution is 3.9%. Hence, the solution computed using this approach is a better approximation than the one computed using the previous approach. This is expected as here, the Heaviside function is replaced by the non-smooth algorithm and hence, an approximation of the Heaviside function is no longer needed. This method is more advantageous as one needs to only vary η to obtain solutions with varying accuracy. The current value of $\eta = 0.025$ is chosen as half the difference between the time instants corresponding to two sub-problems.

4.2.3. Artificial spring-damper

A literature study for the ways to solve the unilateral constraints problem using the harmonic balance approach has revealed that the vibro-impact oscillator has a similar problem. In this approach, the contact with the 'restriction' is modeled as an additional spring-damper element as given in [14][15]. Hence, it appears as if an artificial spring-damper element is placed instead of a rigid bodied 'restriction'. The contact force $\lambda(t)$ in equation (2.15) for such an artificial spring-damper element is given by:

$$-\lambda(t,y,\dot{y}) = \begin{cases} k_c g(t,y) + d_c \gamma(t) & \text{if } (g(t,y) \leq 0) \\ 0, & (g(t,y) > 0) \end{cases} \tag{4.17}$$

where k_c is the spring constant and d_c is the damping constant associated with the artificial spring damper element. $g(t,y)$ is the gap function and $\gamma(t)$ is the relative velocity at the moment of impact. The expression for $\lambda(t)$ is, in fact, the non-smooth contact law for $d_c > 0$ as the contact force jumps at the instant of collision. The contact with the 'restriction' is a partially inelastic impact. For such a contact, it is given in [15] that $d_c = 0$ i.e. no damping element. The presence of a damping element implies a plastic impact. Thus, if one knows the spring constant k_c the contact force is known and so the harmonic balance method can be implemented. This approach is implemented and the solutions are compared.

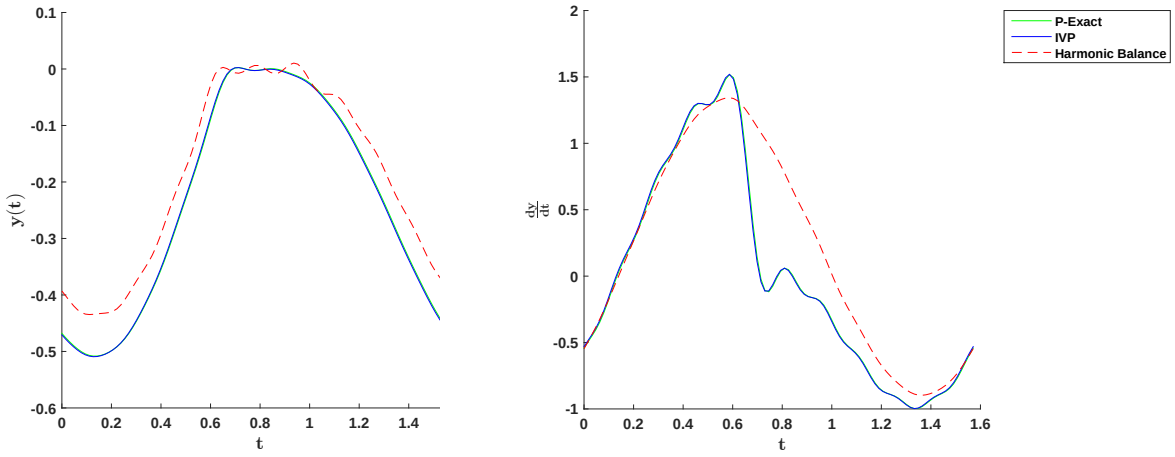

(a) Solution y(t)

(b) Solution $\frac{dy}{dt}$

Figure 4.4: The signal constructed from the harmonic balance solution to (4.12) using n = 10 harmonics with the artificial spring approach. The green and blue curves are the projection of the pseudo-exact and non-smooth IVP solver solutions on the n = 10 harmonic space. The artificial spring constant k_c = 3000Nm. The convergence limit for global iterations was set to 10^{-7}.

Figure 4.4 shows the solution obtained by modeling the impact with the 'restriction' as an artificial spring element with spring constant k_c = 3000Nm. The very high value of k_c (stiffness constant) implies that the 'restriction' tends to rigidity. This value of k_c is chosen by a trial and error method with the value giving the least error with respect to the pseudo-exact solution. The error percentage was 17.7%. The error is very high as compared to the previous two methods. It can be attributed to the fact that this method was developed for vibro-impact oscillator and similar applications where the damping element is important.

Another drawback of this approach is that there is no specific formula or expression relating k_c with the coefficient of restitution. Although, there exists a formula for plastic inelastic impacts which takes into account the damping constant. Thus, it is left to the user as to what specific spring constant to be used.

Also, the method as noted in [15] suffers from issues of convergence and the research in this field is still in the developing stages. But this method is discussed here to check for the accuracy of the resulting solution and for the completeness of the research.

4.3. Conclusion

Until now, the harmonic balance method was applied to obtain steady state solutions to problems having a smooth periodic solution. This chapter discusses 3 solution approaches to solve the periodic non-smooth motion of the lamella/airfoil using the harmonic balance method. For this purpose, the same model problem of spring-mass-damper with 'restriction', as presented in chapter 2, was used. The pseudo-exact and non-smooth IVP solver solutions were used as benchmarks for the solutions obtained from the harmonic balance method.

Out of the three approaches, the first two approaches are developed indigenously as a part of this project. The third approach is obtained from a literature study on modeling unilateral contacts using harmonic balance method. It was seen that, out of the 3 approaches, the second approach-*Modified non-smooth solver* in pseudo-time provides the most accurate solution. Also, this approach is easy to implement within OpenFOAM without many modifications. Hence, it is decided to use this approach for the final problem of the motion of the lamella/airfoil. With this, the second research question is fully addressed.

5

HARMONIC BALANCE METHOD FOR COUPLED FSI PROBLEM

Up to this point, the harmonic balance method was applied to either the structural or fluid flow equations. The problem of modeling the motion of the lamella/airfoil under periodic flow conditions is a fluid-structure interaction problem wherein, both, the structural and the fluid, equations need to be solved using the harmonic balance method. Additionally, the respective governing equations are coupled because there is an interaction between the fluid and structure. Thus, the final implementation would require to solve a *coupled* fluid-structure interaction problem with the harmonic balance method. This will also address the third research question. As has been done previously, a simplified model problem will be tackled: A *loosely coupled* fluid-structure interaction problem.

5.1. Loose coupling using potential flow

In this problem, the airfoil is subjected to potential flow where the solutions of the flow at various time instants are independent of each other. Hence, in this problem there is a coupling between the solutions of the structural model within themselves and with the solutions of the fluid. However, there is *no* coupling between the fluid solutions at various time instants. Hence, in this context, the term *loosely coupled* is used. The problem setup is described in the following section.

5.1.1. Problem setup

The problem under consideration is a potential flow around an airfoil which is hinged at its leading edge. Figure 5.1 shows a symmetric airfoil with time dependent boundary conditions for potential flow in a 2D rectangular domain. The domain is very large as compared to the airfoil dimensions. c represents the chord length of the airfoil. Note that the airfoil is NACA 0009 and was considered because a standard mesh of good quality was readily available for this airfoil. The airfoil is subjected to periodically varying inflow conditions.

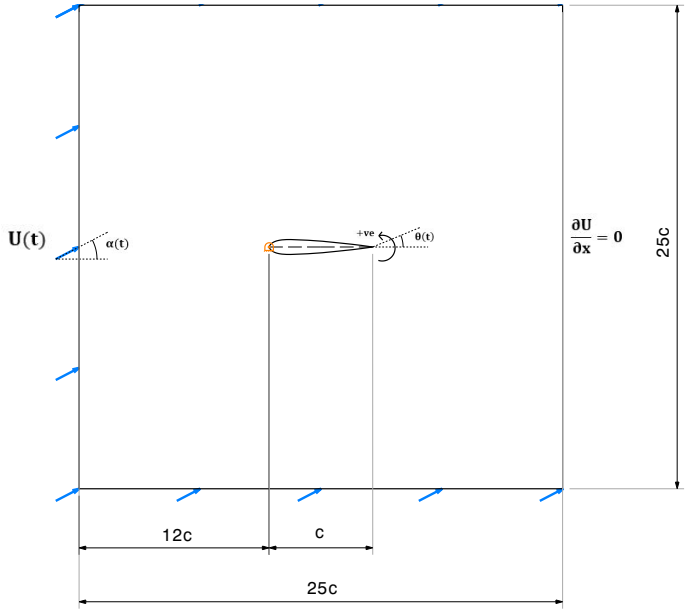

Figure 5.1: Problem setup for a periodic flow around a symmetric airfoil hinged at its leading edge. The boundary conditions are indicated for the inlet and outlet. c represents the chord length of the airfoil.

5.1.2. Fluid model

A potential (ideal) flow is said to be incompressible, irrotational and having no net viscous stresses. The irrotationality implies that the velocity field can be represented by a velocity potential function (ϕ). This relation is given by:

$$\mathbf{u} = \nabla\phi. \tag{5.1}$$

While, the continuity equation in case of incompressible flows is given by:

$$\nabla.\mathbf{u} = 0. \tag{5.2}$$

The equations (5.1) and (5.2) together give the expression for velocity potential as:

$$\nabla^2\phi = 0. \tag{5.3}$$

This is a Laplace equation whose solution will provide the velocity field through the use of (5.1). To solve this equation, appropriate boundary conditions are necessary.

Velocity Boundary Conditions

The periodically varying inflow conditions serve as the inlet boundary conditions. The left boundary of the rectangular domain along with the top and bottom boundaries, together, act as the inlet. At the inlet, the following periodic Dirichlet boundary conditions are applied:

$$\mathbf{U}(\mathrm{t}) = \begin{bmatrix} \mathrm{U_{inf}}\cos(\omega \mathrm{t}) \\ \mathrm{U_{inf}}\sin(\omega \mathrm{t}) \end{bmatrix}, \tag{5.4}$$

where $\mathrm{U_{inf}}$ is the magnitude of the incident velocity and ω is the angular frequency. The boundary conditions at the inlet are time dependent.

The right boundary acts as an outlet and has a homogeneous Neumann boundary condition for velocity.

On the surface of the airfoil, the velocity boundary condition should be a *no penetration* boundary condition.

From the equation (5.3), it is clear that the potential flow is a case of steady flow as the instantaneous solution is independent of time derivatives. But, the velocity boundary conditions are time dependent, which renders the flow unsteady. It is noted in [16] that for such a case of *unsteady* potential flow, the influence of momentary boundary condition is immediately radiated across the whole fluid region. Therefore, steady-state solution techniques can be used to treat such a time-dependent problem by substituting the instantaneous boundary condition at each moment. However, the wake shape *does* depend on the time history of the motion and consequently, an appropriate vortex wake model has to be developed. In this current problem, very low angle of attacks $\pm 10°$ are considered and hence, the lift is very low. On this ground, the vortex wake model has not been considered. But, in reality, the wakes will appear and it has to be treated.

In such a case of unsteady potential flow, the general approach is to change the frame of reference from the inertial frame to a frame fixed to the moving body i.e. airfoil. The potential flow equations are written in this airfoil fixed frame of reference and the boundary conditions are modified accordingly. The velocity potential equation (5.3) in the airfoil fixed frame of reference will not change. But the boundary conditions will change. At the surface of the airfoil, in an inertial frame of reference the no penetration boundary condition is mathematically given by:

$$(\nabla \boldsymbol{\phi}).\hat{\mathbf{n}} = (-\mathbf{v}).\hat{\mathbf{n}}, \tag{5.5}$$

where $\hat{\mathbf{n}}$ is a unit vector normal pointing outwards from the surface of the airfoil and $-\mathbf{v}$ is the velocity of the surface of the airfoil. For a fixed airfoil this value is zero, but in the case of airfoil hinged at the leading edge, this value is non zero. In the frame of reference fixed to the airfoil, this boundary condition translates to:

$$(\nabla \boldsymbol{\phi} + \mathbf{v}).\hat{\mathbf{n}} = 0. \tag{5.6}$$

As the airfoil is rotating about its leading edge, the velocity can simply be given as $\dot{\theta}\mathbf{r}$ where $\dot{\theta}$ is the angular velocity and the vector $\mathbf{r}$ is the position vector of the surface of the airfoil from the leading edge.

For the velocity boundary conditions on the outer boundary (inlet and outlet) of the domain, one should understand that in the case when the domain is very big as compared to the airfoil, the flow disturbance due to the motion of the airfoil should diminish far away from the airfoil. Thus, the airfoil motion doesn't affect the flow at the outer boundaries of the domain which means that the boundary conditions at the outer boundaries are the same in both the frames of references.

Note that, the case of potential flow is inviscous. But, the viscosity effects are considered in the structural model. This will be clear in the next section. The fluid model was implemented in OpenFOAM and the results are visualized.

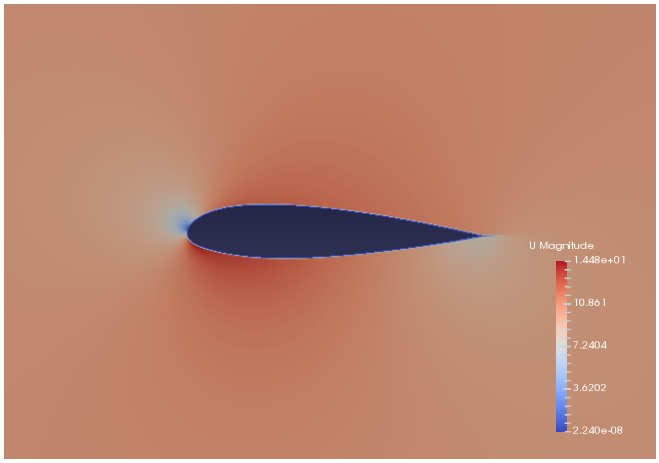

(a) Velocity field

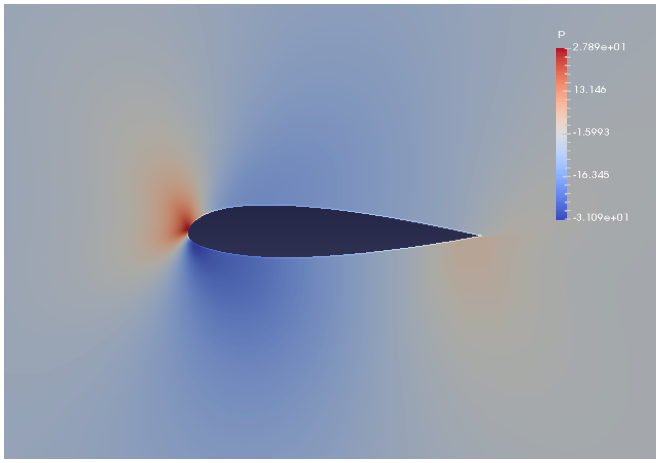

(b) Pressure field

Figure 5.2: The velocity and pressure fields computed using the *potentialFoam* solver of OpenFOAM®. The inlet velocity (**u**) is $[9.9 \quad -1.41]^T$, while $\dot{\theta}(t) = 0c/sec$.

Figure 5.2 shows the velocity and pressure fields computed using the *potentialFoam* solver of OpenFOAM. The value of the inlet velocity (**u**) is $[9.9 \quad -1.41]^T$, which implies that the velocity is incident at an angle of –6.3° with the horizontal. This can be confirmed from the location of the stagnation point in figure 5.2. The location is such that the velocity appears to be incident on the airfoil at some angle less than zero with the horizontal.

For verification of the above results, a Joukowski transform can be used to compute the location of the stagnation point on the corresponding cylinder. As NACA 0009 is a standard symmetric airfoil whose computations have been done for decades. Its Joukowski transform is readily available[17], from which it can be estimated that a stagnation point of –6.3° on the airfoil corresponds to –19.4° on the cylinder. Knowing the location on the cylinder, the pressure at the stagnation point of the cylinder is given by the following expression:

$$p_s = p_{inf} + \frac{1}{2}\rho U_{inf}^2(1-4\sin^2\theta), \tag{5.7}$$

where p_s is the pressure at the stagnation point, p_{inf} is the pressure at infinity (=0 in this case), θ is the angle made by the location of stagnation point with the horizontal cylinder axis. From the above expression, the value of $p_s = 27.8 N/m^2$. This is in accordance with the numerically calculated value, as seen in figure 5.2. This verifies the implementation of the fluid model in OpenFOAM and

lends support to quality of mesh. The description of the fluid model is complete. It remains to see how to obtain $\dot{\theta}$(t) and the correct inlet velocity condition. This input is obtained from the structural model.

5.1.3. Structural model

In chapter 2, the governing equation of the motion of lamella/airfoil was discussed. The following chapters dealt with solving a spring-mass-damper problem using the harmonic balance method. In this section, the governing equation of the motion of the airfoil is presented again and the process of solving it coupled with the solutions from the fluid model is discussed. Here, it will become more clear as to why the spring-mass-damper system was discussed as a representative model. The airfoil nomenclature to be used in this project is presented in the next section.

Airfoil terminology

To better understand the structural model, it is necessary to understand some basic terminology related to airfoils.

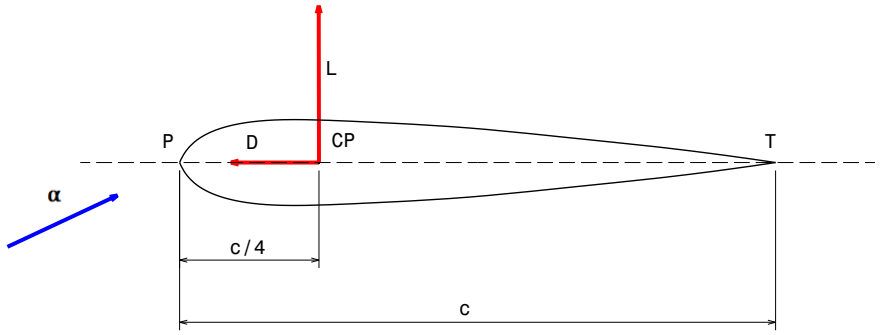

Figure 5.3: Schematic of a symmetric airfoil depicting the important terminology related to airfoils that is required for this project.

Figure 5.3 shows a symmetric airfoil cross-section in 2D. The following is a list of the important parameters in this context adopted from [18]

- P-Point corresponding to the leading edge in 2D.
- T-Point corresponding to the trailing edge in 2D.
- c-Length of the chord line, which is a straight line connecting the leading and trailing edges.
- α-Angle of attack of the fluid flow with respect to the airfoil.
- CP-Center of pressure which is the same as the aerodynamic center for a symmetric airfoil. This point is approximately at distance of $\frac{c}{4}$ from the leading edge for small angles of attack.
- L-Lift force acting at CP perpendicular to the chord.
- D-Drag force acting at CP along the chord opposite to the direction of the flow..

Further, the lift and drag forces are represented by the corresponding lift and drag coefficients.

Lift Coefficient

The expression for the lift (C_l) is:

$$C_l = \frac{L}{\frac{1}{2}\rho U_{inf}^2 c(1)}, \tag{5.8}$$

where ρ is the density of the fluid, U_{inf} is the magnitude of incident velocity (in this case velocity at the inlet of the domain), c(1) is the chord length times a unit span in the direction perpendicular to the airfoil cross-section.

Drag Coefficient

The expression for drag coefficient (C_d) is similar to the lift coefficient and is given by:

$$C_d = \frac{D}{\frac{1}{2}\rho U_{inf}^2 c(1)}, \tag{5.9}$$

where the quantities have the same meaning as given before. The lift and drag forces will exert a torque to an airfoil hinged at its leading edge. The expression for this torque is given by:

$$T_f = L\frac{c}{4} - D\frac{c}{4} + T_m. \tag{5.10}$$

where T_m is the torque acting at CP. This torque is obtained directly from the fluid model. Torque is considered positive in the anticlockwise direction.

The important characteristics of an airfoil have been discussed. Going back to the problem of the motion of an airfoil under potential flow, the governing equation of this motion is given by:

$$I\ddot{\theta}(t) + k_f\theta(t) + c_f\dot{\theta}(t) = T_f + T_{ns}, \tag{5.11}$$

where the terms have the same meaning as given in 2.7. But there is an appearance of two new terms-stiffness and damping. The stiffness term is represented by $k_f\theta$, where k_f is the stiffness constant, while the damping term is represented by $c_f\dot{\theta}$, where c_f is the damping constant. These two terms appear in the above equation because the potential flow model is a case of ideal flow. In reality, it will not be an inviscid but a viscid flow. Hence to compensate for the additional forces because of viscosity, the additional stiffness and damping forces are added to the equation (2.7)[19]. Note that the fluid torque term on the right hand side of (5.11) is a result of the torque because of the integration of pressure stresses on the airfoil. This is essentially the lift force in case of potential flow. The form of equation (5.11) is similar to the spring-mass-damper problem treated earlier. Thus, the similar theory applies here. The equation (5.11) is a second order ODE which is reduced to a system of first order ODEs as given by:

$$\begin{bmatrix} \dot{\theta} \\ \ddot{\theta} \end{bmatrix} = \begin{bmatrix} 0 & 1 \\ -\frac{k_f}{I} & -\frac{c_f}{I} \end{bmatrix} \begin{bmatrix} \theta \\ \dot{\theta} \end{bmatrix} + \begin{bmatrix} 0 \\ \frac{T_f}{I} \end{bmatrix}. \tag{5.12}$$

Note that, the T_{ns} term is absent because only the smooth motion is considered. In the case of potential flow, only lift force is acting, hence, the value of the fluid torque T_f is given by the expression (5.10) where only the lift force component is present. The effect of drag is introduced by adding a suitable damping constant c_f.

The equation (5.12) is now solved with a *partially uncoupled approach* (section 3.2.2) of the harmonic balance method with inputs for the coefficient of lift (C_l) from the fluid model. This input is used to compute the lift force using the expression (5.8) and then the torque using (5.10).

5.1.4. Description of the coupling

In this section, the coupling between the fluid and structural model is described. The following is a detailed procedure to solve the problem of motion of the airfoil under periodic fluid flow.

- The problem is solved using MATLAB and OpenFOAM, where the structural model and the coupling is done in MATLAB, while OpenFOAM is used to solve the fluid model.
- The structural model is implemented in a partially uncoupled approach, thus, for n harmonics, there are $2n+1$ sub-problems.
- The MATLAB script is run with some appropriate initial guess for θ and $\dot{\theta}$.
- In each sub-problem, the coefficient of lift C_l is obtained from the fluid model. To run the fluid model, a MATLAB function is created which takes the inlet velocity, according to the sub-problem number (out of $2n+1$), and $\dot{\theta}$ as input. It is then passed to OpenFOAM where the simulations are executed by commands given through a MATLAB script. The C_l output from these simulations is used to compute the torque T_f. After obtaining the T_f value the sub-problem is run to convergence in pseudo-time.
- This process is continued for all the sub-problems until the global iterations converge.
- Once the solution is obtained for all the sub-problems, the signal is computed for the values of θ and $\dot{\theta}$.

The model problem given at the start of this section is solved using the procedure described above for a NACA-0009 plastic airfoil. This is also referred to as a hydrofoil.

5.1.5. Results and discussion

The parameters of the hydrofoil utilized in this section are summarized in the table below.

Parameters	Plastic Hydrofoil
c (m)	0.1
ρ_s (kg.m^{-3}	7800/7
I (kg.m)	$1.0\times10^{-2}/7$
c_f	2.5
k_f	400

Table 5.1: Parameters of a plastic NACA0009 hydrofoil obtained from [20]

Table 5.1 gives the parameters for plastic NACA0009 hydrofoil to be used in simulations. The lamellas in the OWM are also made of plastic. n = 2 harmonics are considered to obtain a harmonic balance solution for the problem. The inlet has a periodic flow with angles of attack varying from –10° to +10°. Thus, the boundary conditions 5.4 in this case are given by:

$$\mathbf{U}(t) = \begin{bmatrix} U_{inf}\cos\left(\frac{\pi}{18}\left(\sin(\omega t+\frac{3\pi}{2})\right)\right) \\ U_{inf}\sin\left(\frac{\pi}{18}\left(\sin(\omega t+\frac{3\pi}{2})\right)\right) \end{bmatrix}. \tag{5.13}$$

Observing the expression (5.13), it is clear that the incident velocity varies from –10° to +10° in a sinusoidal way with a frequency given by ω. With $U_{inf} = 10$ and $\omega = 4$, the boundary conditions in matrix form for n = 2 harmonics and $\omega = 4$ are given by:

$$\mathbf{u_i} = \begin{bmatrix} 9.9855 & -0.5391 \\ 9.9005 & 1.4073 \\ 9.9005 & 1.4073 \\ 9.9855 & -0.5391 \\ 9.8481 & -1.7365 \end{bmatrix}. \tag{5.14}$$

Each row corresponds to the inlet velocity boundary conditions for each of the 2n+1 sub-problems. The first column gives the x-component while the second gives the y-component of the velocity. The harmonic balance method will provide solutions for the 2n+1 time instants in a single time period. This solution is used to compute the Fourier signal by performing a discrete Fourier transform as seen in chapter 3 section 3.1.1.

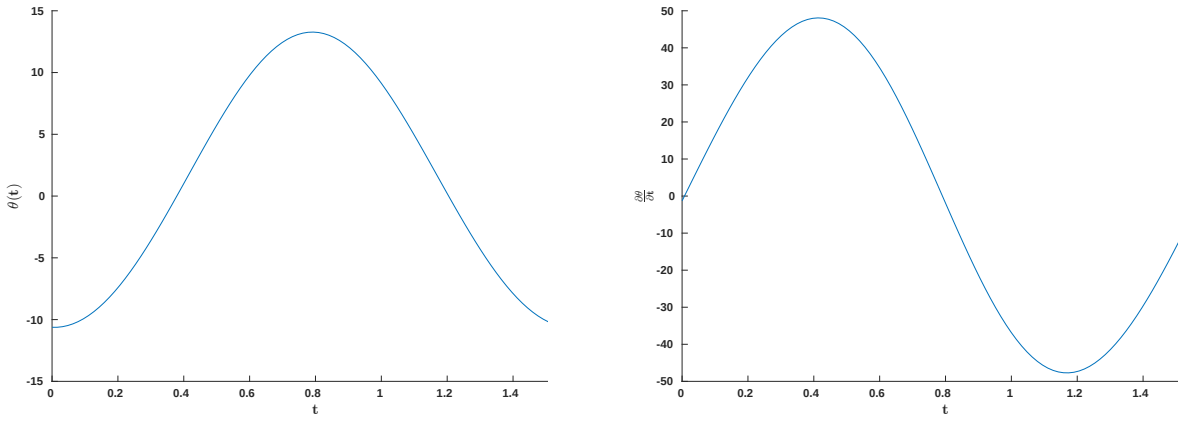

(a) Position (b) Velocity

Figure 5.4: The position and velocity signals for the airfoil under periodic potential flow having inlet velocity given by (5.4). n = 2 harmonics were used for the solution and $\omega = 4$ was considered for periodic inlet velocities. The values of the angle and the angular velocity are in degrees and degrees/sec respectively.

Figure 5.4 shows the solutions for position and velocity of the airfoil obtained by the MATLAB-OpenFOAM coupled solver using the procedure described in the previous section. The solutions are Fourier signals computed from the harmonic balance solution. Further, the coefficients of the Fourier modes are computed for the position and velocity solutions.

Modes	Position	Velocity
sin(ωt)	-0.0051	0.8342
sin(2ωt)	-0.00023	-0.0259
Constant	0.0199	3.07e-08
cos(ωt)	-0.2085	-0.0205
cos(2ωt)	0.0032	-0.0019

Table 5.2: Fourier coefficients obtained from the application of the DFT operator on the harmonic balance solution of the structural model given by (5.11).

Table 5.2 shows the Fourier coefficients of the Fourier modes which define the position and velocity curves of the airfoil. The modes for position show that the solution is a cosine wave of 1 harmonic

which is offset from the origin. And the modes for velocity solution show that is it is a sine wave centered around the origin. Thus, one can also obtain the same solution using n = 1 harmonic. This will be faster as only 2n + 1(= 3) sub-problems are solved instead of 5 in the case of n = 2 harmonics. The solution for loose coupling is not the same as the solution needed for the airfoil under laminar flow. But, it serves as a good starting point and verification that the procedure for loose coupling indeed provides a realistic solution.

It is also worthwhile to see if a non-smooth solution can be obtained for the loose coupling problem. To investigate, consider that the airfoil is restricted at a position by a mechanical stopper, similar to how a lamella is constrained.

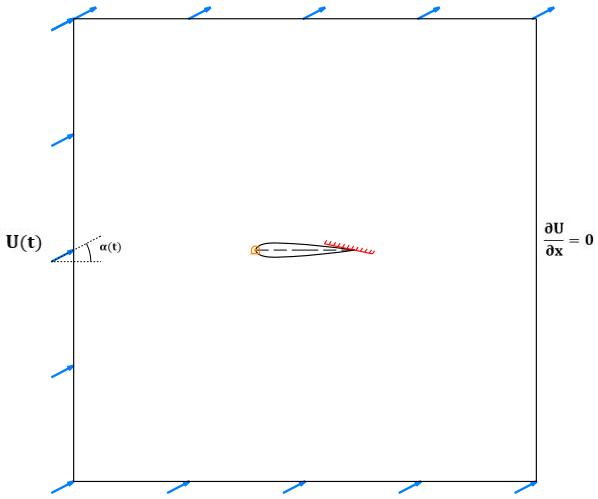

Figure 5.5: Problem setup for the non-smooth airfoil problem. The boundary conditions are indicated for the inlet and outlet. The airfoil motion is restricted by a mechanical stopper when the airfoil is horizontal with respect to the flow.

Figure 5.5 shows the same airfoil problem of figure 5.1 with a restriction to the motion of the airfoil when it becomes horizontal i.e. parallel to the x-axis. This will result in the airfoil having a non-smooth motion similar to the one discussed for the spring-mass-damper system with 'restriction' (2.7). Note that the flow starts from –10°. To solve this problem, the fluid model is the same as discussed for the smooth problem. But the structural model has an additional torque which acts because of the collision with the restriction/stopper. Thus, the governing equation of the airfoil in this case is given by:

$$\begin{bmatrix} \dot{\theta} \\ \ddot{\theta} \end{bmatrix} = \begin{bmatrix} 0 & 1 \\ -\frac{k_f}{I} & -\frac{c_f}{I} \end{bmatrix} \begin{bmatrix} \theta \\ \dot{\theta} \end{bmatrix} + \begin{bmatrix} 0 \\ \frac{T_f}{I} + \frac{T_{ns}}{I} \end{bmatrix}, \tag{5.15}$$

where T_{ns} is the torque because of the non-smooth contact force. The above problem is solved using the second approach discussed in chapter 4.

In a gist, the non-smooth airfoil problem can be solved using the *loose coupling* procedure discussed previously with the addition of a torque due to the non-smooth force. This torque is computed using the *modified non-smooth solver* as discussed in chapter 4. The procedure is implemented and a solution is computed with the same problem parameters as used in the smooth case.

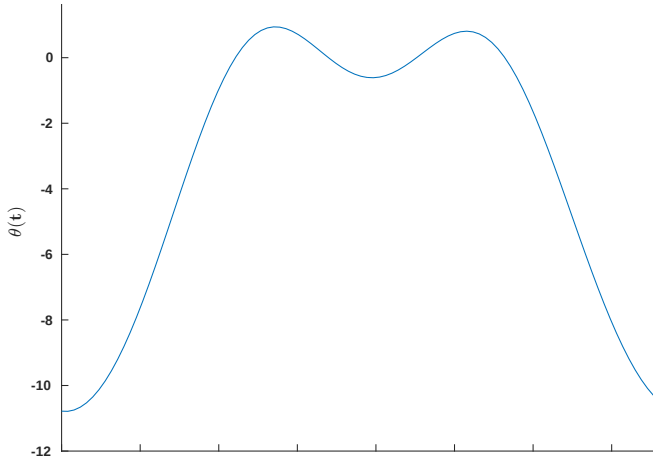

(a) Position

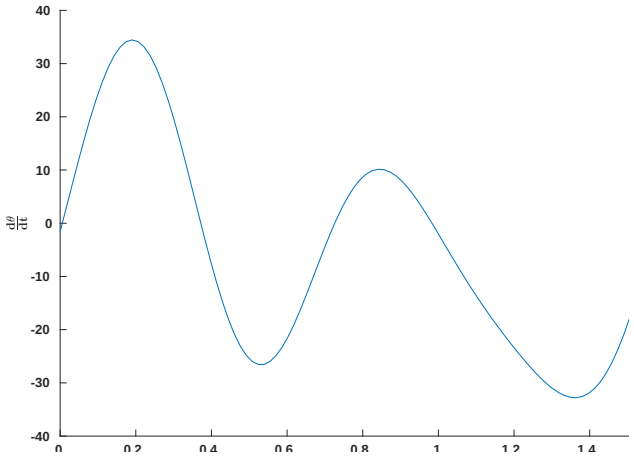

(b) Velocity

Figure 5.6: The position and velocity signals for the non-smooth motion of the airfoil under periodic potential flow having inlet velocity given by (5.4). n = 3 harmonics were used for the solution and $\omega = 4$ was considered for periodic inlet velocities. The values of the angle and the angular velocity are in degrees and degrees/sec respectively.

Figure 5.6 shows the Fourier signals computed from the harmonic balance solution to the non-smooth airfoil motion under periodic potential flow conditions. The solution was computed for n = 3 harmonics. The signal for the position of the airfoil shows that the airfoil is restricted at the 0° mark, which is expected because of the stopper at that position. This gives confidence to the obtained solution. Nonetheless, the solution does go over the 0° mark by a small amount. This is due to the fact that the non-smoothness renders the problem highly non-linear and hence, the above 3 harmonic solution is a Fourier approximation of the exact solution. This fact has already been presented in chapter 4. Thus, the non-smooth motion of the airfoil under periodic potential flow conditions is solved using the harmonic balance method with the approach of a modified non-smooth solver in a MATLAB-OpenFOAM coupled environment.

5.2. Tight coupling using laminar Navier-Stokes

The loose coupling was simple because only the structural model had coupling within its solutions at various time steps, while the solutions of fluid model were not coupled within themselves. This was due to the assumption of potential flow. But the case of potential flow is an ideal case and so, in this section, a fluid flow described by the laminar Navier-Stokes model is considered. Again, only a smooth problem is initially discussed.

5.2.1. Problem Setup

The problem setup is the same as considered for the loose coupling, but with a laminar flow model. Figure 5.1 shows this setup. The boundary conditions for velocity at the inlet and outlet remain the same. On the surface of the airfoil, the boundary condition is a no slip boundary condition as this is a case of laminar flow.

5.2.2. Fluid model with implementation of HB method for N-S equations

The fluid flow is laminar, and hence it is governed by the unsteady Navier-Stokes equations. The unsteadiness implies the presence of time derivative terms and hence, the fluid flow equations will also require a harmonic balance implementation which couples the fluid solutions at all the time instants. This makes the coupling more *tight*. At this point, a detour is taken to discuss the harmonic balance implementation of Navier-Stokes equations. It is imperative to initially discuss the Navier-Stokes equation to have a clear picture of the application of the harmonic balance method.

The Navier-Stokes equations for incompressible flow

The momentum equation of the Navier-Stokes equations in vector form is given by:

$$\rho \frac{\mathrm{D}\mathbf{u}}{\mathrm{D}t} = -\nabla \mathrm{p} + \mu \nabla^2 \mathbf{u} + \rho \mathbf{f_b}, \tag{5.16}$$

while the continuity equation is given by:

$$\nabla . \mathbf{u} = 0. \tag{5.17}$$

The description of the terms in the above equation is as follows:

- $\rho \frac{\mathrm{D}\mathbf{u}}{\mathrm{D}t}$-This term represents the density times the material derivative of velocity, where ρ is the density of the fluid and $\mathbf{u}$ is the velocity vector. In the context of Newton's Second law, one can think of this term as the mass times acceleration term.
- $-\nabla$p-This term represents the gradient of pressure p which is also the hydrostatic forces.
- $\mu \nabla^2 \mathbf{u}$-This term represents the viscous forces in the flow. μ is the dynamic viscosity of the fluid. The term is obtained from the divergence of the deviatoric stress tensor.
- $\rho \mathbf{f_b}$-This term represents external body forces like gravitational force.
- $\nabla . \mathbf{u}$-This term represents the divergence of the velocity field. Further, the incompressibility condition that this velocity field should be divergence free.

The equation (5.16) is simplified and represented in a condensed form as:

$$\rho \frac{\partial \mathbf{u}}{\partial t} + \mathbf{R}(t) = 0, \tag{5.18}$$

where $\mathrm{R} = \nabla \mathrm{p} - \mu \nabla^2 \mathbf{u} + \mathbf{u}.(\nabla \mathbf{u}) - \rho \mathbf{f_b}$.

Semi-discretization on a spatial grid using an appropriate finite volume discretization method gives:

$$\rho \frac{d\mathbf{U}}{dt} + \hat{\mathbf{R}}(t) = 0, \tag{5.19}$$

where $\hat{\mathbf{R}}(t)$ is the operator containing the terms obtained from the discretization of the terms in $\mathbf{R}(t)$ of the equation (5.18). The equation (5.19) is an ODE for velocity vector $\mathbf{U}$ containing the value of velocity at all the cell centers of the grid. It should be noted that this equation is the same as (3.1) which was considered for the derivation of the harmonic balance method.

By now, it is clear that the harmonic balance transformation of (5.19) provides a set of coupled steady state problems. These set of coupled steady state problems in the discrete form for the velocity ($\mathbf{u_{t_j}}$) are represented as:

$$\nabla.(\mathbf{u_{t_j}}\mathbf{u_{t_j}}) - \nabla.(\nu\nabla\mathbf{u_{t_j}}) = -\nabla p_{t_j} - \omega\left(\sum_{i=1}^{2n} B_{i-j}\mathbf{u_{t_i}}\right), \quad \text{for} \quad j = 1\ldots 2n+1, \tag{5.20}$$

where ν is the kinematic viscosity. Note that a partially uncoupled approach is used where the above equation represents each sub-problem of the 2n+1 sub-problems. The operator $\boldsymbol{B}$ (3.15) is expanded for each sub-problem. Observing the form of the matrix $\boldsymbol{B}$ hints that, one needs to store only a vector of values given by:

$$B_j = \sum_{k=1}^{n} k\sin(k\omega j t_1), \quad \text{for} \quad j = 1\ldots 2n+1.$$

With these, one can construct the entire matrix $\boldsymbol{B}$ or obtain directly the source term for each sub-problem as given in (5.20). This helps in reducing the storage requirements in case of huge grids and is thus a computationally better alternative. Similar harmonic balance transformation if applied to the continuity equation (5.17) gives $\mathbf{u}$ replaced by its discrete counter part $\mathbf{u_{t_j}}$:

$$\nabla.\mathbf{u_{t_j}} = \mathbf{0}. \tag{5.21}$$

The equations (5.20) and (5.21) have to be solved for all the sub-problems. The nature of the equations implies that they are a set of coupled steady state Navier-Stokes equations with an additional source term (temporal source term) which couples them. The SIMPLE algorithm is known to provide a solution to steady state Navier-Stokes equations. So, with some modification to the SIMPLE solvers to add an extra source term, one can easily develop a harmonic balance solver for the Navier-Stokes equations based on the partially uncoupled approach. This is the beauty of the harmonic balance method.

Going back to the problem of the motion of an airfoil, similar to the potential flow model, in this case too, the frame of reference is fixed to the body of the airfoil. Such a change of reference can be done as the rate of rotation of the airfoil is constant during the process of obtaining a *steady state* solution to the sub-problem. For this formulation, OpenFOAM already has a SIMPLE algorithm based solver by the name of *SRFSimpleFoam*[21], which means a single rotating frame SIMPLE solver. Using the SRFSimpleFoam solver, a *MATLAB-OpenFOAM harmonic balance solver* is developed to solve the fluid model. This model is in a frame of reference fixed to the airfoil and hence, the force from the fluid will also have the centrifugal and Coriolis force components in it. Note that, as only the steady state equations were solved it was possible to change the frame of reference. But, this is not possible in a case when the problem is solved as an IVP with transient solutions as the rate of rotation is not constant in that case.

In the MATLAB-OpenFOAM coupled solver, the harmonic balance algorithm and temporal source term evaluations for all the sub-problems is done in MATLAB. These are given as inputs to OpenFOAM where the sub-problems are solved using the SIMPLE algorithm to obtain a steady state solution in pseudo-time[22].

This solver is tested for a problem of a fixed airfoil in the periodic inflow conditions given by (5.4). It is expected to provide a converged periodic steady-state solution for a certain number of time steps depending on the number of harmonics. A Fourier transform of this solution will provide the coefficients of the Fourier series which represents the solution. Knowing the Fourier coefficients, the solution can be computed for any other time instant.

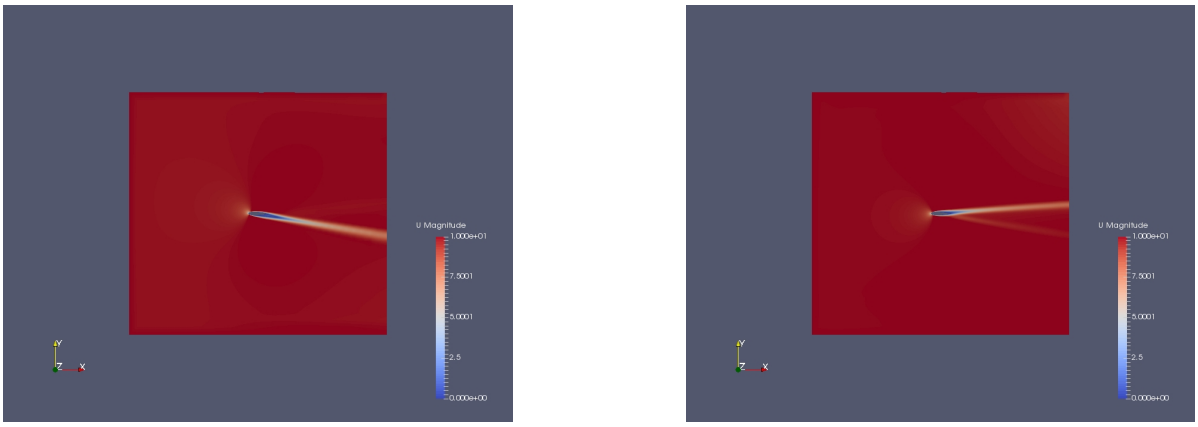

(a) t = 0s (b) t = 0.5024s

(c) t = 1.099s (d) t = 1.57s

Figure 5.7: The velocity field for 4 different time instants computed using the Fourier signal. The Fourier signal was developed from the harmonic balance solution to the problem with n = 1 harmonic. The time period is T = $\frac{\pi}{2}$ because the inlet velocity has an angular frequency of $\omega = 4$. The convergence limit for the global iterations is set to 10^{-7}.

Figure 5.7 shows the velocity field computed for certain time instants of the total period T = $\frac{\pi}{2}$ using the developed MATLAB-OpenFOAM harmonic balance solver. The solver is set a global convergence limit of 10^{-7}. The steady state solution for any time instant can be computed quickly using this solver. Thus, a faster and efficient way is developed for obtaining steady state solutions to problems with periodic flow conditions.

Note that, there is no observable vortex shedding in the results which is contrary to the expectations. This is because the solution is computed for n = 1 harmonic and thus, the computed velocity field is 1 harmonic field. The vortex shedding is highly non-linear, and to observe this in the solution an expansion in higher harmonics is required. The current implementation cannot be used to compute such a solution in a reasonable time.

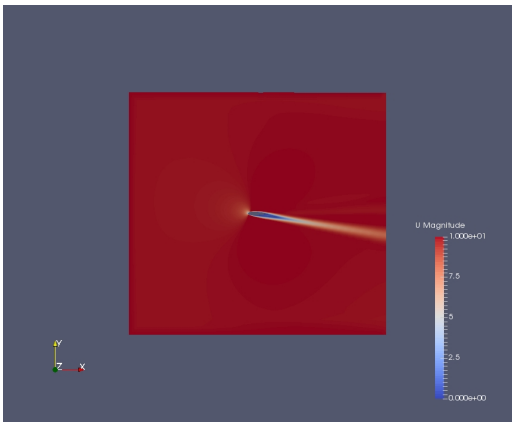

(a) t = 0s

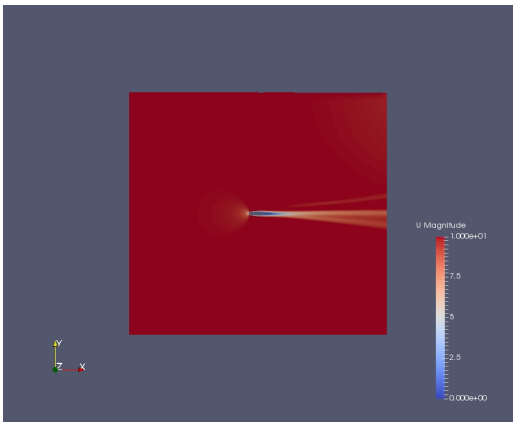

(b) t = 0.40s

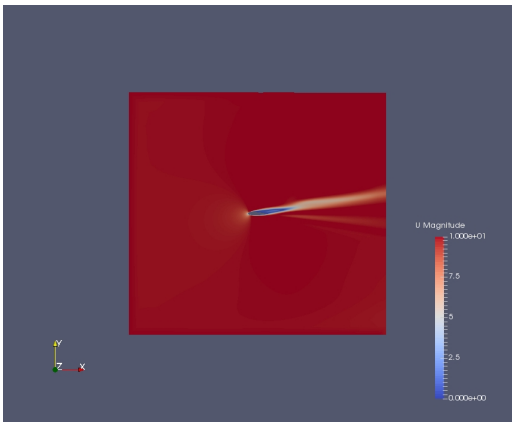

(c) t = 0.8s

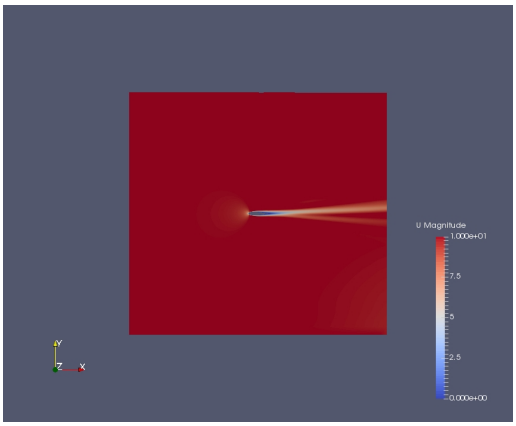

(d) t = 1.18s

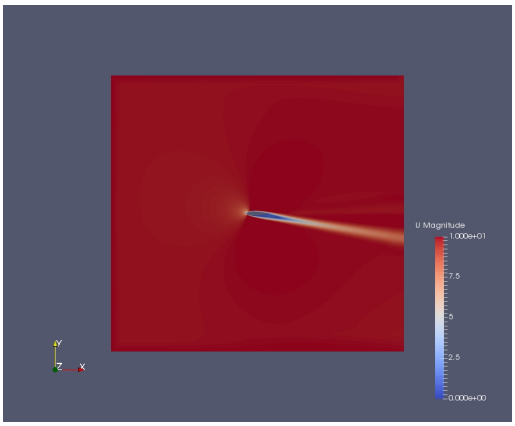

(e) t = 1.57s

Figure 5.8: The velocity field for 5 different time instants computed using the Fourier signal of the solution. The Fourier signal was developed from the harmonic balance solution to the problem with n = 5 harmonics. The time period is T = $\frac{\pi}{2}$ because the inlet velocity has an angular frequency of $\omega = 4$. The convergence limit for the global iterations is set to 10^{-7}.

Figure 5.8 shows the solutions for the same problem computed for n = 5 harmonics. The separations can be noted in figure (c) at the top. This means that with higher harmonics, the non-linear velocity field can be visualized. It has already been noted in [8] that the harmonic balance approach will provide an approximate in less computational time to such a problem of airfoil fixed under periodic flow. One is referred to [8] for a more detailed analysis on this front. Here, only the results of the implementation of the method are shown as it is not the focus of this project to analyze the harmonic balance method. In the next section, the structural model is presented.

5.2.3. Structural model

The structural model, in this case, is represented by the governing equation of the lamella (2.7) given in chapter 2. The equation (5.12) presented in the structural model for loose coupling is modified to suit for the current case of tight coupling. The modified equation is:

$$\begin{bmatrix} \dot{\theta} \\ \ddot{\theta} \end{bmatrix} = \begin{bmatrix} 0 & 1 \\ 0 & 0 \end{bmatrix} \begin{bmatrix} \theta \\ \dot{\theta} \end{bmatrix} + \begin{bmatrix} 0 \\ \frac{T_f(\theta,\dot{\theta})}{I} \end{bmatrix}. \tag{5.22}$$

As this is a case of laminar flow and the fluid and structural model will be coupled to obtain the final solution, the fluid torque T_f also contains the stiffness and damping components in its value. Hence, the damping and stiffness components from the loose coupling case are not present in this case.

The expression for T_f is given in (5.10) which implies that, once the C_d, C_l and T_m values are known from the fluid model, the structural model can be solved using the partially uncoupled approach as was done in the case of loose coupling. This completes the description of the structural model.

5.2.4. Description of the coupling

The coupling of the fluid and structure models was easy for the loose coupling problem. In the case of tight coupling, the following procedure is adopted to combine and couple the solutions from the structure and fluid.

- The fluid and structural models are solved with the same number of harmonics and so, they will have the same number of sub-problems. With n harmonics, there will be $2n+1$ sub-problems.
- The inlet velocity vector is formed for the $2n+1$ sub-problems. This provides the fixed value of inlet velocity for all the sub-problems. Note that the inlet velocity vector will be obtained by computing the effective angle of attack. If α is the angle of attack of the inflow with respect to an inertial frame, then the angle of attack with respect to the airfoil will be $\alpha - \theta$. This effective angle of attack is used to compute the inlet velocity vector.
- The θ and $\dot{\theta}$ are assigned some appropriate initial values for all the $2n+1$ sub-problems.
- Only one single loop is considered for the global iterations and within this loop, each sub-problem of the fluid and solid is solved in the following way:
  - Initially, the fluid model is provided with the input of angular velocity $\dot{\theta}$ and the inlet velocity corresponding to that sub-problem. The MATLAB-OpenFOAM coupled fluid solver provides the harmonic balance solution for this sub-problem. The output from this solution is the fluid torque T_f
  - The corresponding sub-problem in the structural model is then solved to convergence in pseudo-time using the value of the fluid torque computed previously.

  - The new values of θ and $\dot{\theta}$ from the structural model are fed back to the fluid model.
  - Again the fluid model is run to convergence in pseudo-time and the updated fluid torque T_f is obtained.
  - The structural model is run again with the updated fluid torque.
  - This process continues until a sufficient convergence is reached between the successive values of the θ and $\dot{\theta}$.

- This completes the solution procedure for one sub-problem. For the next sub-problem, the similar procedure is adopted but with updated source terms for the fluid and structural models from the solutions of the previous sub-problem. This gives a partially uncoupled way of implementation.
- The solutions are converged when the global iterations converge. The global iteration convergence is based on the errors of both the fluid and structural model. Both the errors should be within a certain convergence limit to stop the iterations.

A *MATLAB-OpenFOAM coupled smooth motion solver* is developed with the coupling described above.

5.2.5. Results and discussion

The solver was run for the same inlet velocity conditions as given in (5.13). Again n = 2 harmonics are considered and hence, the inlet velocity vector is given by (5.14).

It was seen in the simulations that the individual sub-problems didn't converge to a solution in pseudo-time for the structural model. But, it was converging in the loose coupling case and also in the case of the spring-mass-damper system. So, to understand why they don't converge in pseudo-time the individual sub-problems of the structural model are considered here.

$$\begin{bmatrix} \frac{1}{\Delta\tau} & 1 \\ 0 & \frac{1}{\Delta\tau} \end{bmatrix} (\Delta\boldsymbol{\theta})_i = \boldsymbol{A}(\boldsymbol{\theta})_i + \begin{bmatrix} 0 \\ \frac{T_f(\theta,\dot{\theta})}{I} \end{bmatrix}_i - (\omega \boldsymbol{B}\hat{\boldsymbol{\theta}})_i. \tag{5.23}$$

where $\boldsymbol{A} = \begin{bmatrix} 0 & 1 \\ 0 & 0 \end{bmatrix}$. Note that, T_f is constant in the above formulation and depends on θ and $\dot{\theta}$ from the previous iteration.

The form of the matrix $\boldsymbol{A}$ hints that it is not suitable to obtain a converged solution because both the eigenvalues of the matrix are zero. It is known from numerical analysis of ODEs that the eigenvalues of the matrix $\boldsymbol{A}$ should have a negative real part for the equation (5.23) to converge to a solution. The only difference of the above system from the spring-mass-damper system is the absence of the stiffness and damping terms. Hence, it hints that such stiffness and damping terms can be used to obtain convergence in pseudo-time.

The question is: How to obtain these stiffness and damping terms to make the equation (5.22) suitable for numerical implementation?

To target this problem, it is necessary to understand the equation (5.23). Currently, for some initial values of θ^0 and $\dot{\theta}^0$ the fluid solver computes the fluid torque for a sub-problem. Then, this value is used to run the corresponding sub-problem of the structural model which gives the updated θ^1 and $\dot{\theta}^1$ for the next iteration between the fluid and structural models. Now, $T_f(\theta^0,\dot{\theta}^0)$ is at a previous iteration level and is used to compute a θ^1 and $\dot{\theta}^1$. Thus, T_f is not implicit in the current formulation.

To make it implicit, consider a linearization of the fluid torque (T_f) term:

$$T_f(\theta^1,\dot{\theta}^1) \approx T_f(\theta^0,\dot{\theta}^0) + \frac{\partial T_f}{\partial \theta}(\theta^1-\theta^0) + \frac{\partial T_f}{\partial \dot{\theta}}(\dot{\theta}^1-\dot{\theta}^0). \tag{5.24}$$

The equation (5.23) for one sub-problem is written as:

$$\begin{bmatrix} \frac{1}{\Delta\tau} & 1 \\ 0 & \frac{1}{\Delta\tau} \end{bmatrix} (\Delta\boldsymbol{\theta})_i = \boldsymbol{A}(\boldsymbol{\theta})_i + \begin{bmatrix} 0 \\ \frac{T_f(\theta,\dot{\theta})}{I} \end{bmatrix}_i - (\omega \boldsymbol{B}\hat{\boldsymbol{\theta}})_i. \tag{5.25}$$

On using the linearization (5.24), the equation transforms to:

$$\left[\frac{\boldsymbol{I}}{\Delta\tau} - \hat{\boldsymbol{A}}\right] (\Delta\boldsymbol{\theta})_i = \hat{\boldsymbol{A}}(\boldsymbol{\theta})_i + \begin{bmatrix} 0 \\ \frac{T_f(\theta^0,\dot{\theta}^0)}{I} - \frac{\partial T_f}{I\partial\theta}\theta^0 - \frac{\partial T_f}{I\partial\dot{\theta}}\dot{\theta}^0 \end{bmatrix}_i - (\omega \boldsymbol{B}\hat{\boldsymbol{\theta}})_i, \tag{5.26}$$

where $\hat{\boldsymbol{A}} = \begin{bmatrix} 0 & 1 \\ \frac{\partial T_f}{I\partial\theta} & \frac{\partial T_f}{I\partial\dot{\theta}} \end{bmatrix}$ is the modified coefficient matrix. Now, there are terms present in this modified coefficient matrix which correspond to the stiffness and damping terms. The next question is: How to compute the partial derivatives of the fluid torque?

The derivative can be computed using the value of θ for two different iterations in pseudo-time. But, there were problems in this, as the value of $\delta\theta$ tends towards zero when it reaches convergence. Thus, making the derivative undefined. So, this option is rejected.

It is clear that the eigenvalues of this modified matrix $\hat{\boldsymbol{A}}$ should have negative real parts and, from the previous analysis of the spring-mass-damper system, they correspond to the stiffness and damping constants. So instead of the partial derivative terms, if some stiffness and damping constants are used, one can still obtain a convergence in pseudo-time of the problem (5.26). But these cannot be any constants and should be such that the eigenvalues of the modified matrix $\hat{\boldsymbol{A}}$ should have a negative real part. From the comparison of equations (5.26) and (5.12) it is clear that $\frac{\partial T_f}{\partial\theta}$ has the form of a stiffness constant while $\frac{\partial T_f}{\partial\dot{\theta}}$ has the form of a damping constant.

Let k_a and c_a be the stiffness and damping constants which replace the partial derivative terms. The modified matrix $\boldsymbol{A}$ is then, given by:

$$\hat{\boldsymbol{A}} = \begin{bmatrix} 0 & 1 \\ \frac{k_a}{I} & \frac{c_a}{I} \end{bmatrix} \tag{5.27}$$

To obtain the eigenvalues of this matrix, the equation $|\boldsymbol{A}-\lambda\boldsymbol{I}| = 0$ is solved where λ denotes the eigenvalues. The resulting quadratic equation is:

$$\lambda^2 - \lambda\frac{c_a}{I} - \frac{k_a}{I} = 0. \tag{5.28}$$

The solution of the above equation is:

$$\lambda = \frac{c_a}{I} \pm \sqrt{\frac{c_a^2}{I^2} + \frac{4k_a}{I}}.$$

The values of k_a and c_a should be such that the above expression should compute to a value with negative real part.

Knowing that the stiffness and damping constants from the loose coupling were providing a converged solution, it prompts one to use those values and see if the eigenvalues have a negative real part. Hence, $k_a = -400$ and $c_a = -2.5$. The eigenvalues are: $\lambda_1 = -356.26$ and $\lambda_2 = -3143.7$. Both have negative real parts and thus, it can be concluded that the sub-problems will indeed converge. But it should be understood that these values do not affect the final solution of the coupled problem.

Optimized values of k_a and c_a can be computed so that it will help in a faster convergence of the structural sub-problems in pseudo-time and also, the convergence of the coupling between the fluid and structural solutions for one sub-problem. This analysis is not done here and can be a part of future research.

The simulations are now run for the tight coupling problem. It was seen that the individual sub-problems were indeed converging and also, the global iterations converged.

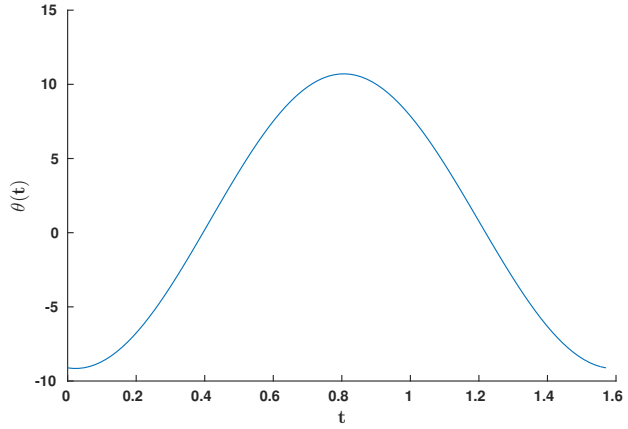

(a) Position

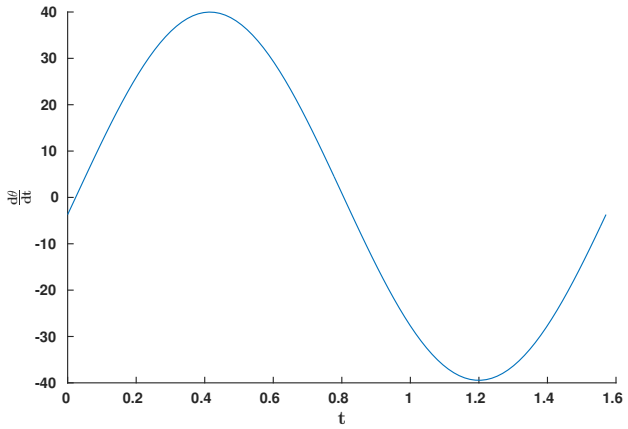

(b) Velocity

Figure 5.9: The position and velocity signals for the tight coupling problem having inlet velocity given by (5.13). n = 2 harmonics were used for the solution and $\omega = 4$ was assumed for periodic inlet velocities. The values of the angle and the angular velocity are in degrees and degrees/sec respectively. The global iterations are set a convergence limit of 10^{-5}.

Figure 5.9 shows the Fourier signals obtained from the converged solution to the tight coupling problem. The solution was computed for n = 2 harmonics, but the form of the solution is a 1 harmonic solution. This is expected, as the inflow velocity is also 1 harmonic. Further, this can be confirmed from the coefficients of the Fourier modes. Table 5.3 shows the coefficients of the Fourier modes of the structural solution of the tight coupling problem. The values of coefficients indeed confirm that the position is a cosine curve while velocity is a sine curve. These are compared to the Fourier coefficients from the loose coupling problem which involves a potential flow. The coefficients in the loose coupling case are similar to the ones for this tight coupling problem. This implies that one can use a potential flow model to obtain a faster but less accurate solution which can serve as a good starting point.

Modes	Position	Velocity
sin(ωt)	-0.015	0.6906
sin(2ωt)	-0.00047	-0.0013
Constant	0.0135	3.07e-08
cos(ωt)	-0.1727	-0.0605
cos(2ωt)	0.0094	-0.0043

Table 5.3: Fourier coefficients obtained from the application of the DFT operator on the harmonic balance solution of the structural part of the tight coupling problem.

As the flow is incident $\pm 10^{\circ}$, the steady state airfoil motion also varies around the same angular positions as seen in figure 5.9. There is definitely some phase lag due to the inertia of the airfoil. This phase lag is visualized here.

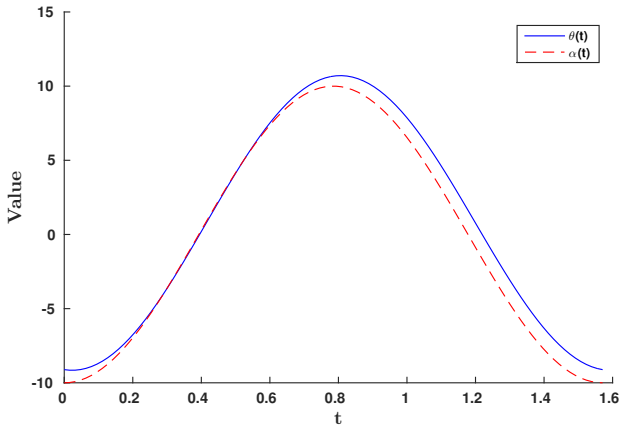

Figure 5.10: Phase lag between the angle of attack α(t) and the airfoil angle θ(t) over a single time period.

Figure 5.10 shows that, in steady state, there is a small phase lag between the angle made by the airfoil with the horizontal and the angle of attack. As the airfoil is plastic, it has low inertia. Hence, the phase lag is small. Another striking observation is that the θ curve is offset from the zero. This is clear from the non-zero value of the *constant* Fourier mode in the solution of the position (θ(t)) of the airfoil as seen in Table 5.3. This is contrary to the physical intuition and further analysis on this front is needed.

The tight coupling problem is completely solved. This problem is actually a coupled fluid-structure interaction problem of a *smooth* motion of an airfoil hinged at its leading edge under a periodic laminar flow. This is closest to the actual problem of this project: the *non-smooth* motion of the airfoil under periodic laminar flow. The next section deals with the non-smooth motion of the airfoil under periodic laminar flow.

5.3. Non-smooth motion of airfoil under periodic laminar flow

The solver developed for the problem of smooth motion is modified to obtain the non-smooth force according to the approach 2 discussed in chapter 4. A non-smooth solution can then be obtained. This is similar to what has been done for the loose coupling problem. Thus, a new *MATLAB-OpenFOAM coupled non-smooth motion solver* is developed to solve this final problem.

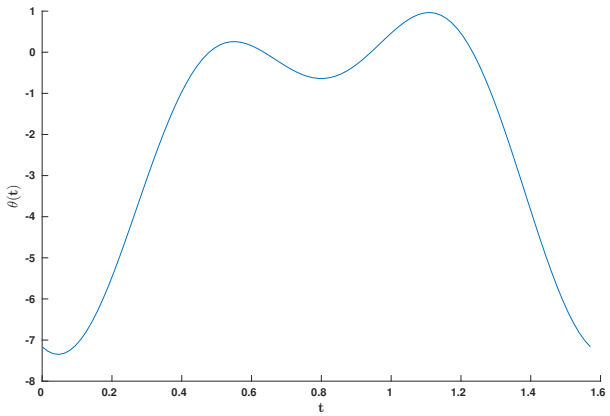

(a) Position

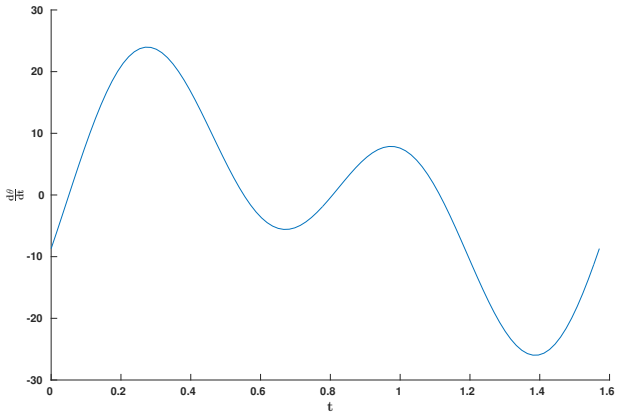

(b) Velocity

Figure 5.11: The position and velocity signals for the problem of non-smooth motion of the airfoil having inlet velocity given by (5.13). n = 2 harmonics were used for the solution and $\omega = 4$ was assumed for periodic inlet velocities. The values of the angle and the angular velocity are in degrees and degrees/sec respectively. The global iterations are set a convergence limit of 10^{-4}.

Figure 5.11 shows the signals computed from the non-smooth solution to the problem of the motion of an airfoil hinged at its leading edge under laminar flow. The signal for the position shows that the airfoil is limited at the 0° angle by the stopper. As this is an approximate solution on a 2 harmonic space, there is little bulge above 0°. Hence, this solution cannot be used for further analysis. To obtain a better solution, higher harmonics are needed. In chapter 4, to treat the spring-mass-damper system with 'restriction' as much as 10 harmonics were needed to obtain a solution with high accuracy. Due to limitations of resources, a higher harmonic solution is not obtained in this project. Nonetheless, the solution above serves as a verification that the entire numerical solution procedure developed in this project is capable of solving the problem of non-smooth motion of the airfoil under periodic laminar flow.

5.4. Conclusion

The chapters 2, 3, and 4 dealt with understanding the lamella dynamics and developing the harmonic balance method to treat the equations governing the lamella dynamics. The first two research questions were addressed. The final research question of coupling the fluid and structural models still remains. Solving this part will provide the solution to the model problem of restricted airfoil motion under periodic fluid flow. In view of this, initially, a simpler loose coupling problem is solved. The loose coupling implies that the solutions of the fluid model are not coupled at all the time instants while only the solutions of the structural model are coupled with each other and with the fluid model. This is achieved by considering a potential flow case, instead of a laminar flow (actual problem). Thus, it simplifies the coupling, and the harmonic balance method along with non-smooth dynamics was tested for this simple problem. It is seen that the method indeed provides a converged and realistic solution. This partially addressed the coupling problem.

The next is the tight coupling problem in which the fluid solutions are also coupled at all the time instants along with the structural solution. This problem considers a laminar flow. Thus the problem is effectively a *smooth* motion of an airfoil hinged at its leading edge under a periodic laminar flow. A coupling procedure is devised for this problem and a *MATLAB-OpenFOAM coupled smooth motion* solver is developed which implements the coupling. In the process of solving this problem, certain issues occur regarding the convergence of sub-problems. These are tackled through a better analysis of the governing equations of the problem and eventually, a converged solution is obtained. The nature of the obtained solution is known to correspond with the physical understanding of the problem. Thus, the third research question of coupling the fluid and structure models for the harmonic balance method is achieved.

Having a smooth solution to the problem of airfoil motion is closest to the actual problem of non-smooth motion. Now, using this smooth solver and the approach 2 discussed in chapter 4, regarding non-smooth solutions using the harmonic balance method, a new *MATLAB-OpenFOAM coupled non-smooth motion* solver is developed. This solver provides a converged solution where the position of the airfoil appears to be restricted at 0°. But, this solution is an approximate one and a solution with higher harmonics is desired. Due to limitations of resources, this higher harmonic solution is not computed here. However, it can be said that the problem which was envisioned at the start of this thesis can be solved with the numerical solution procedure developed in this project.

6

CONCLUSIONS AND RECOMMENDATIONS

This project deals with two different aspects of modeling the motion of the lamella, one is the non-smooth dynamics part and the other is an efficient solution to the FSI problem of a flow around a single lamella. The conclusions in this chapter are also divided into these two parts.

6.1. Conclusions

Each chapter dealt with a part of the problem of modeling the non-smooth motion of the lamella under periodic flow. At the end of every chapter, there are some conclusions which provide answers partly/completely to the research questions presented in 1.3. The first sub-section below presents the conclusions about the modeling of the non-smooth motion of the lamellas.

6.1.1. Modeling non-smooth dynamics

The lamella collides with the stopper which causes the motion of the lamella to become 'non-smooth'. This non-smooth motion is governed by Newton-Euler equations for collisions which are solved using a numerical solution procedure referred to as *event-driven approach*. Then, a *non-smooth IVP solver* is developed to implement this numerical solution procedure and is tested for a model problem of the spring-mass-damper system with 'restriction' (2.12). The solver is verified using a *pseudo-exact solution* developed for this model problem (2.12). In this pseudo-exact solution, only the point of impact is determined numerically while the rest of the solution is determined analytically. Thus, the first research question of the project about modeling the non-smooth motion of the lamella/airfoil was addressed. The next section is about the harmonic balance method.

6.1.2. HB method for obtaining smooth and non-smooth solutions to FSI problems

The developed numerical model is expected to be faster and efficient. Keeping this in mind, a harmonic balance method to solve for flow and structural problems having periodic solutions was selected based on a thorough literature study. The method is implemented and tested for some model problems using the various approaches of the harmonic balance method. It was seen that the *fully uncoupled approach* had problems in convergence. Further research was not done on this front as it is not the main topic of this project.

The harmonic balance method gave a faster and efficient approach of obtaining steady state periodic solutions. But there is still the problem of how to solve the non-smooth problem using the harmonic balance method? The non-smooth solution procedure is based on IVP formulation, and the harmonic balance approach directly provides a steady state solution. There are 3 solution approaches given in chapter 4 to solve this periodic non-smooth motion of the lamella/airfoil using the harmonic balance method. It was seen that, out of the 3 approaches, the second approach- *Modified non-smooth solver* in pseudo-time provides the most accurate solution. This is a unique and indigenous approach developed as a part of this project. There is no literature available where someone has attempted to solve this problem by using such an approach. With this, the second research question is addressed.

Now, the problem of non-smooth motion of an airfoil with the harmonic balance method is solved, but its coupling with the fluid model is still remaining. Initially, a *loose coupling* model is solved using a periodic potential flow. This incorporates a coupling between the structural solutions at various time instants and between the structure and the fluid. But there is no coupling between the fluid solutions at various time instants. The harmonic balance method along with non-smooth dynamics was tested for this comparatively simple problem. It was seen that the method indeed provides a converged, realistic solution. This partially addressed the coupling problem.

The next is the *tight coupling* problem in which the fluid solutions are also coupled at all the time instants along with the structural solution. This problem considers a laminar flow. Thus the problem is effectively a *smooth* motion of an airfoil hinged at its leading edge under a periodic laminar flow. A coupling procedure is devised for this problem and a *MATLAB-OpenFOAM coupled smooth motion* solver is developed which implements the coupling. In the process of solving this problem, certain issues occur regarding the convergence of sub-problems. These are tackled through a better analysis of the governing equations of the problem and eventually, a converged solution is obtained. The nature of the obtained solution is known to correspond with the physical understanding of the problem. Thus, the third research question of coupling the fluid and structure models for the harmonic balance method is addressed.

Using the above developed smooth solver and the approach of modified non-smooth solver in pseudo-time a new *MATLAB-OpenFOAM coupled non-smooth motion* solver is developed. This solver provides a converged solution where the position of the airfoil appears to be restricted at 0°. But, this solution is not suitable for further analysis and a solution with higher harmonics is desired. Due to limitations of resources, this higher harmonic solution is not computed here. However, it can be said that the problem which was envisioned at the start of this thesis can be solved with the numerical solution procedure developed in this project.

The MATLAB-OpenFOAM coupled non-smooth motion solver incorporated a fluid model solver. This fluid model solver is also a MATLAB-OpenFOAM coupled solver which was developed to solve periodic flow problems using the harmonic balance method. This solver is solely for the fluid flow analysis and considers structural components, if any, to be fixed. Such solvers are being developed in the industry to obtain periodic solutions to the problems in turbomachinery.

6.2. Recommendations

Based on the above conclusions, the following are some recommendations or possible future work or research that can be carried out on this project.

Research on fully uncoupled approach

The *fully uncoupled approach* had problems with convergence. A research on finding the convergence criteria for this method can be worthwhile. As this method is similar in implementation to the block Gauss Jacobi method, it can be good to start by analyzing the convergence criteria for block Gauss-Jacobi. On similar lines, the convergence criteria for the fully uncoupled approach can be formulated.

Implementation

The solvers developed in this project are a form of coupled MATLAB and OpenFOAM solvers. The interaction between MATLAB and OpenFOAM is time consuming and heavy for the processor. It is desirable to have a completely OpenFOAM based harmonic balance solver which also incorporates the non-smooth motion. This will make the solution process significantly faster. Additionally, Python can be used instead of MATLAB to make the current solver a completely open source one.

As a partially uncoupled approach is used, each sub-problem can be solved in parallel, thus, reducing the time of computation. So, parallelization of the above solvers is recommended.

Analysis on different solution methods

The individual sub-problems in the structural model for the tight coupling case had issues with convergence so some stiffness and damping terms were added. Currently, these terms were motivated by the loose coupling model. A research can be done regarding optimized values of these constants so that there is a faster convergence between the structural and fluid models for each sub-problem. Further, instead of the present approach to solve the sub-problems, there can be a further research on better solution methods to solve the problem.

Verification for more problems

The novel approach developed for solving the non-smooth motion using the harmonic balance method is verified for a couple of problems. It needs more mathematical analysis to understand its applicability to a wide variety of problems. This can be a good research topic as not many solutions are available for such problems of unilateral contacts to be solved using the harmonic balance method.

Comparison with IVP solutions

Currently, the solutions obtained for the smooth or non-smooth motion of the airfoil are not compared to any benchmark. It is necessary to compare these solutions to the ones obtained from an IVP formulation of the same problem. This will corroborate the numerical solution procedure developed in this thesis.

Construction of 3D model of OWM

The non-smooth motion of the simple lamella is completely understood and a numerical model for this problem is successfully developed. The final problem of a 3D numerical model of the OWM can be now be developed based on this numerical model of a single lamella.

There are now three types of scientists: experimental, theoretical and computational

-Anonymous

A

DETAILS OF NON-SMOOTH DYNAMICAL FORCE

Some more details of the non-smooth dynamical force 4.4 discussed in chapter 4 are presented here. This is a non-linear force, and hence, its Jacobian is essential for the harmonic balance implementaion. The non-smooth dynamical force is given by:

$$\begin{aligned} &\Lambda_{hb}(y,\dot{y},t) = H(y-y_{max})\left(H(\dot{y}-\epsilon_r)F_{col} + (1-H(\dot{y}-\epsilon_r))F_{res}\right), \\ \text{where}\quad &F_{col} = -m(1+\epsilon)\dot{y}(t))\delta\left((y-y_{max})\frac{1}{\dot{y}_{ref}}\right), \\ &F_{res} = H(f_0\sin(\omega_e t))(-f_0\sin(\omega_e t). \end{aligned} \tag{A.1}$$

Using the regularization of the Dirac and Heaviside functions discussed in chapter 4, the approximated non-smooth force is given by:

$$\hat{\Lambda}_{ns}(y,\dot{y},t) = \left(\frac{1+\tanh(\kappa(y-y_{max}))}{2}\right)\left[\left(\frac{1+\tanh(\kappa(\dot{y}-\epsilon_r}\right)\left(-\frac{m(1+\epsilon)\dot{y}}{\eta} + f_0\sin(\omega_e t)\left(\frac{1+\tanh(\kappa f_0\sin(\omega_e t)}{2}\right)\right) - f_0\sin(\omega_e t)\left(\frac{1+\tanh(\kappa f_0\sin(\omega_e t)}{2}\right)\right] \tag{A.2}$$

The above shows that the force $\hat{\Lambda}_{ns}(y,\dot{y},t)$ is non-linear. From the derivation of the harmonic balance method, and it's application to the van der Pol's equation it is clear that one needs to obtain a Jacobian of this force for the computations. Thus, the differentiation of the approximate non-smooth force with respect to y and $\dot{y}$ is given by:

$$\frac{\partial\hat{\Lambda}_{ns}}{\partial y} = \left(-\frac{\tanh^2(\kappa(y-y_{max}))}{2}\right)\left[\left(\frac{1+\tanh(\kappa(\dot{y}-\epsilon_r}\right)\left(-\frac{m(1+\epsilon)\dot{y}}{\eta} + f_0\sin(\omega_e t)\left(\frac{1+\tanh(\kappa f_0\sin(\omega_e t)}{2}\right)\right) - f_0\sin(\omega_e t)\left(\frac{1+\tanh(\kappa f_0\sin(\omega_e t)}{2}\right)\right] \tag{A.3}$$

$$\frac{\partial\hat{\Lambda}_{ns}}{\partial \dot{y}} = \left(\frac{1+\tanh(\kappa(y-y_{max}))}{2}\right)\left[\left(\frac{-\tanh^2(\kappa(\dot{y}-\epsilon_r}\right)\left(-\frac{m(1+\epsilon)\dot{y}}{\eta} + f_0\sin(\omega_e t)\left(\frac{1+\tanh(\kappa f_0\sin(\omega_e t)}{2}\right)\right) - \left(\frac{1+\tanh(\kappa(\dot{y}-\epsilon_r}\right)\frac{m(1+\epsilon)}{\eta}\right] \tag{A.4}$$

The expressions A.3 and A.4 are used in the harmonic balance implementation of this force.

BIBLIOGRAPHY

[1] V. Maniyara, *Computational modeling of the oryon watermill*, Master's thesis, TU Delft (2017).

[2] C. Studer, *Numerics of unilateral contacts and friction*, edited by Springer (Lecture notes in applied computational mechanics, 47, 2009).

[3] D. Baraff, *An introduction to physically based modeling*, SIGGRAPH Course Notes.

[4] C. Glocker, *On frictionless impact models in rigid-body systems*. The Royal Society (2001), 10.1098/rsta.2001.0857.

[5] G. Takacs and B. Rohal-IIkiv, *Model predictive vibration control*, (springer, 2012) Chap. Basics of vibration dynamics, pp. 25–64.

[6] M. B. S. Rowan J. Gilmore, *Nonlinear circuit analysis using the method of harmonic-balance-a review of the art*, Internation Jouranl of Microwave and Millimeter-Wave Computer-Aided Engineering (1991).

[7] W. S. Clark, K. C. Hall, and J. P. Thomas, *Computation of unsteady nonlinear flows in cascades using a harmonic balance technique*, AIAA journal Vol. 40 (2002).

[8] G. Cvijetic, *Analysis and implementation of the harmonic balance method in computational fluid dynamics*, Master's thesis, University of Zagreb (2015).

[9] A. K. G. A. Jameson, *Time spectral method for periodic unsteady computations over two- and three- dimensional bodies*. AIAA Aerospace Sciences Meeting and Exhibit (2005).

[10] M. W. K.J. Badcock, *Implicit computational fluid dynamics methods for fast analysis of rotor flows*, AIAA Journal Vol.50 (2012).

[11] *Sylvester*.

[12] M. Evans, *Lecture notes on methods of mathematical physics*, .

[13] R. F. Hoskins, *Delta functions*, edited by Elsevier (Elsevier, 2009).

[14] R. I. L. Frederic Schreyer, *A mixed shooting-harmonic balance method for unilaterally constrained mechanical systems*, Archive of mechanical engineering (2016).

[15] B. Brogliato, *Nonsmooth mechanics*, edited by Communications and control engineering (Springer, 2016).

[16] A. P. Joseph Katz, *Low-speed aerodynamics*, edited by C. U. Press (Cambridge University Press, 2001).

[17] *Naca0009-joukowskitransform*, .

[18] J. Anderson, *Fundamentals of aerodynamics*, edited by Mcgraw-Hill (Mcgraw-Hill Education-Europe, 2001).

[19] M. P. Paidoussis, S. J. Price, and E. de Langre, *Fluid-structure interactions*, edited by Cambridge (Cambridge University Press, 2010).

[20] Y. L. Young, E. J. Chae, and D. T. Akcabay, *Hybrid algorithm for modeling of fluid-structure interaction in incompressible, viscouse flows*, Acta Mechanica Sinica (2012), 10.1007/s10409-012-0118-3.

[21] *OpenFOAM User Guide v05*.

[22] *OpenFOAM programmer's guide*.